

THESIS

DEVELOPMENT OF A LOW-FIREPOWER BIOMASS DUST COMBUSTOR

Submitted by

Kyle C. Greer

Department of Mechanical Engineering

In partial fulfillment of the requirements

For the Degree of Master of Science

Colorado State University

Fort Collins, Colorado

Fall 2018

Master's Committee:

Advisor: John Mizia

Co-Advisor: Bret Windom

Jay Ham

Copyright by Kyle C. Greer 2018

All Rights Reserved

## ABSTRACT

### DEVELOPMENT OF A LOW-FIREPOWER BIOMASS DUST COMBUSTOR

As of 2017, the World Health Organization estimates that 2.3 billion people globally lack access to basic sanitation facilities such as toilets or latrines. 892 million of these people defecate in the open, which increases the spread of disease and intestinal parasites. Incinerating desiccated human waste provides a low-cost opportunity to safely mitigate this public health risk. Over the last five years, the Advanced Biomass Combustion lab at CSU has developed a 2-kW fecal gasifier as part of the Gates Reinvent the Toilet Challenge, but the combustor lacks scalability to low firepowers.

Continuous low-firepower biomass combustion has eluded development due to several technical challenges, however it is advantageous in many situations and opens the door for many low energy devices. Development of a low-firepower fecal combustor could act as a pilot light for the existing gasifier, it could be a low-cost standalone incinerator for household use, it may have higher combustion efficiencies and lower emissions than the gasifier, and it could be scaled to high firepowers by creating arrays of flames.

A 100 Watt idealized biomass dust combustor has been developed to investigate the feasibility of creating a low-firepower fecal dust burner. Despite extensive research on dust explosion dynamics, few stable dust-flame burners have been researched and developed. This project utilized dust combustion fundamentals and iterative hardware development to create a low-firepower biomass dust combustor. Cornstarch, wheat flour, and lycopodium spores were explored as idealized biomass fuels, and human feces was briefly tested in the combustor. The hardware development process will help guide the transition to a stable low-firepower fecal dust burner.

## ACKNOWLEDGEMENTS

My deepest thanks goes to those that have helped the completion of this work and create balance during my graduate studies.

John Mizia, without whom this endeavor would truly not be possible, has provided tremendous support and guidance, challenging and engaging projects, good-humor, and an enjoyable workplace. The friends and colleagues at the Energy Institute have fostered an engaging, enjoyable, and educational atmosphere throughout my master's degree. Thank you to Bret Windom for his guidance on combustion fundamentals, and to Jay Ham for teaching me how to (among other things) revamp my backyard farm with Arduino boards.

I have great thanks to the whole team at MSR, notably Linden Klein, who provided incredible support with hardware development and fabrication for this project.

To my best friend and wife, Dana, who brings great joy and adventure to my life. And I have such gratitude to my parents, who brought me into the world and raised me with unending love and support.

And to the wild and windy places, who clear my head and lighten my heart.

## TABLE OF CONTENTS

ABSTRACT . . . . .	ii
ACKNOWLEDGEMENTS . . . . .	iii
LIST OF TABLES . . . . .	vii
LIST OF FIGURES . . . . .	viii
Chapter 1    Introduction . . . . .	1
1.1        Human Waste Disposal and Project Background . . . . .	1
1.2        Development of a Biomass Dust Nano-Combustor . . . . .	2
1.3        Project Goals and Deliverables . . . . .	4
Chapter 2    Dust Combustion Theory . . . . .	6
2.1        Combustion Basics . . . . .	6
2.1.1    stoichiometry . . . . .	6
2.1.2    Fuel Heating Values . . . . .	7
2.1.3    Premixed and Diffusion Flames . . . . .	8
2.1.4    Other Flame Characteristics . . . . .	10
2.2        Dust Combustion History . . . . .	12
2.3        Dust Combustion Dynamics . . . . .	13
2.3.1    Ignition and Limits of Flammability . . . . .	14
2.3.2    Stoichiometric Concentration . . . . .	15
2.3.3    Additional Challenges of Dust Combustion . . . . .	16
Chapter 3    Fuels . . . . .	19
3.1        Idealized Biomass Fuels . . . . .	19
3.2        Feces as Fuel . . . . .	20
3.3        Fuel Comparisons . . . . .	21
3.4        Combustible Dust Properties . . . . .	23
3.4.1    Particle Size Distribution . . . . .	24
3.4.2    Aerosol Physics . . . . .	24
3.4.3    Material Transport . . . . .	26
3.4.4    Powder Generation . . . . .	27
Chapter 4    Risk Assessment . . . . .	28
4.1        Risk Assessment . . . . .	28
4.1.1    Primary Risks . . . . .	28
4.1.2    Secondary Risks . . . . .	30
4.2        Project Trajectory . . . . .	31
Chapter 5    Initial Hardware Development . . . . .	32
5.1        Standing Flame Dust Combustors - Literature Review . . . . .	32
5.2        Powder Coating Gun . . . . .	34
5.3        Venturi Nozzle . . . . .	36

5.3.1	Combustion Results . . . . .	39
Chapter 6	Fluidized Bed . . . . .	43
6.1	Fluidized Bed Theory . . . . .	43
6.2	Hardware Development . . . . .	45
6.2.1	First Generation Fluidized Bed Burner . . . . .	45
6.2.2	Intermediate Hardware Revisions . . . . .	49
6.2.3	Second-Generation Fluidized Bed Burner . . . . .	50
6.3	Conclusions . . . . .	52
Chapter 7	Fuel Delivery System . . . . .	53
7.1	Auger Design . . . . .	53
7.2	Firepower Set points . . . . .	55
7.3	Control System . . . . .	56
Chapter 8	Final Nano-Combustor Design and Testing . . . . .	57
8.1	Third-Generation Nano-Combustor . . . . .	57
8.1.1	Gen-3, Revision 1 Results . . . . .	59
8.1.2	Gen-3, Revision 2 . . . . .	61
8.1.3	Nozzle Rim Flameholders . . . . .	62
8.1.4	Gen-3, Revision 3 . . . . .	64
8.1.5	Further Auger Development . . . . .	65
8.2	Final Nano-Combustor . . . . .	67
8.2.1	Testing Results and Summary . . . . .	69
Chapter 9	Fuel Challenges . . . . .	72
9.1	Observations From Testing . . . . .	72
9.2	Flow Regimes . . . . .	73
9.3	Agglomeration and Particle Microscopy . . . . .	75
Chapter 10	Further Hardware Improvements . . . . .	78
10.1	Flameholders . . . . .	78
10.2	Fuel Delivery . . . . .	79
10.3	Lofting Orifices . . . . .	81
Chapter 11	Fecal Processing and Testing . . . . .	83
11.1	Grinding and Size Selection . . . . .	83
11.1.1	Sieve Vibrator . . . . .	84
11.2	Fecal Combustion Testing . . . . .	85
11.2.1	Test Enclosure . . . . .	85
11.2.2	Nano-Combustor Fecal Testing . . . . .	85
Chapter 12	Conclusions . . . . .	89
12.1	Summary of Findings . . . . .	89
12.2	Suggestions for Future Work . . . . .	90

Bibliography	92
Appendix A Combustion Calculator	97
Appendix B Fecal Fuel Analysis	103
Appendix C Venturi Calculations and Hardware Design	109
Appendix D Arduino Controller Code	116
Appendix E Primary EES Design Calculator	120
Appendix F Additional Images and Charts	122
F.1 Fluidized Bed Burner	122
F.2 Powder Microscopy	123

## LIST OF TABLES

3.1	Ultimate Fuels Analysis . . . . .	21
3.2	Powdered Fuels Properties - Empirically Derived . . . . .	21
3.3	Powdered Fuels Calculated stoichiometric Concentrations . . . . .	22
3.4	Lycopodium and cornstarch flame speeds as a function of dust concentration . . . . .	24
6.1	Summary of fluidized bed burner operating parameters, cornstarch as fuel . . . . .	52
7.1	1/4" pitch auger firepower setpoints . . . . .	56
8.1	Summary of first revision results with third-generation Nano-Combustor using lycopodium fuel . . . . .	59
8.2	Summary of third-gen. Rev 2 Nano-Combustor using lycopodium fuel . . . . .	61
8.3	Summary of Third-Gen. Rev 3 Nano-Combustor using lycopodium fuel . . . . .	64
8.4	Summary of third-generation Nano-Combustor set points using lycopodium fuel . . . . .	65
8.5	Differences in primary augers' geometry . . . . .	66
8.6	Summary of initial test with the final Nano-Combustor design using lycopodium fuel . . . . .	69
8.7	Summary of final Nano-Combustor set points . . . . .	70
11.1	Summary of Nano-Combustor fecal testing . . . . .	85

## LIST OF FIGURES

1.1	Helminth Parasite . . . . .	1
1.2	RTTC concept proposed by RTI and CSU . . . . .	2
1.3	CSU’s Micro-monofold updraft fecal gasifier . . . . .	2
1.4	Nano-Combustor Project Deliverables . . . . .	5
2.1	Bunsen burner flame speed . . . . .	10
2.2	Liftoff and flashback . . . . .	11
2.3	Lycopodium Dust Flame Propagation Model . . . . .	13
2.4	Dust Explosion Pentagon . . . . .	14
2.5	Scanning electron microscope image of lycopodium . . . . .	17
2.6	75 watt lycopodium flame on the Nano-Combustor . . . . .	18
3.1	Lycopodium laminar flame propagation sequence . . . . .	20
3.2	Cornstarch, Wheat Flour and Lycopodium Laminar Flame Speeds . . . . .	22
3.3	Lycopodium Flame Speed . . . . .	23
5.1	Typical dust flame burner schematic . . . . .	32
5.2	Schematics of standing flame dust combustors from various sources . . . . .	33
5.3	Powder Coating Gun Cross-section . . . . .	35
5.4	Powder Coating Gun with Cornstarch Flame . . . . .	35
5.5	Fox venturi nozzle . . . . .	36
5.6	Nozzle diameters as a function of cornstarch concentrations . . . . .	37
5.7	Venturi nozzle with hopper, nozzle, and torch . . . . .	38
5.8	Venturi nozzle assembly . . . . .	38
5.9	Venturi Nozzle Flames . . . . .	40
5.10	Fox venturi nozzle firepower results . . . . .	41
5.11	Fox venturi nozzle concentration results . . . . .	41
5.12	Venturi nozzle with pick-up tube . . . . .	42
6.1	Fluidized bed flow regimes . . . . .	44
6.2	Fluidized Bed Burner . . . . .	46
6.3	First generation fluidized burner (a) dust cloud and (b) resulting flame. 10.5 SLPM air, firepower ~275 watts . . . . .	48
6.4	Firepower sweeps for 1.25" diameter fluidized bed burner . . . . .	48
6.5	Fluidized bed burner with swirl . . . . .	49
6.6	Fluidized burner with aluminum nozzle . . . . .	49
6.7	Second-generation fluidized bed burner . . . . .	51
6.8	Second-generation flame. ~100-200 watts, 1.5 SLPM air. . . . .	51
7.1	First generation auger and hopper assembly . . . . .	54
7.2	Firepower vs RPM curve, first generation auger versions . . . . .	55
7.3	Arduino stepper-motor controller . . . . .	56

8.1	Third-generation Nano-Combustor . . . . .	58
8.2	third-Gen Nano-Combustor, Rev. 1 flame . . . . .	60
8.3	third-Gen Nano-Combustor, Rev. 2 flame, with flattened-wire flameholder . . . . .	62
8.4	Nozzle rim flameholders . . . . .	63
8.5	Third-Gen Nano-Combustor, Rev. 3 flame, with flared nozzle . . . . .	65
8.6	Original and final augers . . . . .	66
8.7	3/8" OD auger firepower set points . . . . .	66
8.8	Final Nano-Combustor Assembly . . . . .	67
8.9	Section view schematic of final Nano-Combustor . . . . .	68
8.10	3/8" OD 3/16" pitch augers. New auger on top with thinner flights . . . . .	71
8.11	Firepower set points for old and new 3/8" OD augers . . . . .	71
9.1	Lycopodium accumulating on Nano-Combustor nozzle and occluding bulk flow . . . . .	73
9.2	9/32"OD nozzle velocity factor with lycopodium . . . . .	74
9.3	9/32"OD nozzle Reynolds numbers . . . . .	74
9.4	Fresh lycopodium, 80x magnification . . . . .	75
9.5	Used lycopodium, 80x magnification, agglomerates circled . . . . .	76
9.6	Human Feces, 0-44 $\mu\text{m}$ , 80x magnification . . . . .	76
9.7	Auger with decreasing pitch creates partially-full flights . . . . .	77
10.1	Examples of flameholder designs at MSR . . . . .	79
10.2	Redesigned augers at MSR including variable pitch and variable shaft diameter (bottom) . . . . .	80
10.3	Updated tee-fitting with interchangeable lofting orifices, developed at MSR . . . . .	81
10.4	Lofting orifices ranging from 0.013" to 0.125" developed at MSR . . . . .	82
11.1	Sieve stack with coarsest mesh on top . . . . .	83
11.2	Sieve vibrator made out of a re-purposed palm-sander . . . . .	84
11.3	Initial powdered fecal flames with Nano-Combustor hardware . . . . .	86
A.1	Matlab combustion calculator GUI . . . . .	101
A.2	Example results from combustion calculator . . . . .	102
C.1	Dust concentration vs. air flowrate . . . . .	110
C.2	Concentration vs. venturi nozzle diameter . . . . .	111
C.3	Hopper design equations [1] . . . . .	112
C.4	Hopper design equations [1] . . . . .	113
C.5	Hopper design equations [1] . . . . .	114
C.6	Hopper design equations [1] . . . . .	115
F.1	Fuel/Air Concentrations as a function of air flowrate, 1.25" diameter fluidized bed burner . . . . .	122
F.2	Fresh lycopodium, 80x magnification . . . . .	123
F.3	Fresh lycopodium, 200x magnification . . . . .	124
F.4	Fresh lycopodium, 800x magnification . . . . .	125
F.5	Used lycopodium, 80x magnification . . . . .	126
F.6	Used lycopodium, 80x magnification . . . . .	127
F.7	Used lycopodium, 80x magnification, agglomerates circled . . . . .	128
F.8	Used lycopodium, 200x magnification . . . . .	129

F.9	0-45 um sieved feces powder, taken straight from sieve and sprinkled on microscope slide . . . . .	130
F.10	0-45 um sieved feces powder, 80x magnification . . . . .	131
F.11	0-45 um sieved feces powder, 80x magnification . . . . .	132
F.12	0-45 um sieved feces powder, 200x magnification . . . . .	133
F.13	0-45 um sieved feces powder, 200x magnification . . . . .	134
F.14	0-45 um sieved feces powder, 800x magnification . . . . .	135
F.15	45-75 um sieved feces powder, taken straight from sieve and sprinkled on microscope slide . . . . .	136
F.16	45-75 um sieved feces powder, 80x magnification . . . . .	137
F.17	45-75 um sieved feces powder, 80x magnification . . . . .	138
F.18	45-75 um sieved feces powder, 200x magnification . . . . .	139
F.19	45-75 um sieved feces powder, 200x magnification . . . . .	140
F.20	45-75 um sieved feces powder, 200x magnification . . . . .	141
F.21	45-75 um sieved feces powder, 200x magnification . . . . .	142
F.22	45-75 um sieved feces powder, 800x magnification . . . . .	143

# Chapter 1

## Introduction

### 1.1 Human Waste Disposal and Project Background

Public health depends on access to hygienic sanitation facilities, yet much of the global population lacks these services. As of 2017, the World Health Organization estimates that 2.3 billion people globally lack access to basic sanitation facilities such as toilets or latrines. 892 million of these people defecate in the open, such as in streets, open spaces, or bodies of water [2].

Poor sanitation is linked to the spread of cholera, dysentery, hepatitis A, typhoid, and polio. It is also responsible for the spread of intestinal worms such as Helminth, which cause malnutrition, suffering, and death for thousands. The World Health Organization estimates that 280,000 annual deaths occur due to inadequate sanitation [2]. Improved access to sanitation facilities reduces the spread of these intestinal parasites and disease, eases malnutrition, and can increase the quality of life for millions globally.

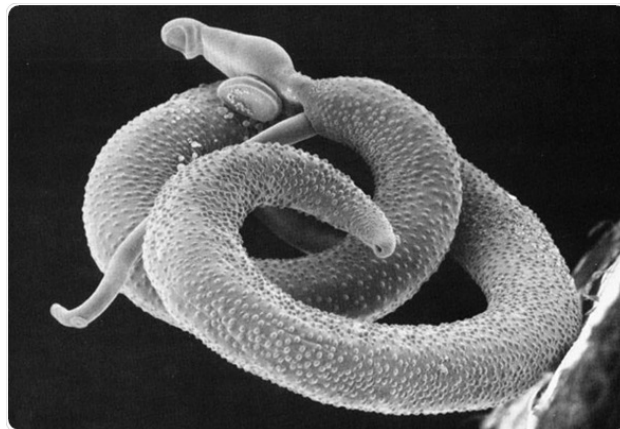


**Figure 1.1:** Helminth Parasite [3]

In 2011, the Bill and Melinda Gates Foundation initiated the *Reinvent the Toilet Challenge* (RTTC). This effort awarded grants to sixteen research groups around the world to explore innovative approaches to safely and sustainably manage human waste. Primary criteria for the RTTC

initiative includes removing pathogens from human waste, recovering valuable byproducts (e.g. energy/nutrients/water), off-grid operation, and a maximum operating cost of \$0.05 per user per day [4].

Colorado State University's (CSU) Advanced Biomass Combustion Lab was contracted by Research Triangle Institute (RTI) as one of the sixteen research groups for the RTTC to develop a human feces combustor as part of a full toilet system. This system (Figure 1.2) aims to include solid/liquid waste separation, liquid sanitation treatment, fecal drying using ambient air and waste heat from combustion, automated fuel (feces) sizing and delivery, and complete, efficient dried feces combustion. In the last six years the team at CSU has developed a robust and efficient 2 kW human feces combustor (Figure 1.3), automated fuel delivery, and heat exchangers to dry incoming fresh feces [5]. This combustor integrates into RTI's toilet and fresh waste processing system and as of Summer 2018 the project is in its Phase 3: Commercialization stage.

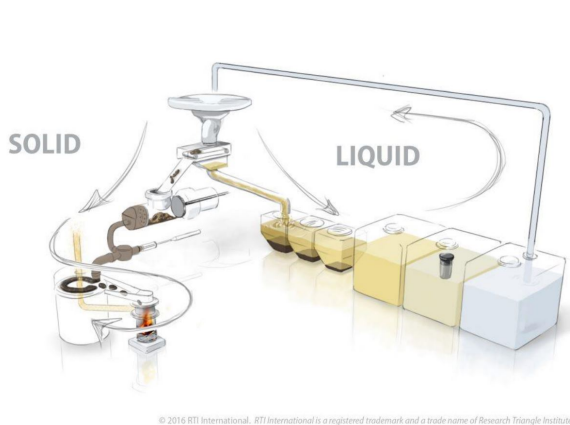


**Figure 1.2**  
RTTC concept proposed by RTI and CSU [5]



**Figure 1.3**  
Micro-monofold continuous-feed updraft fecal gasifier developed by CSU [5]

## 1.2 Development of a Biomass Dust Nano-Combustor

Some of the challenges faced by the current CSU/RTI toilet system include: a high input-energy startup phase, a startup phase with a high level of particulate matter (PM) in the exhaust,

and difficulty scaling down to low-firepower operation. The current system is designed to serve about 15 people per day, but the combustor requires daily startup. It is feasible to scale up the current combustor to service more people per day, but it does not scale down effectively below 1-1.5 kW. In response to these limitations, the Advanced Biomass Combustion Lab at CSU proposed a smaller combustor design that operates on premixed dust combustion, henceforth referred to as the Nano-Combustor.

Continuous low-firepower biomass combustion has eluded development due to several technical challenges, however it is advantageous in many situations and opens the door for many low energy devices. Current high firepower biomass combustors consume fuel quickly, are relatively large, and do not offer scalability like modern gaseous fuel burners. Combustors operating at 1.5 kW may be well suited for large scale processing of feces, but they are unable to offer the efficiencies needed for small scale processing. By developing a low-firepower combustor, near continuous fuel drying could occur, thus improving the overall thermal processing efficiencies and energy balance.

The primary goal of the Nano-Combustor is to reduce the firepower of the combustion by over an order of magnitude to 100 watts. For perspective, a standard butane lighter flame is approximately 80 watts. At 100 watts, the system consumes approximately 20 grams of dried fecal fuel per hour. This would allow the Nano-Combustor to burn the feces of a small family (1-6 people) under continuous operation. Continuous combustion is an improvement over the larger system because it would reduce the poor startup emissions and energy inputs needed for the ignitor and fan start-up.

Another advantage of the Nano-Combustor is that it operates as a quasi premixed flame. This helps avoid the emissions penalties associated with typical solid biomass diffusion flames, which is characteristic of the the larger fecal combustor. In diffusion flames, the fuel diffuses into ambient air, which limits the fuel's access to oxidizer and can increase the products of incomplete combustion. The premixed flame, on the other hand, has the fuel suspended in the air, which provides more complete combustion by increasing the fuel's access to oxidizer. It is also easier to scale the

premixed flame to larger firepowers by either increasing the flowrates of the fuel-air mixture or by creating an array of flames, which is analogous to a gas cooking range. The Nano-Combustor could also be used as a pilot light for the larger system, which would offset the energy burden of the ignitor at start-up. Combustion fundamentals and final system design will be discussed in much more detail in Chapter 2 - Dust Combustion Theory, and Chapter 8 - Final Nano-Combustor Design.

### **1.3 Project Goals and Deliverables**

CSU's Advanced Biomass Combustion Lab partnered on this project with Mountain Safety Research (MSR), a Seattle-based company well-known for being a leader in designing and manufacturing single-burner camping cookstoves and drinking water filtration. The 18-month project was split into two phases beginning August 2017. The first phase was led primarily by the CSU group and involved initial research, development, and testing of the Nano-Combustor technology. The larger RTTC project provided insight into the difficulty in burning feces, so the first phase of the Nano-Combustor used idealized biomass powders as surrogate fecal powder. This will be discussed in-depth in Chapter 3 - Fuels. The project also took a trajectory where initial hardware would demonstrate a stable 500 watt flame at CSU and the final Nano-Combustor would be 100 watts at MSR. Stable was defined as hands-free operation for greater than 15 minutes. This allowed an opportunity to vet the combustion physics and hardware setup at the high firepower and then scale into the final goal of 100 watts.

The hardware development was initially focused on fast iterative design and testing to allow for smooth hardware changes and a broad understanding of the combustion dynamics. As the hardware and the combustion became more robust and well-understood, hardware design became more solidified. MSR's strength in design and manufacturing made them strong partners by being able to provide the CSU team quick hardware manufacturing and also the ability to design a visually streamlined end-product. The Advanced Biomass Combustion Lab at CSU has over a decade of experience with high-volume biomass cookstove design and testing, including full in-house emis-

sions testing capabilities. The group at CSU also had a complete metal shop, a CNC waterjet, and a workshop available for in-house fabrication, which provided great flexibility in the iterative hardware design.

Figure 1.4 shows an overview of the 18-month project deliverables split between CSU and MSR, beginning August 2017. This thesis will focus primarily on CSU’s deliverables. Unless otherwise noted, all hardware was fabricated, assembled, and tested by the author. MSR was a key contributor at points of the project and will be recognized appropriately.

Deliverables	CSU			MSR		
	Q1	Q2	Q3	Q4	Q5	Q6
1). Flame modeling and Fuel Prepreparation/Testing	→					
2). Demonstration of 500W Flame		→				
3). Demonstation of 100W Flame			→			
4). Recommendations / Report						→

**Figure 1.4:** Nano-Combustor Project Deliverables

# Chapter 2

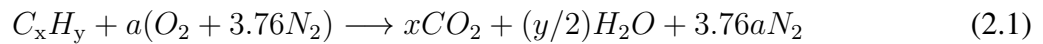
## Dust Combustion Theory

### 2.1 Combustion Basics

Any combustion event requires fuel, oxidizer, and ignition. For combustion to be sustained, fresh incoming fuel must be introduced into the flame zone and will react with either excess oxidizer or additional incoming oxidizer. A stoichiometric mixture of fuel and oxidizer means that all of the fuel and oxidizer are consumed in combustion. Fuel-lean mixtures result in products with excess oxidizer, and fuel-rich mixtures result in a myriad of products such as unburned or partially burnt hydrocarbons often including carbon monoxide (CO) [6].

#### 2.1.1 stoichiometry

For a hydrocarbon fuel (e.g.  $C_xH_y$ ) and assuming an ideal set of products, a general stoichiometric reaction can be written by using simple atom balances, as in equation 2.1:



$$\text{Where: } a = x + y/4$$

The equivalence ratio,  $\phi$ , will be used here to refer to stoichiometric ( $\phi = 1$ ), fuel lean ( $\phi < 1$ ), or fuel rich ( $\phi > 1$ ) conditions. The equivalence ratio is defined by:

$$\phi = \frac{(m_{\text{fuel}}/m_{\text{air}})_{\text{actual}}}{(m_{\text{fuel}}/m_{\text{air}})_{\text{stoic}}} \quad (2.2)$$

With:

$$\left(\frac{m_{\text{fuel}}}{m_{\text{air}}}\right)_{\text{stoic}} = \frac{1}{4.76a} \frac{MW_{\text{fuel}}}{MW_{\text{air}}} \quad (2.3)$$

Where  $MW_{\text{air}}$  and  $MW_{\text{fuel}}$  are the molecular weights of the air and fuel respectively.

## 2.1.2 Fuel Heating Values

The heat of combustion (kJ/kg) is the difference in enthalpy between reactants and products during combustion. The higher heating value (HHV) is the heat of combustion plus the energy liberated when water vapor in the products condenses. The HHV is aptly named because the most energy is released when energy from water vapor condensation is taken into account. The lower heating value (LHV) is the energy released during combustion assuming the water in the products remains in vapor state [6]. This paper utilizes the lower heating value for energy calculations because one of the RTTC's goals is to explore the utilization of waste heat in the exhaust. It is assumed that energy from the waste heat will be extracted above the temperature at which water condenses, so the LHV is used.

The relationship between HHV and LHV is summarized in Equation 2.4, where  $W$  is the mass percent of water in the combustion products and  $\lambda$  is the latent heat of water [7].

$$HHV = LHV + W\lambda \quad (2.4)$$

### Firepower

Firepower (W or kW) is a function of the fuel's heating value and mass flowrate, shown below in Equation 2.5. Note that firepower is not a function of the equivalence ratio, and assumes that all of the fuel ends as gaseous combustion products. In reality, the inorganic solid ash created in combustion is present in the mass of the original fuel and does not contribute to the firepower. The fuel calculator often used in this project and reproduced in Appendix A takes this into account and subtracts the ash content from the original fuel mass. This was important for feces calculations because of the relatively high ash content compared to wood (see Chapter 3). For this project, the LHV will be used when expressing firepower because it is assumed that any available energy in the exhaust is extracted above water's condensation temperature. The two main benchmark firepowers for the Nano-Combustor are 500 W and 100 W dust combustors. Firepower is a valuable metric because it represents the maximum (ideal) power that can be extracted from exhaust.

$$\dot{m}_{\text{fuel}} [\text{kg/s}] * LHV [\text{kJ/kg}] = \text{Firepower} [\text{kW}] \quad (2.5)$$

Appendix A contains the combustion calculator written in MATLAB by the author. Given fuel composition (mass or molar-based), equivalence ratio, exhaust temperature, mass flowrate of the fuel, and the lower heating value of the fuel, the calculator will balance the combustion equation, provide exhaust flowrate, and give the expected firepower. The calculator was used extensively on this project (and others in the Advanced Biomass Combustion Lab) to help guide hardware developments as a function of changing combustion conditions. Note that the calculator only operates with  $\phi \leq 1$ .

### 2.1.3 Premixed and Diffusion Flames

A flame can be classified as a premixed or diffusion (nonpremixed) flame. In a premixed flame, the fuel and oxidizer are mixed at the molecular level before combustion occurs (e.g. a spark-ignition engine). On the other hand, in a diffusion flame the fuel and oxidizer are initially separated and combustion occurs at the interface between the two. The reactants combine via diffusion and thus the rate of reaction is largely determined by the diffusion rate of the reactant molecules [6]. A candle flame or burning match are quintessential examples of diffusion flames.

### Gasification

The 1.5 kW fecal combustor under development for the RTTC operates on the principal of "updraft gasification." Gasification is not relevant to this study, but will be reviewed briefly here as a form of comparison and was used to guide this project's development. Gasification is the process by which solid fuel (e.g. dried feces) is heated in a low-oxygen environment to the point when volatile and semi-volatile compounds transition to vapor phase. This pyrolysis gas represents the combustible constituents of the solid fuel, but a gasifier has the benefit of being able to route the pyrolysis gas to a specific combustion zone.

An updraft gasifier routes the pyrolysis gas through the unburned fuel bed using forced air. At a point above the fuel bed, while the vapors are still hot enough to combust once in contact with

oxygen, secondary air is introduced at the proper velocity and volume to create stoichiometric combustion. This resulting flame is still considered a diffusion flame because the fuel and oxidizer are kept separate until the combustion event [5]. More specifically, this is considered an inverse diffusion flame because the oxygen diffuses into the fuel at the secondary air inlet.

## **Emissions**

From an emissions perspective, employing a premixed flame has many benefits. Diffusion flame fronts contain complex combustion phenomena especially from the perspective of the fuel air ratio. Certain regions of the diffusion flame front may be locally fuel lean, while others may be fuel rich. The fuel rich zones may contain incomplete combustion, which can result in unburned hydrocarbons as combustion products [6]. Some of these products (notably particulate matter and carbon monoxide) can cause health implications when inhaled in confined spaces [8].

Particulate matter (PM) is another negative byproduct characteristic of diffusion flames that can cause negative health implications. PM is often observed as soot, which is formed in the fuel-rich zones of the diffusion flame [6]. Soot reduces combustion efficiency and can cause health problems when inhaled. PM inhaled from combustion is mostly below a diameter of  $2.5 \mu\text{m}$ , which can impact in the nasal cavity, throat, or in the lungs. The smallest particles can embed themselves deep in the lungs and enter the bloodstream, potentially causing heart complications in the host [8]. Clearly reducing PM and gaseous products of incomplete combustion reduces possible public health risks and increases combustion efficiency. One way of doing this is to employ premixed combustion, which characteristically has low-levels of CO and PM [6]. Thus from an emissions and public health perspective, the Nano-Combustor development offers a compelling alternative to the fecal gasifier.

It should be noted that sulfur is contained in fecal material and is present in its combustion products as  $\text{SO}_2$  or  $\text{SO}_3$  [5]. These oxides of sulfur can degrade exhaust materials and create negative health impacts when inhaled in high-enough concentrations. At the moment, efforts on fecal combustion under the RTTC umbrella are primarily focusing on the challenges of fecal combustion and are minimally addressing the issue of mitigating sulfur in the exhaust [5]. Yet

technologies already exist for sulfur mitigation from coal and oil industries that employ lime or limestone "filters" in the exhaust. The calcium in the lime reacts with the sulfur, which precipitates out as calcium sulfite dihydrate ( $\text{CaSO}_3$ ) and is disposed of as a solid waste [6].

### 2.1.4 Other Flame Characteristics

A flame can freely propagate, such as in a tube filled with fuel and air, or a flame can be stationary, such as a Bunsen burner. In both cases, the flame consumes the unburned mixture at a velocity, the *flame speed*,  $S_L$  (m/s, or cm/s). In a one-dimensional flame neglecting heat losses at the edges, the flame speed will be constant for a given equivalence ratio. On the premixed, inner cone of a Bunsen burner, the flame speed is the velocity of the fuel normal to the surface of the flame as shown in Figure 2.1 below and in Equation 2.6.

$$S_L = v_{u,n} = v_u \sin \alpha \quad (2.6)$$

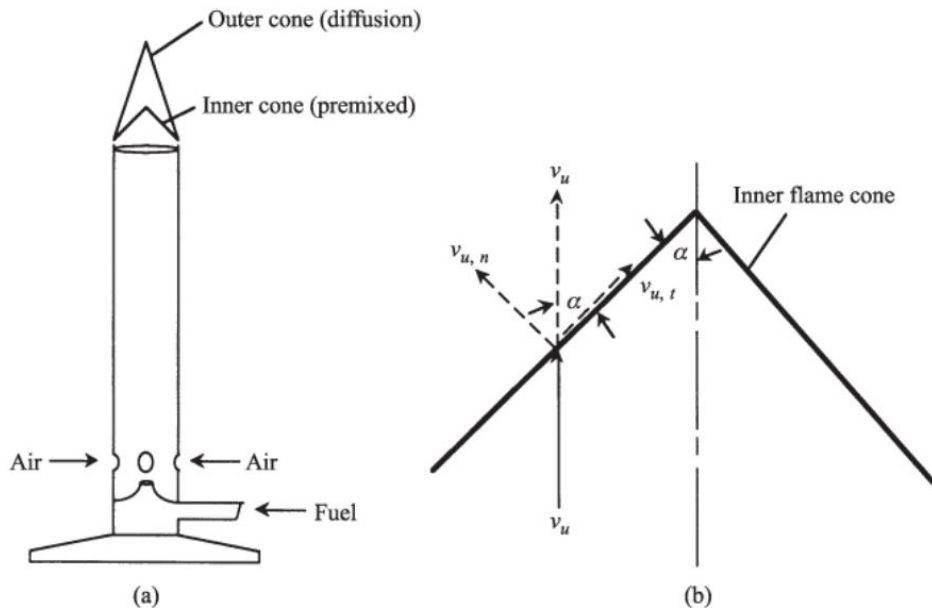


**Figure 2.1:** (a) Bunsen burner (b) Laminar flame speed is the normal component of the unburned mixture velocity [6].

For a simplified understanding of flame speed and flame stabilization, the rate of incoming unburned fuel and air must balance the flame speed at the flame front in order for the flame to remain stationary. If the rate of incoming fuel and air exceeds the flame speed, the flame will *lift off*. The flame may become stationary while lifted off of the edge of the nozzle, but as the unburned velocity increases, heat losses will eventually extinguish the flame. If the local unburned mixture velocity is less than the local flame speed at the flame front, the flame will *flashback*. Flashback usually results in the flame quenching, but can also be a danger in certain applications where the flame flashing back can ignite a reservoir of unburned fuel-air and cause an explosion. Figure 2.2 shows flashback and liftoff conditions at the edge of a burner.

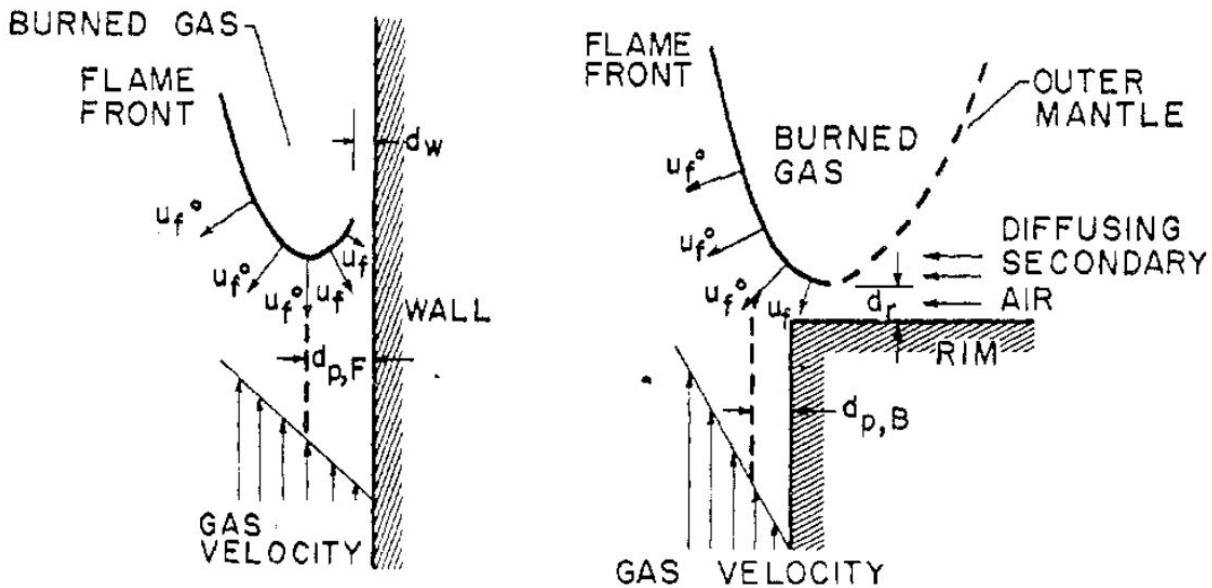


**Figure 2.2:** Velocity vectors for (a) flashback and (b) liftoff [9]

Flame speed and flame stabilization can quickly become a multifaceted concept. When considering an unburned mixture in a tube, the flow's velocity profile becomes parabolic because of the no-slip condition at the boundaries. On a nozzle like a Bunsen burner, premixed combustion will occur in the inner cone, but a diffusion flame occurs at the outer boundary (Fig 2.1). Additionally, the flow of gas at a nozzle edge will create micro-eddies, which further complicates the fluid dy-

namics of matching incoming mixture velocity to flame speed. Flame speed is also affected by heat loss to the surroundings. Because of this, the local flame speed around the edge of a nozzle will be lower due to conduction through the nozzle body. A local decrease of flame speed at a nozzle edge due to heat losses coupled with slower gas velocity at boundaries and increased mixing from micro-eddies can help anchor the flame to the edges of the nozzle. These three factors (heat loss to the nozzle, micro-eddies, and the no-slip condition) were critical in establishing a stable flame in the Nano-Combustor and will be discussed more in Chapters 8 and 10.

## **2.2 Dust Combustion History**

The field of dust combustion has been primarily investigated as a safety measure to better mitigate hazards from dust explosions in industries that pulverize or grind combustible material. The first documented and investigated dust explosion occurred in 1785 in a Turin, Italy bakery [10]. As the industrial revolution progressed through the 19th Century, industries such as agriculture, manufacturing, and mining developed new technologies and scales of operation that made them particularly susceptible to dust explosion hazards. The materials-processing in these industries results in a large amount of suspended organic particles that are often combustible. If these suspended dusts reach a high enough concentration and come into contact with an ignition source, the resulting explosion can be devastating. Ignition sources can include a hot surface, a spark, an overheated bearing, or a flame. From coal dust in mining operations to suspended grain flour in large mills, dust explosions have resulted in many lost lives and destroyed facilities.

Dust explosions are particularly devastating because the primary explosion from the suspended dust can create a pressure wave that lofts dust which had settled onto surfaces of the building and re-suspends it in the air. Once lofted, this dust can create a secondary explosion and feeds the intensity of the primary combustion. The pressure wave from the re-lofted secondary explosion can occur in confined spaces, which may amplify the pressure wave in confined spaces and cause additional escalation [11].

## 2.3 Dust Combustion Dynamics

Dust combustion is a unique phenomenon, appearing as a homogeneous premixed flame on the macro-level, but acting as many diffusion flames on the micro-scale. The phase change from solid particle to combustible vapor on the particle-scale is a complex and dynamic process when considering the pre-heating zones within a dust cloud. Figure 2.3 shows a model of flame propagation in a lycopodium dust cloud.

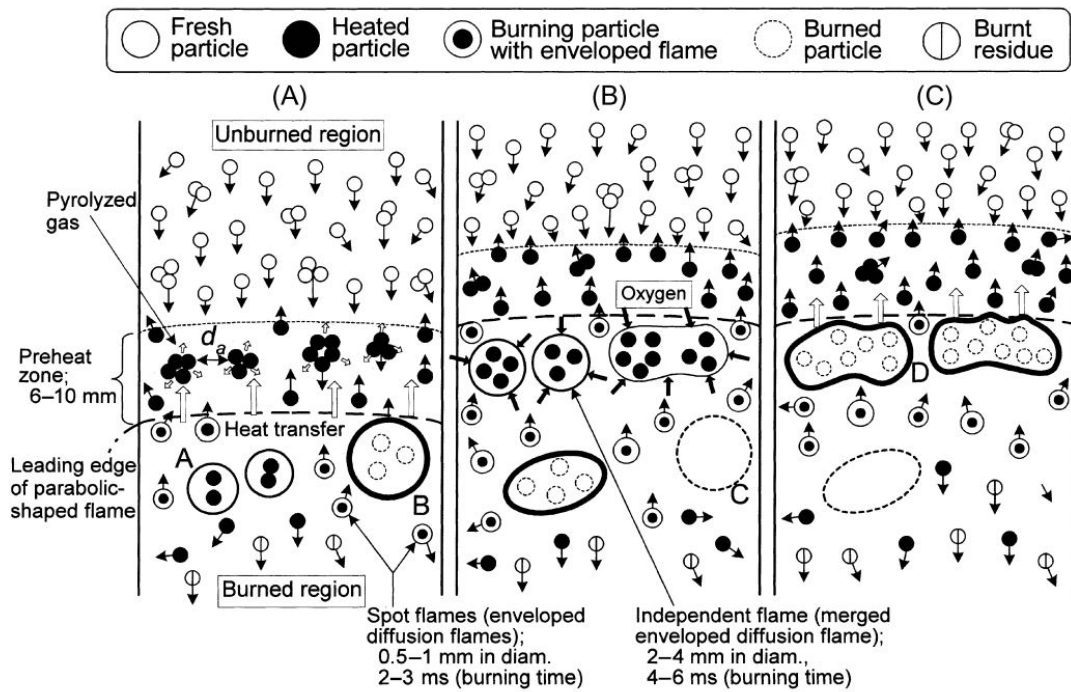


**Figure 2.3:** Model of lycopodium dust flame propagation: (A) heating and ignition of single particles; (B) heating and ignition of particle agglomerates; and (C) final pyrolysis and combustion [12]

A dust explosion requires two conditions in addition to the basic combustion triangle (ignition, fuel, and oxidizer): containment of the dust cloud, and suspension of the dust such that the fuel concentration lies within the ignitable range. This can be visualized by the dust explosion pentagon depicted in Figure 2.4. The explosion is characterized by the pressure wave that arises due to containment of the fuel-air mixture. This pressure wave is one of the main conditions that make

dust explosions so devastating. For the purposes of the Nano-Combustor, there is no pressure wave (removing the "explosion" designation) and thus containment is unnecessary.

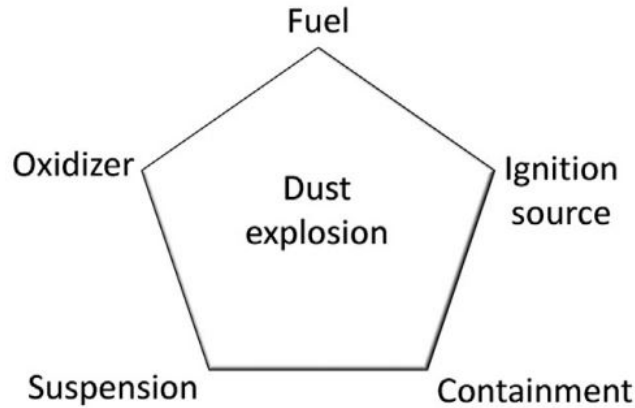


**Figure 2.4:** Dust explosion pentagon [12]

### 2.3.1 Ignition and Limits of Flammability

There are some crucial differences between gas and liquid combustion vs. dust combustion. One difference is the increased energy required to ignite the fuel and air mixture in the latter case. For combustion to occur, the fuel and air must mix on a molecular level in vapor phase. The additional phase changes to vaporize the volatiles in a solid particle carry an additional energy burden. Because of this, the rate of combustion is slowed down compared to gaseous fuels [12].

In order for the particles to initially vaporize and begin combustion, ignition must occur. Ignition can take the form of an electric spark or hot surface (including hot bearings). Minimum ignition energy (MIE) is a property sometimes measured in dust combustion, but will not be discussed further in this paper.

For any fuel and air mixture, there is a range of fuel concentrations that will lead to combustion. The bounds of combustion are called the *upper* and *lower* limits of flammability (UFL and LFL, respectively). For gaseous fuels, the upper flammability limit is well defined, but the complex combustion phenomena within a dust cloud makes it difficult to clearly establish the UFL for dust

mixtures [12]. The LFL is a convenient property that will be reviewed again in Chapter 3 for the powdered fuels explored in this study.

### 2.3.2 Stoichiometric Concentration

Dust combustion stoichiometry expands on the fundamentals discussed above in Section 2.1.1. In dust combustion, stoichiometric concentrations are expressed in units of *grams of fuel per cubic meter of air* ( $\text{g}/\text{m}^3$ ). The stoichiometric concentration is a theoretical value based on moles of fuel reacting with moles of oxygen, but is often determined empirically using flame speed [12]. Both empirical and theoretical stoichiometric concentrations of idealized fuels used in this study are shown in Tables 3.2 and 3.3. Since stoichiometric concentrations are a function of air volume (and thus density), stoichiometric concentrations were calculated to adjust for altitude in Ft Collins, Colorado.

For a given hydrocarbon fuel  $\text{C}_x\text{H}_y\text{O}_z$ , the stoichiometric concentration ( $\rho_{\text{dust,stoic}}$ ) can be found following Equation 2.7:

$$\rho_{\text{d,st}} = \frac{m_{\text{d,st}}}{V_{\text{air}}} = \frac{n_{\text{d,st}}\mathcal{M}_{\text{d}}}{V_{\text{air}}} = \frac{n_{\text{O}_2,\text{st}}\mathcal{M}_{\text{d}}}{(x + y/4 - z/2)V_{\text{air}}} = \frac{0.21\mathcal{M}_{\text{d}}}{(x + y/4 - z/2)} \left( \frac{P}{R_g T} \right) \quad (2.7)$$

Where the subscripts  $_{\text{d,st}}$  refer to *dust, stoichiometric*,  $x$ ,  $y$  and  $z$  come from the hydrocarbon subscripts,  $\mathcal{M}_{\text{d}}$  is the molecular weight of the fuel ( $\text{g}/\text{mol}$ ),  $P$  and  $T$  are the local pressure (Pa) and temperature (K), and  $R_g$  is the ideal gas constant ( $\text{J}/\text{mol}\cdot\text{K}$ ).

Similar to Equation 2.2, equivalence ratio for dust combustion can be expressed as in Equation 2.8 below:

$$\phi = \frac{\rho_{\text{d,act}}}{\rho_{\text{d,stoic}}} \quad (2.8)$$

### **2.3.3 Additional Challenges of Dust Combustion**

Compared to gas and liquid fuel combustion, dust combustion poses key differences. These differences mainly arise due to the fact that gaseous fuels already interact with air on the molecular level, where particles must undergo a physical or chemical transformation in order to interact with air molecules.

#### **Surface Effects**

It's often straightforward to determine a gaseous fuel's purity and chemical formula, but the surface conditions of a particle can pose interesting challenges in combustion analysis. The surface of a dust particle can have a completely different chemical composition than the body of the dust due to adsorption of compounds in the air [13]. Of the possible particle surface changes, surface adsorption (and sometimes absorption) of water can dramatically alter the combustion properties of the dust and perhaps increase its likelihood to agglomerate into larger particle clusters [12].

#### **Shape and Size**

A particle's size and shape can have dramatic effects on its combustion, its ability to become suspended, and its ease of transport. A dust is defined in NFPA 654 as a particle with diameter less than 500  $\mu\text{m}$  based on sieve analysis [14]. But as the particle size decreases, a greater specific surface area becomes available which increases the rate of combustion.

Particle size also affects the suspension, and thus concentration, of the dust in the air. Not only will larger particles be more difficult to ignite, they will also be more difficult to loft and will drop out of suspension more quickly. Smaller particle diameters are more beneficial for achieving a quasi-uniform concentration and ignite readily, but are not always realistic in a dust sample.

Particle shape can also affect the way a dust combusts. A particle with circuitous surface geometry will have more available surface area to volatilize pyrolysis gases and will combust more quickly than a purely spherical particle. For the purposes of this investigation, particles are assumed to be spherical when discussing diameters and terminal velocities. Figure 2.5 shows the spherical and textured lycopodium spore under high magnification.

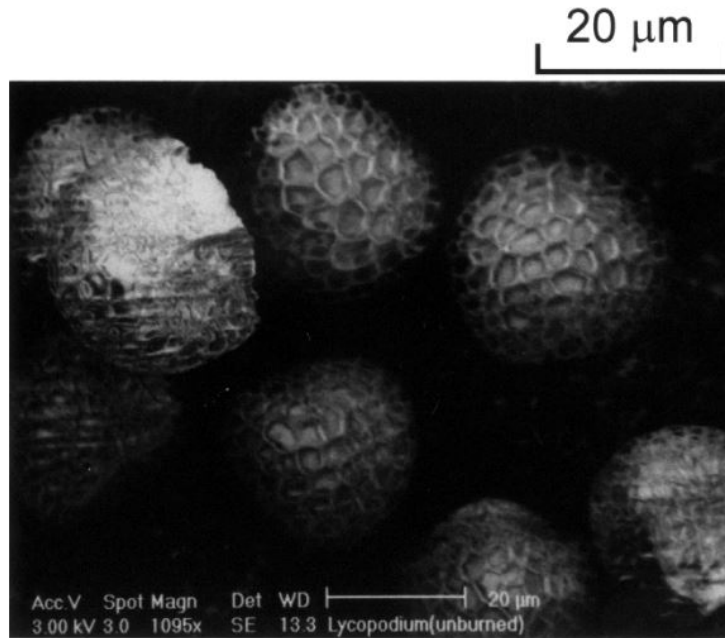


**Figure 2.5:** Scanning electron microscope image of lycopodium, magnified at 1095x [15]

The flame-stability challenges discussed in Section 2.1.4 are further complicated because dust shape and size will create a concentration and velocity gradient across a cross-section of a nozzle. Since flame speed is a function of the equivalence ratio, the local equivalence ratio in a dust-combustion nozzle will be a function of the distance from the nozzle's axis. In a gaseous mixture, the equivalence ratio can be assumed constant across the flow profile, but in dust combustion this is not the case.

Section 3.4 contains a more in-depth discussion of particle physics, dust creation, particle size distributions, and elutriation.

### **Uniformity of Fuel Concentration**

A gaseous fuel mixes with air and will eventually become a homogeneous mixture through forced or natural convection and diffusion. This mixing allows gaseous fuels to ignite even in quiescent environments. Dust, on the other hand, will eventually settle out of a quiescent environment and requires physical disturbance to become re-suspended.

Additionally, dusts created through mechanical means (pulverizing, grinding, etc) will have a poly-disperse aerodynamic diameter distribution. This means that even in the event that all particles are equidistant from each other (the most homogeneous case), the differences in particle sizes will create a non-uniform combustion event when compared to a homogeneous mixture of gaseous fuel and air. Additionally, the dust suspension concentration is time dependent, with the largest diameter particles falling out of the mixture first and creating a gradient of particle sizes based on terminal velocities.

For the purposes of this investigation, the goal of creating a uniform dust suspension is one of the primary factors that guided hardware development. Calculations assume a homogeneous particle suspension, even though this is very difficult to achieve even in the best laboratory settings. Figure 2.6 shows a 75 watt lycopodium flame from this project; notice the streaking of the fuel burning within the flame.

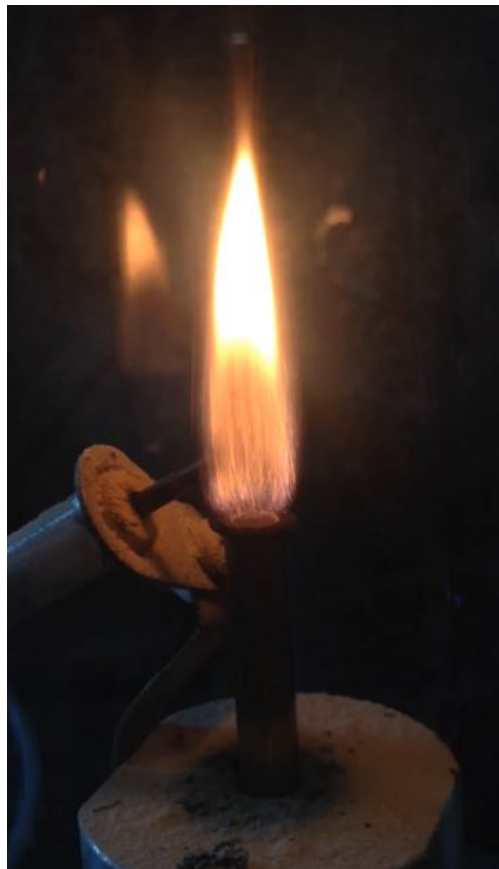


**Figure 2.6:** 75 watt lycopodium flame on the Nano-Combustor

# Chapter 3

## Fuels

### 3.1 Idealized Biomass Fuels

Based on CSU's past experience with the fecal gasifier development, it was expected that powdered fecal fuel would present tremendous challenges. Because of this, idealized biomass powder guided the first phase of the Nano-Combustor's development, which is the main focus of this thesis. Developing a stable low-firepower dust combustor with idealized fuel was an ambitious goal in itself, and it provided a strong foundation for transitioning to fecal fuel.

The Nano-Combustor hardware development was overwhelmingly guided by experiments using idealized biomass powders. Three idealized fuels were considered at the onset: (1) wheat flour, which was a notable consideration because of the many industrial flour mill explosions that had occurred in the last 150 years, and its affordability; (2) corn starch, which had been studied in a number of dust combustion experiments ([10] [11] [12] [16] [17]) and was very economical; and (3) lycopodium spores, which are the spores of a common club moss and known for their high lipid content and monodisperse particle size distribution, as well as their use in early flash photography. Lycopodium combustion has been studied in a number of dust combustion experiments ([10] [12] [11] [16] [18] [19] [20] [17]). Lycopodium was initially considered only peripherally because of its high cost (~\$250/lb), but became the primary fuel of final hardware iterations. Figure 3.1 shows a lycopodium flame propagating in a vertical duct.

The remainder of this chapter provides an overview of the properties of these three fuels and includes a brief discussion of feces as a fuel. The idealized biomass fuels' properties will continue to be referenced in subsequent chapters discussing hardware development. Early hardware developments mainly used cornstarch to guide design iterations because of its low-cost. Certain factors, though, such as cornstarch's propensity to clump and pack (to be discussed in-depth in Chapters 5 - 7) steered the project towards using lycopodium for the final hardware development. Despite its

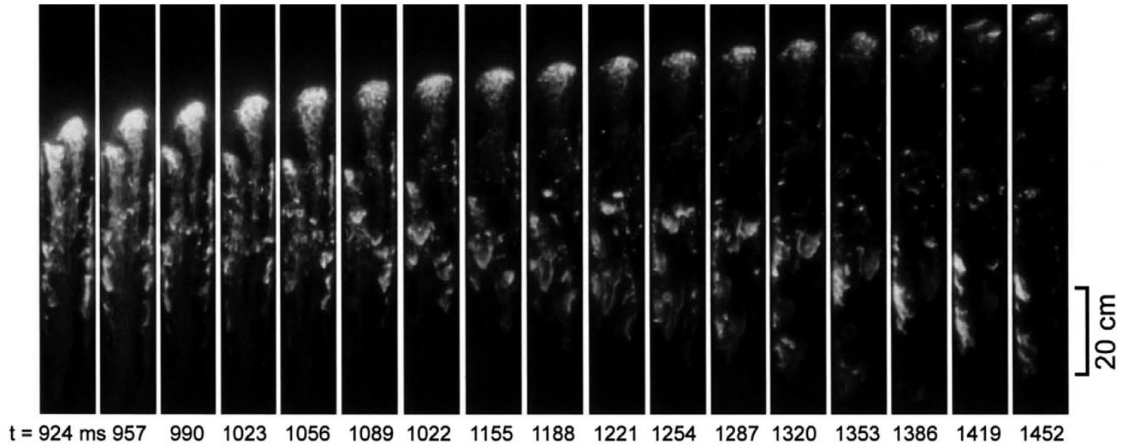


**Figure 3.1:** Lycopodium laminar flame propagation sequence at a concentration of  $592 \text{ g/m}^3$  [15]

high-cost, lycopodium ended up being a superior idealized fuel because of its free-flowing nature, ease of ignition, and monodisperse particle size distribution.

### 3.2 Feces as Fuel

Although feces was minimally tested in this version of the Nano-Combustor, the following brief fecal facts might help provide guidelines for further hardware development. Fresh feces has a median moisture content of 74.6%. In low income countries, the average person produces 250 g of fresh feces per day, which equates to 38 g of dry material [21].

With a LHV of 18831 (India feces, Table 3.1), this equates to 715.6 kJ/day per person. If this dry feces burned for 2 hours at a steady rate, it would produce a 100 W flame, which is the final target for this project. A 100 W flame burning for 24 hours would require dried feces from 12 people. CSU's deliverable of a steady 500 W flame would require the dried feces of 60 people per day to burn continuously for 24 hours/day.

Feces has a much higher ash content than the other biomass fuels considered, as shown in Table 3.1. Ash management has presented some challenges in the fecal gasifier because it will fuse into a hard "glass" at combustion chamber temperatures. The present solution to this in the gasifier is to implement an ash wiper that grinds the ash over a grate to break it up. For a fecal dust burner, ash

fusing will probably not be an issue, but managing the waste ash from combustion may provide some material transport and disposal challenges.

### 3.3 Fuel Comparisons

Ultimate fuel analysis was performed on human and canine feces by Hazen Research Inc., summarized in Table 3.1 and reproduced fully in Appendix B. Table 3.1 summarizes ultimate analysis data for the various possible fuels used in the Nano-Combustor, taken from various sources. Wood pellet data is included in Table 3.1 just for reference; wood dust was not explored as an idealized fuel for the Nano-Combustor because cornstarch, wheat flour, and lycopodium spores already existed as powdered fuels and required no processing.

**Table 3.1:** Ultimate Fuels Analysis

	<b>Carbon (%)</b>	<b>Hydrogen (%)</b>	<b>Oxygen (%)</b>	<b>Sulfur (%)</b>	<b>Ash (%)</b>	<b>LHV (kJ/kg)</b>
<b>Wood Pellets [5]</b>	47.2	6.5	45.4	~0	1.0	20023
<b>Human Feces (N. Carolina) [5]</b>	48.85	6.63	20.88	0.91	14.83	20854
<b>Human Feces (India) [5]</b>	56.15	6.04	20.32	0.45	12.25	18831
<b>Canine Feces [5]</b>	36.45	5.00	22.99	0.65	28.52	14114
<b>Corn Starch [22] [23]</b>	46.9	5.4	47.4	0.06	2.9	16500
<b>Wheat Flour [24] [23]</b>	38.86	5.45	55.56	0.13	0.65	15400
<b>Lycopodium Spores [16] [19] [18] [25]</b>	68	9.6	20	0.1	1.4	30554

Of the idealized powdered fuels, Table 3.2 shows each fuel’s combustible dust properties, derived empirically in the literature.

**Table 3.2:** Powdered Fuels Properties - Empirically Derived

	<b>Mean Particle Diameter (<math>\mu\text{m}</math>)</b>	<b>Minimum Explosive Concentration (<math>\text{g}/\text{m}^3</math>)</b>	<b>Stoichiometric Concentration (<math>\text{g}/\text{m}^3</math>) (empirical)</b>	<b>LHV (kJ/kg)</b>
<b>Corn Starch [16] [23] [20]</b>	28	63.9	230	16500
<b>Wheat Flour [26] [23] [20] [17]</b>	110.98	64.7	240	15400
<b>Lycopodium [16] [20] [19]</b>	31	37.9	300	30554

**Table 3.3:** Powdered Fuels Calculated stoichiometric Concentrations

	<b>Empirical Formula</b>	<b>Molar Mass (g/mol)</b>	<b>Stoic. Concentration (g/m<sup>3</sup>)</b>
<b>Corn Starch</b>	CH <sub>2.01</sub> O <sub>0.80</sub>	26.84	174
<b>Lycopodium</b>	CH <sub>1.65</sub> O <sub>0.22</sub>	17.19	94
<b>Human Feces</b>	CH <sub>1.62</sub> O <sub>0.32</sub>	18.76	99

There can be variation in these empirically derived values, which rely on flame speed data and flame temperature to determine the stoichiometric concentration. Because of the discrepancy of the different fuels in the literature and because the stoichiometric concentration for combustible dusts is a function of altitude (g/m<sup>3</sup>), theoretical stoichiometric concentrations will be used. Table 3.3 shows the reduced chemical formula for each combustible dust [12] and its calculated stoichiometric concentration, calculated using Equation 2.7 and the local average pressure taken at Ft Collins, Colorado (85 kPa). The stoichiometric concentrations in Table 3.3 will be used henceforth for equivalence ratios and other calculations because they are adjusted for local conditions. Cornstarch and Lycopodium are shown because they were the two idealized powders primarily tested. Human feces is also included for comparison.

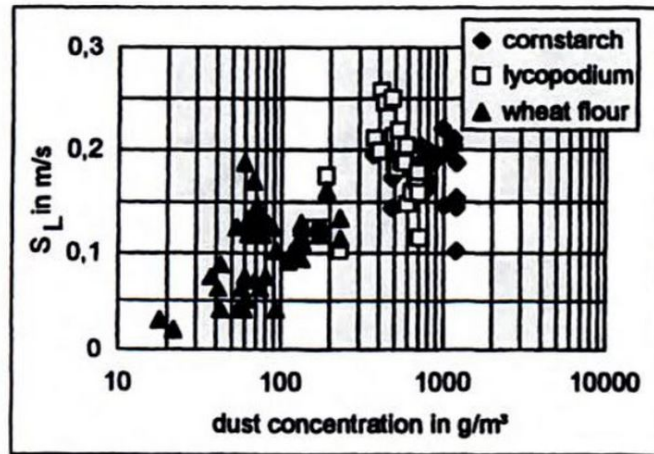


**Figure 3.2:** Laminar flame speeds of cornstarch, wheat flour, and lycopodium as a function of dust concentration in air [17]

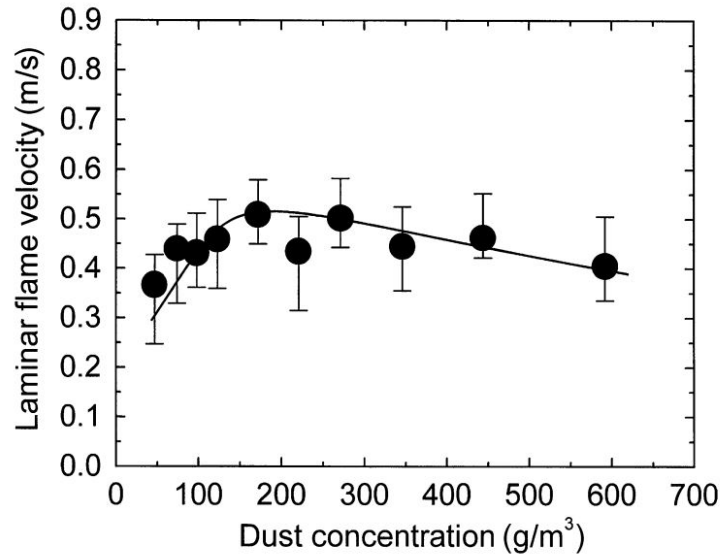


**Figure 3.3:** Lycopodium flame speed as a function of concentration [15]

Figures 3.2 and 3.3 show flame speeds for cornstarch, wheat flour and lycopodium at varying concentrations. Note the ~50% discrepancy between the lycopodium flame speeds in the two studies. Han et al. point out that the limited experimental results for dust combustion found in literature are often apparatus dependent and often contradict each other [15].

Figure 3.2 shows that cornstarch and lycopodium have similar flame speeds, but Figure 3.3 establishes a more definitive trend line for flame speed as a function of concentration. For future calculations, Figure 3.3 will be used for first-order approximations with both cornstarch and lycopodium. The Nano-Combustor concentrations often exceeded 1000 g/m<sup>3</sup> dust concentration, so Figure 3.3 was extended linearly to higher concentrations. The trend line was digitized and tabulated below in Table 3.4.

### 3.4 Combustible Dust Properties

It is natural to assume that combustible particles are spherical in shape and consistent in diameter, but this is rarely the case. Often particles have irregular shapes, form a broad size distribution with diameters that can span an order of magnitude, and may clump together and form agglomerations which behave like large particles. Additionally, particles size distributions may change

**Table 3.4:** Lycopodium and cornstarch flame speeds as a function of dust concentration

<b>Dust Concentration</b> (g/m <sup>3</sup> )	<b>Laminar Flame Speed</b> <b>Lycopodium/cornstarch Combined</b> (m/s)
50	0.3141
100	0.4387
200	0.5178
500	0.4265
750	0.3518
1000	0.2750
1250	0.1982
1500	0.1215

over time with successive handling or transport and may become smaller or have a propensity to agglomerate [12].

### 3.4.1 Particle Size Distribution

For this investigation, particle diameters for the idealized biomass fuels are taken from the literature and assumed to be spherical (Table 3.2). Since spores and pollen are monodisperse, it is a reasonable assumption to use lycopodium's mean particle diameter in calculations [8]. But cornstarch and wheat flour are polydisperse and so using the mean particle diameter for calculations is a simplification that carries some error. For first-order approximations involving terminal velocities and lofting forces, the mean diameter was deemed sufficient.

Feces was processed at the end of the project and sorted into four size bins using three ASTM sieves: 40 mesh (420  $\mu\text{m}$ ), 200 mesh (74  $\mu\text{m}$ ), and 325 mesh (44  $\mu\text{m}$ ). This will be discussed further in Chapter 11.

### 3.4.2 Aerosol Physics

Air moving through a burner nozzle will have a Reynolds number associated with the operating conditions. The Reynolds number is the ratio of a fluid's inertial effects to viscous effects, and will describe is the fluid flow is laminar, turbulent or in transition. For a pipe, laminar flow is when  $Re < 2000$  and turbulent flow is when  $Re > 4000$  [8]. The transition zone is between these

values. The Reynolds number in terms of the fluid's properties is shown in equation 3.1, where  $\rho$  is fluid density and  $\eta$  is the fluid viscosity. For a first-order approximation, air properties at normal temperature and pressure (NTP: 293.15 K, 101.3 kPa) can be used and Equation 3.1 simplifies to Equation 3.2, where  $V$  is the velocity of the fluid (m/s) and  $d$  is the diameter of the pipe (m).

$$Re = \frac{\rho V d}{\eta} \quad (3.1)$$

$$Re = 66,000 V d \quad (3.2)$$

Particles moving through a fluid can also carry an associated Reynolds number based on the relative motion between the particle and the fluid. Equations 3.1 and 3.2 can be used for particles as well, with  $V$  as the particle's relative velocity to the fluid (m/s) and  $d$  as the particle's diameter (m). For the purposes of this investigation, particles are assumed to loft at the same velocity as the surrounding fluid and particle Reynolds numbers are neglected.

The settling velocity of a particle in still air is an important consideration when discussing particle lofting for dust combustion. A falling spherical particle will quickly reach its terminal settling velocity, which is an equilibrium state where drag forces,  $F_D$ , acting upwards on the particle balance gravitational effects,  $F_G$ , acting downward on the particle:

$$\begin{aligned} F_D &= F_G = mg \\ 3\pi\eta V d &= \frac{(\rho_p - \rho_g)\pi d^3 g}{6} \end{aligned} \quad (3.3)$$

For particles with  $d > 1 \mu\text{m}$  and assuming  $\rho_p \gg \rho_g$ , Equation 3.3 can be rearranged to solve for the terminal settling velocity,  $V_{TS}$  (Eq. 3.4), and simplified to Equation 3.5 assuming standard particle density ( $1000 \text{ kg/m}^3$ ), NTP, and with  $d_p$  in  $\mu\text{m}$ :

$$V_{TS} = \frac{\rho_p d^2 g}{18\eta} \quad (3.4)$$

$$V_{TS} = 3 \times 10^{-5} d_p^2 \text{ m/s} \quad (3.5)$$

When designing hardware and establishing air velocity set-points to loft particles in the Nano-Combustor, Equation 3.5 was used as a first-order approximation to make sure that air velocity was much greater than the settling velocity of the mean particle diameter for the idealized fuel.

### 3.4.3 Material Transport

A collection of particles can behave like a solid (static pile, certain flow inside a hopper) or a fluid (dust cloud, fluidized bed, auger transport). If a hopper, for example, is designed without taking into account the inter-particle or particle/wall shear forces, the material can bridge above the out-feed and act as a stable solid [1]. If the hopper is designed with these forces in mind, the particles will flow like a fluid and there will be no discontinuities. Similarly, particles will pour out of an auger and act like a fluid.

Particles can also be lofted and conveyed via forced air, utilized in the pneumatic conveying industry. This is of particular interest to the Nano-Combustor because the dust concentration in a pneumatic conveyor can be tuned to specific combustible concentrations. In a horizontal tube, gravitational effects must be considered because the dust will want to settle out from the air stream before reaching its destination, creating constrictions in the flow.

One step less aggressive than pneumatic conveying is creating a fluidized bed. In a fluidized bed, powder sits on a permeable membrane with a mesh size smaller than the particles, and air flows up through the bed of powder. At a certain air velocity, the particles will agitate and develop fluid-like properties, and particles on the surface will begin to loft. The air velocity can be tuned to create specific concentrations and lofting velocities above the fluidized bed, which can be siphoned for controlled dust combustion.

As powders are handled, their size and properties can change. Particles can break and become smaller, or they can stick to particles next to them through physical or electrostatic bonds and

agglomerate into bigger particles. The changes that particles undergo while being conveyed is a complex field, and had strong bearing on the development of the Nano-Combustor.

### **3.4.4 Powder Generation**

Powders are created through mechanical wear, milling, grinding, impaction, pulverizing, or through a number of processing industries. They can be primary products (e.g. grain flour, pharmaceutical powders) or byproducts of other processing (e.g. coal dust from mining). Particle size distributions will vary greatly between materials and processes, but will always be polydisperse compared to spores and pollen in nature that are characteristically monodisperse. In a polydisperse size distribution, there are different ways to classify the sizes into different bins.

A rudimentary way to sort particles based on sizes is to pass them through a series of successively finer-meshed sieves placed on a vibrating table. After the material passes through the sieve stack, there will be different bins of particle sizes. The classification of particles based on size, shape and/or density using air is called *elutriation*. Elutriation sorts particles using their terminal velocities. This project does not intentionally use elutriation to classify particles based on size, but it invariably plays a role when using air for mechanical transport of powders, as is done in the different hardware revisions.

# Chapter 4

## Risk Assessment

### 4.1 Risk Assessment

Establishing primary and secondary risks at the onset of the project helped focus the hardware development path. Many of the identified challenges stem from the fundamental complexities and challenges of dust combustion that have been explained in Chapters 2 and 3.

As the project progressed, new challenges arose and guided further hardware improvements. The initial identified risks will be discussed here, and the sections on hardware development will address more specific challenges.

#### 4.1.1 Primary Risks

The primary risks of constructing a low-firepower biomass combustor were proper fuel-air concentrations, homogeneous fuel-air mixing, proper lofting velocities, flame stability and scalability. These concepts can be broadly simplified into fuel selection and delivery, air delivery, mixing chamber, and nozzle geometry.

The challenge of entraining dust into the primary air stream was multifaceted. The issues of fuel-air mixing and proper fuel-air concentrations can be split into fuel delivery systems and control and air delivery and control. In any case, settled dust must become lofted into a dust cloud to combust. Settled dust as a static bulk mass (as opposed to lofted dust) requires more force to loft directly into an air stream than the individual particles because the inter-spatial air pockets have decreased in size, increasing the bulk density and requiring a higher air velocity to loft the bed [27]. An example of this situation would be a fluidized bed (Chapter 6), and to a lesser extent, a venturi nozzle (Section 5.3). Another way to introduce fuel into an air stream is with a gravity-fed (hopper) system. A hopper must be designed for proper friction coefficients to prevent complications such as bridging, as discussed in Section 3.4.3. The venturi nozzle in Section 5.3

and the final Nano-Combustor design (Chapter 8 use a hopper for fuel delivery. A hopper can feed material into a horizontal air stream (e.g. the venturi) or it can lead into a auger that conveys the material horizontally. The horizontal auger can introduce the fuel in a controlled manner into a vertical air stream and create a range of ignitable concentrations. The final Nano-Combustor (Ch. 8) used an auger in this manner.

As discussed in section 2.3, proper fuel-air concentration is critical for combustion to occur. Unlike gaseous fuels, dust combustion doesn't have a well-defined upper explosive concentration limit, so design parameters were focused on creating highly adjustable fuel-air concentrations ranging from the lower flammability limit to quite rich mixtures. The concentrations were adjusted initially by changing nozzle geometry and *only* air flowrate (in the fluidized bed and venturi nozzle). Final hardware versions provided independent control of fuel and air flowrates and nozzle geometry.

Air flowrate was controlled exclusively with an Alicat MCR-100SLPM mass-flow controller connected to a pressurized air line. Air flow was measured in SLPM. For velocity calculations, SLPM was converted local volumetric flow rate in  $m^3/s$  (using Ft Collins, CO, ambient pressure: 85 kPa) using the relationships:

$$\begin{aligned}
 V &= Q/A = \frac{4Q}{\pi D^2} \\
 Q [m^3/s] &= \frac{LPM}{60,000} \\
 LPM &= \frac{P_o}{P} SLPM \\
 &\vdots
 \end{aligned}
 \tag{4.1}$$

$$V = \frac{1}{39,541} \frac{SLPM}{D^2}
 \tag{4.2}$$

Where  $V$  is the air velocity in a tube (m/s) and  $D$  is the diameter of the tube (m). This relationship was used to help balance the particles' terminal velocity and the mixture's flame speed with the bulk air velocity through the burner nozzle.

Turbulence and residence time was necessary to provide the proper mixing of the fuel and air once the fuel was delivered into the primary air-stream. It was assumed that an air velocity much greater than the terminal particle velocity would create a homogeneous mixture in a nozzle, so air velocity became the primary mixing mechanism rather than nozzle geometry. Increased residence time complicated the conditions by increasing dust settling inside the nozzle.

Flame stability was a risk item first addressed by balancing bulk flow velocity with flame speed at the nozzle's exit. It later became clear that nozzle exit geometry was an important piece in anchoring the flame. More thorough discussion of nozzle geometry and flame holders is in Chapters 8 and 10.

Scalability was addressed by first creating high firepower dust flames, starting above 5000 watts, to better-understand flowrate set points and geometry configurations. Operating fuel-air concentrations and nozzle velocities were established at each step and then geometries and flowrates were scaled down to create similar concentrations and velocities. In this way, hardware could be scaled down quickly while gaining a better understanding of the most successful dust combustion conditions.

### **4.1.2 Secondary Risks**

Additional criteria considered at the onset of hardware design included ignition source and temperature, steady fuel feedrate, flashback prevention, automated operation, and fuel processing/sizing.

At first, a hand-held propane torch was used to ignite the dust mixtures. Final hardware versions utilized a ceramic hot surface igniter commonly used in furnaces and other gas-fueled appliances (see Ch. 8).

Steady fuel feedrate became an iterative process and its evolution will be described in the following chapters.

Flashback prevention was a concern at first, but then it became clear that there was not a sufficient reservoir of fuel-air mixture upstream of the nozzle to be dangerous. This will be touched on briefly in Chapter 6.

The primary phase of this investigation used idealized biomass fuels whose size distribution fell within a narrow band. This allowed for independent investigations of nozzle design criteria without over complicating the investigation with more polydisperse fuels. For the overall success of the project, though, fuel sizing is a primary concern because the fuel sources will be non-idealized and must be processed for use in the nano-combustor.

## **4.2 Project Trajectory**

The next four chapters walk through the iterative design process that led to a stable sub-100 watt Nano-Combustor (project deliverables only required sub-500 watts). The primary risks discussed above guided macro-developments and each phase of the project provided new insights toward further iterations.

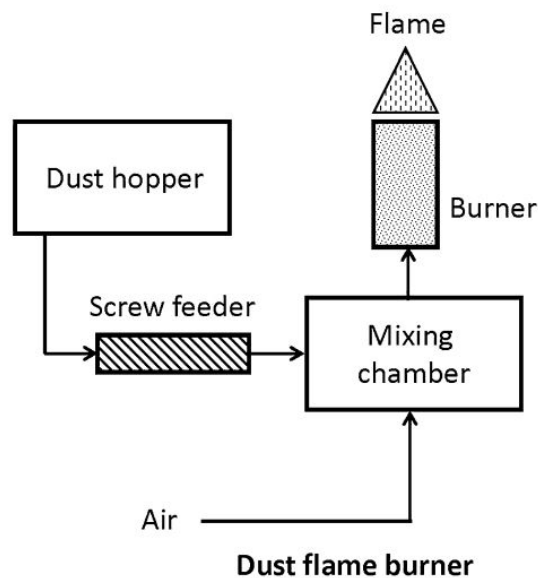
At each phase of development, both qualitative and quantitative observations were recorded. Flame stability was a subjective observation and was established by observing the flame's relative strength, how well it attached to the nozzle perimeter, the flame's color, its shape, and presence of fugitive unburned powder. Quantitative measurements such as flame height and burn duration supported qualitative observations. Other quantitative measurements that guided development include firepower, fuel-air concentration, and nozzle exit velocity.

# Chapter 5

## Initial Hardware Development

### 5.1 Standing Flame Dust Combustors - Literature Review

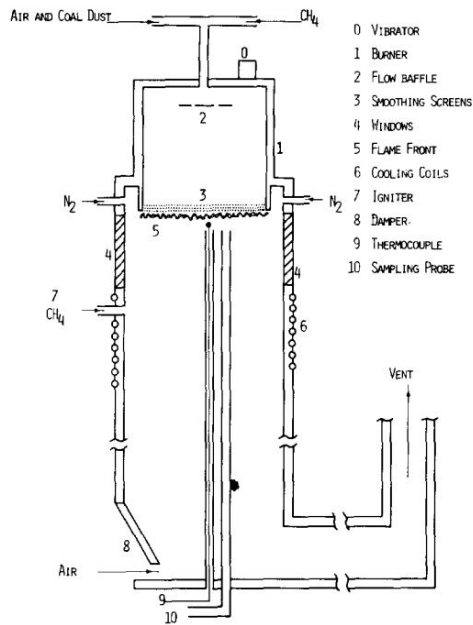
Unconfined standing dust flame studies exist in the literature and the apparatus developed for those experiments helped guide the first hardware concepts of the Nano-Combustor. Figure 5.1 shows a standard configuration for a typical dust flame burner.



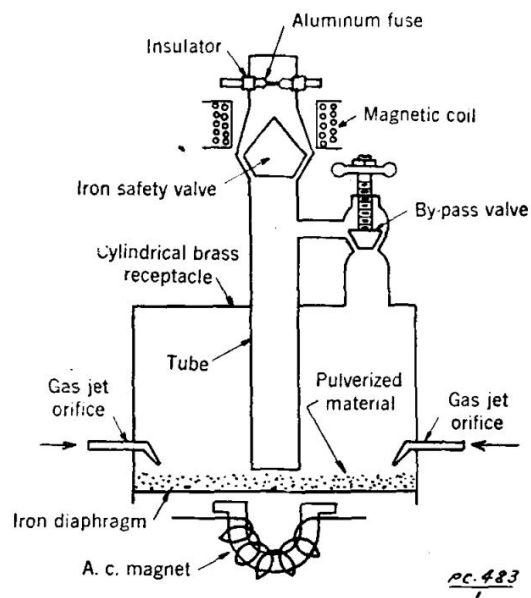
**Figure 5.1:** Typical dust flame burner schematic [12]

Figure 5.2 shows schematics from three standing flame dust burners in the literature. Note that Fig. 5.2a uses methane mixed with air for the experiments. Also note the flashback screens in Figs. 5.2b and 5.2c.

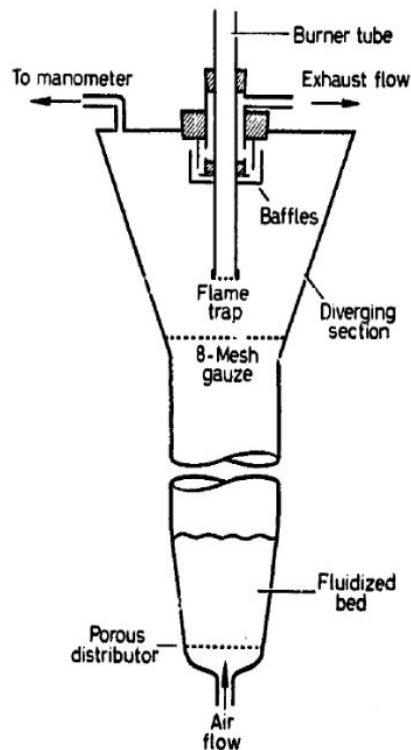
These were the best schematics of stable flame burners found in the literature to use as a starting point on the Nano-Combustor. Even though fuel-air concentration was adjustable in these apparatus, none of these studies wrote about firepower or the ability to create a stable low-firepower



(a) Schematic for a flat-flame dust combustor. Coal dust is mixed with methane and air [28]



(b) Aluminum dust disperser. Includes a vibrating floor driven by magnet to help loft particles. Includes adjustable fuel-air concentration at bypass valve, and flashback prevention [29]



(c) Apparatus for a laminar flame lycopodium combustor. Includes fluidized bed lofting, flashback prevention, and adjustable fuel-air concentration with baffles [30]

**Figure 5.2:** Schematics of standing flame dust combustors from various sources

flame. Of the diagrams above, Fig. 5.2c seemed like the best to emulate. Not only did Mason et al. create the hardware specifically to test lycopodium, it provided enough controls to suit the Nano-Combustor. The main problem, though, was that it was batch-fed with fuel and the Nano-Combustor required the ability to continuously add fuel. Key elements from Fig. 5.2c are the fluidized bed, the adjustable fuel-air concentration, and the vertical burner tube. Early Nano-Combustor versions explored each of these elements and ultimately end with a combustor that is mechanically more simple and more adjustable in firepower and concentration than Fig. 5.2c.

## 5.2 Powder Coating Gun

As a proof of concept at the onset of this project, a modified Eastwing powder-coating paint gun was operated with various powders to observe a steady dust flame. This quick and simple investigation provided initial verification that various biomass dusts were, indeed, combustible as a stable flame. The paint nozzle was removed from the gun so that powder exited without any hindrance.

Fuels tested in this configuration were wheat flour, cornstarch, and desiccated, powdered dog feces (ground in an electric coffee grinder). Lycopodium was not used because of its expense. A hand-held propane torch was used as the ignitor.

The powder coating gun was connected to pressurized air and had a hopper hanging off the bottom which was filled with the powder of choice. When the trigger was pulled, the air was routed vigorously through the hopper, which lofted the powder and then exited the nozzle. There was no venturi effect that diluted the fuel-air mixture downstream of the fuel lofting. As a result, the mixture was quite fuel rich and ignited easily. Figure 5.3 shows a cross-section of the device.

This demonstration was to subjectively observe how well the different powders ignited when lofted into an air stream. No fuel-air ratios were measured, nor was firepower calculated. The wheat flour and cornstarch ignited quite well and a flame about 7 feet long was observed (as shown in Figure 5.4). The firepower was estimated to be greater than 10 kW based on past firepower measurements at the CSU lab. The powdered dog feces had a less vibrant flame and a large amount of

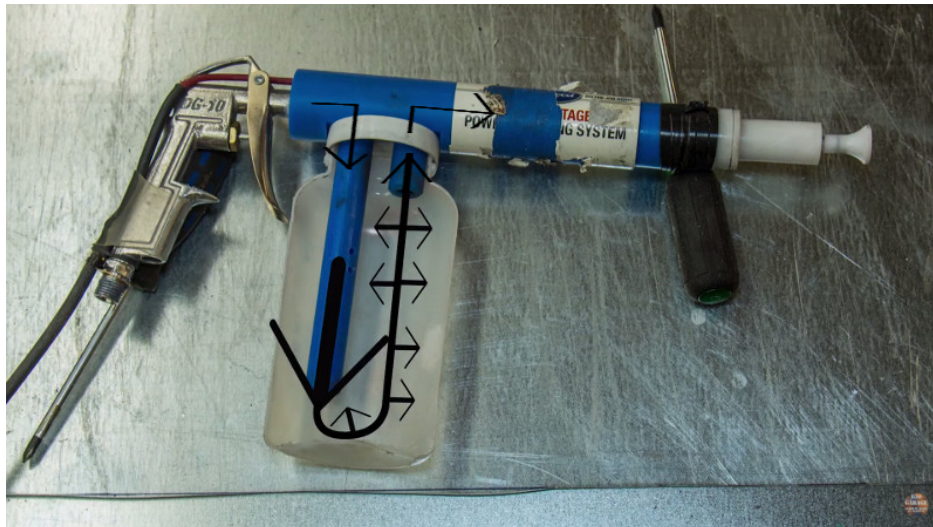


**Figure 5.3:** Eastwing Powder Coating Gun Cross-section

unburned powder settled downstream of the nozzle, which foreshadowed difficulty igniting feces. Although there was anticipated difficulty in lighting the feces, this test showed that a powdered fecal flame was a feasible achievement given proper fuel-air ratios, velocities, and nozzle geometry.

None of the powders sustained a flame when the torch igniter was removed. If the torch was removed, the flame would lift off the tip of the gun and extinguish. This confirmed the importance of proper exit velocity for the fuel-air mixture to maintain a steady flame after ignition. It was also not possible to adjust fuel-air ratios in this setup.



**Figure 5.4:** Powder Coating Gun with Cornstarch Flame

### 5.3 Venturi Nozzle

A mini-eductor venturi nozzle [31] pictured in Figure 5.5 was sourced from Fox Venturi Products. The expected powder delivery to air flowrate ratio was provided by the company, shown in Equation 5.1:

$$SLPM_{\text{air}} = 2.5 * \dot{m}_{\text{fuel}} \text{ [lb/hr]} \quad (5.1)$$

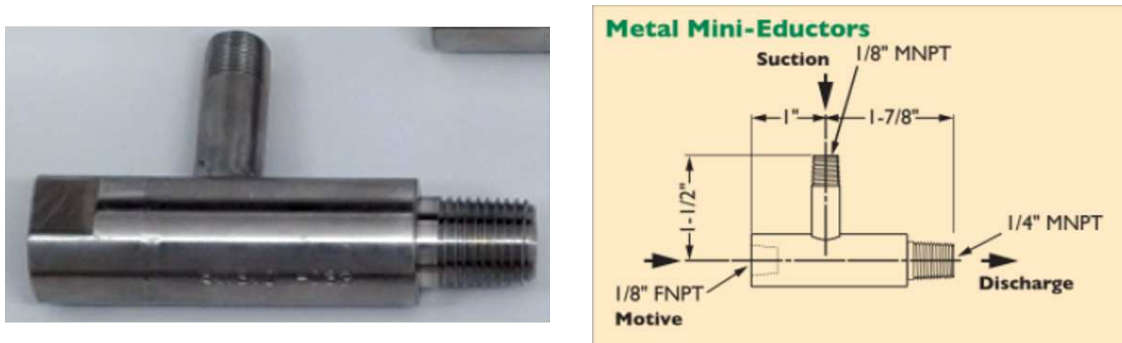


**Figure 5.5:** Fox 1/4" mini eductor venturi nozzle [31]

The initial idealized powder used with the venturi nozzle was cornstarch because it ignited the most readily in the powder coating gun. Using the lower heating value for starch: 15,227 kJ/kg [32], the expected flowrate for a 500 watt flame was 0.6515 SLPM of air through the nozzle, using Equations 2.5 and 5.1 for firepower and venturi air flowrate.

A hopper for the powder delivery was fabricated from stainless steel. The slope of the hopper sides were calculated from hopper design tables [1] using cornstarch friction coefficients given by Fitzpatrick [33]. For unobstructed bulk mass flow in the hopper, a slope angle of 20° from vertical was calculated. See Appendix C for details on conical hopper design. The hopper was extended with cardboard in order to hold a greater volume during sustained testing.

An Alicat mass-flow controller (Model: MCR-100SLPM) connected to a pressurized air line was used to regulate the incoming air flowrate.

Anticipating high exit velocity, a diverging nozzle diameter was calculated for the end of the venturi. High exit velocity would result in flame blow-off similar to the powder coating gun and a stable flame would not be achieved without redesigning the nozzle. As a result, a simple diverging nozzle was fabricated to attach to the FNPT threads of the venturi nozzle.

Using the flame speed data in Figure 3.3 and Table 3.4 coupled with nozzle velocity (Eq. 4.2), theoretical nozzle velocity was calculated as a function of fuel-air concentration for a 500 W cornstarch flame and plotted in Figure 5.6. Note that the lower flammability limit for cornstarch is  $63.9 \text{ g/m}^3$  and the stoichiometric concentration is  $174 \text{ g/m}^3$  (from Tables 3.2 and 3.3). For this first-order calculation, flame angle was not accounted as it was assumed that a stable flame would occur when flame speed equals exit velocity rather than using the flame speed equation (Eq. 2.6). A copy of the EES code used to generate Figure 5.6 can be found in Appendix C.

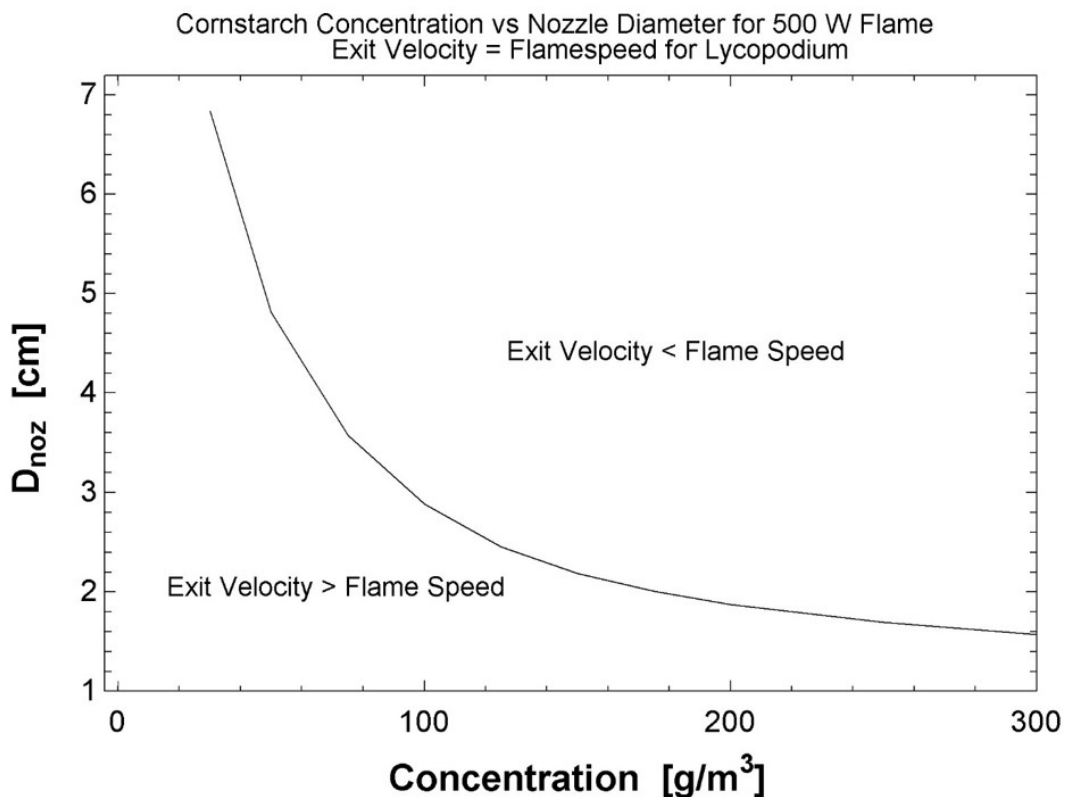


**Figure 5.6:** Nozzle diameters for various cornstarch concentrations

Using Equation 5.1 from Fox, the expected fuel-air concentration for cornstarch was a constant  $2537 \text{ g/m}^3$ , independent of air flowrate. Despite this rich equivalence ratio ( $\phi = 14.58$ ), a 2.5 cm diameter nozzle was chosen in order to keep the exit velocity much less than the flame speed. A 1-inch black pipe 12 inches long was used as an approximation for this calculated nozzle diameter.

A hand-held propane torch was mounted to a magnetic stand with six degrees of freedom that locked the torch at any distance from the end of the nozzle. This provided a convenient way to keep the ignition in a constant location. Figure 5.7 shows a close-up of the venturi nozzle with the hopper, 2.5 cm diameter nozzle (a shorter length), and torch. Figure 5.8 shows an overview of the entire venturi apparatus including the Alicat mass-flow controller.



**Figure 5.7:** Venturi nozzle with hopper, nozzle, and torch



**Figure 5.8:** Venturi nozzle assembly

### 5.3.1 Combustion Results

Cornstarch was tested in the Fox eductor venturi nozzle initially at the desired air flowrate of 0.6515 SLPM. As discussed in the previous section, this was the flowrate expected to produce a 500 watt cornstarch flame using Equation 5.1 provided by Fox. Unfortunately, this air flowrate was not high enough to draw the cornstarch through the hopper into the air stream. Despite physically agitating the cornstarch in the hopper and trying to gradually pour cornstarch into the hopper, clogging occurred before being entrained into the air stream.

In order to produce enough force at the venturi to draw the cornstarch into the air stream, the supply air was increased to a flowrate where eduction began. This occurred between 6 and 20 SLPM of air. Below 6 SLPM, the air stream was insufficient to entrain the powder. The line air pressure was not high enough to produce air flowrates over 20 SLPM, and higher flowrates were unnecessary due to the resulting high firepower.

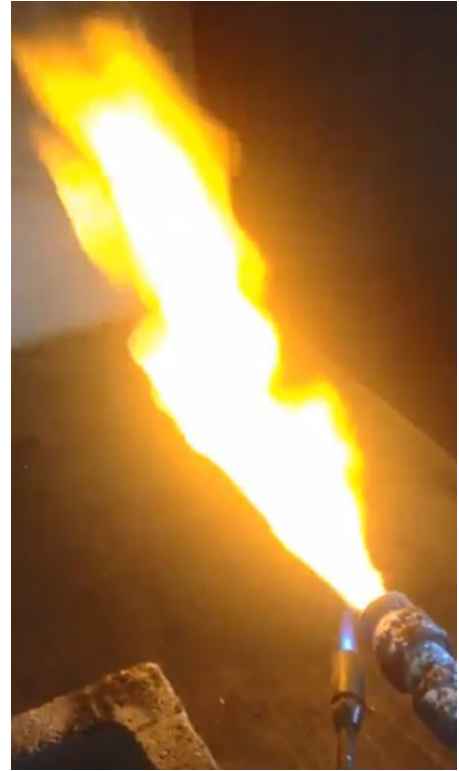
The venturi was initially tested without any diverging nozzle to observe the flame. Figure 5.9a shows the high exit velocity and flame liftoff of the cornstarch flame using the stock nozzle diameter. 8 SLPM of air created a flame about 1.5 feet long.

The 1-inch diameter, 12-inch long nozzle was tested on the end of the venturi. The flame was much closer to attaching to the nozzle in a stable manner, but the horizontal configuration caused the powder to fall out of the air stream before exiting. This powder build-up created a constriction in the nozzle, reducing its cross-sectional area and increasing exit velocity. A shorter nozzle was chosen, which was an improvement on the settling, and the flame was close to attaching to the end of the nozzle. The flame wasn't nearly stable enough, though, and the torch remained lit through the experiments (Figure 5.9b).

Cornstarch firepower was tested at flowrates of 7, 8, 10, and 12 SLPM using the 1-inch nozzle and regulated by the Alicat mass-flow controller. Even though these air flowrates sufficiently entrained the powder, the hopper was physically agitated to ensure that all the powder exited the hopper during the test.



(a) Fox venturi flame lifting off without a diverging nozzle



(b) Venturi flame with 1-in nozzle

**Figure 5.9:** Venturi Nozzle Flames

For each of these firepowers, cornstarch was weighed at 15 g and 20 g batches. A minimum of three tests were conducted at each flowrate. Figure 5.10 shows the results from these firepower tests.

The expected firepower in Figure 5.10 comes from the expected fuel mass consumption given by Equation 5.1, where the experimental data comes from measuring the actual fuel consumption in batches. This shows a minimum expected firepower of 6000 watts, which is an order of magnitude more than the Nano-Combustor target of 500 watts.

The calculated fuel-air concentration was theoretically constant ( $2537 \text{ g/m}^3$ ) given by Equation 5.1, but was calculated to vary slightly as a function of air flowrate, as shown in Figure 5.11.

The discrepancy between calculated and experimental values may stem from the manner in which cornstarch flows, its particle size, and the fact that Equation 5.1 is a general approximation of fuel-air concentration and not material specific.

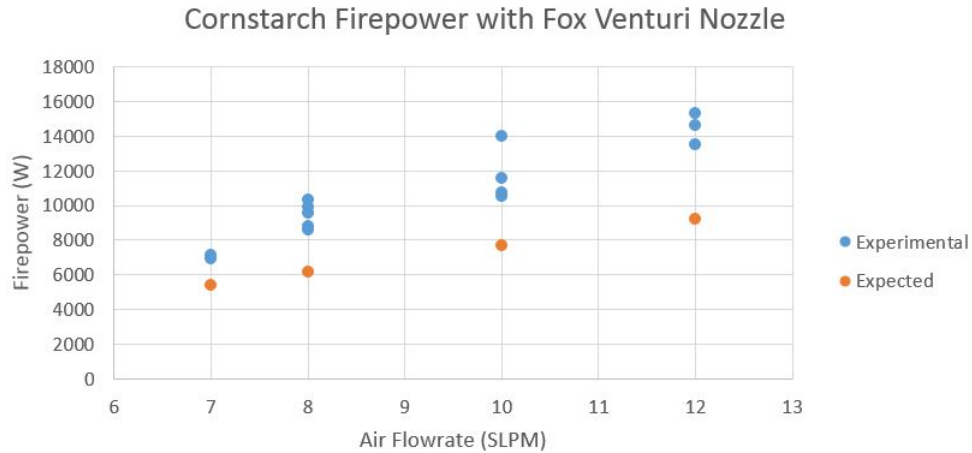


**Figure 5.10:** Fox venturi nozzle firepower results

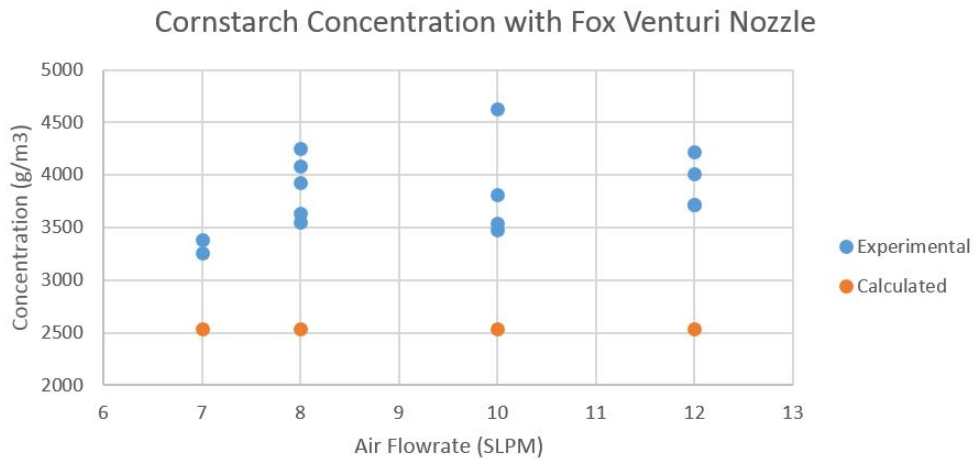


**Figure 5.11:** Fox venturi nozzle concentration results

Air flowrates below 6 SLPM were attempted using a fuel pick-up tube and a line of powder, but the suction was not strong enough to sufficiently convey the powder (Figure 5.12).

This experiment provided insight into constant fuel feed hoppers, nozzle diameter design, calculating firepower, and adjusting overall bulk flow, but ultimately there was still no way to isolate fuel and air flowrates and the firepower was far too high. Given that there was no obvious way to scale down the venturi nozzle to the sub-1000 watt level, the venturi nozzle was abandoned and other hardware configurations were considered.



**Figure 5.12:** Venturi nozzle with pick-up tube

The main project goals at this point were to drastically reduce firepower to below 1000 watts. Fluidized bed technology seemed a worthy next-step because of the possibility to scale to low firepowers. Various hardware configurations were created based on fluidized beds and are the subject of the next chapter.

# Chapter 6

## Fluidized Bed

Fluidized beds are a complicated phenomena, but their utility was integral to the development of the Nano-Combustor. Fluidized bed fundamentals will be discussed first, followed by the relevant hardware development and combustion tests.

### 6.1 Fluidized Bed Theory

Fluidization occurs when a fluid is passed through a bed of particles at a sufficient velocity where the bed begins to exhibit fluid-like properties. Fluidized beds have utility in certain industrial processes because they have a high rate heat transfer, low pressure drop, and uniform temperature [34].

As a fluid is passed through a fixed bed of particles and the fluid's velocity increases, there will be a point where local fluid velocity creates enough drag to overcome the gravitational effects of the particles. In this flow regime, *bubbles* begin to appear in the particle bed. As fluid velocity is increased further, the bubbles become more frequent and larger. Increasing velocity further reaches a point where the bubbles break down and the bed of particles appears to *boil*. At this point of fluidization, the bed exhibits fluid-like properties and has reached a *turbulent fluidized regime* [34]. Through these different flow regimes, the particle bed increases in height.

Even though the fluid passed through the bed can be liquid or gas, gas is often used. The fluid velocity in this case is termed the superficial gas velocity,  $U_g$ . The velocity that causes the onset of fluidization is termed the *critical velocity*,  $U_c$ .

The surface of a fluidized bed in this regime contains local particle lofting, but no actual mass transfer away from the bed. A gradient will exist above the fluidized bed that can be equated to the fuel-air concentration in a combustible dust cloud.

As  $U_g$  increases beyond  $U_c$ , the height of the particle bed continues to increase and the dust cloud above the surface of the bed becomes more extended. At a point where  $U_g$  exceeds the

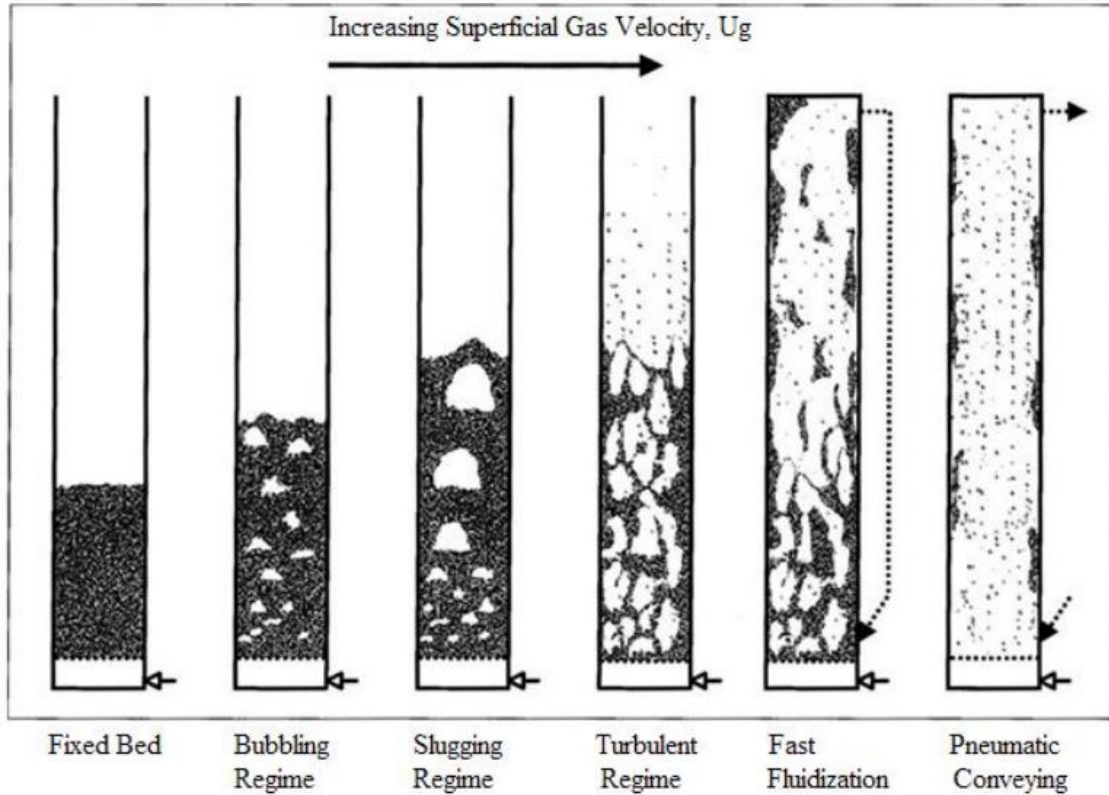


**Figure 6.1:** Fluidized bed flow regimes [35]

terminal velocity of the particles, pneumatic conveying will occur and the bed will eventually no longer exist.

Figure 6.1 summarizes these different flow regimes.

The minimum transport velocity for a particle occurs when  $U_g$  equals the terminal velocity of a particle, given in Equation 3.5. For a bed of particles with diameters below 0.1mm, the Reynolds number is relatively small and the Kozeny-Carman Equation below can be used to find the critical fluidization velocity [27]:

$$U_c = \frac{(\rho_p - \rho_f)gD_p^2}{150\mu} \frac{\varepsilon^3}{1 - \varepsilon} \quad (6.1)$$

Where  $\rho_p$  and  $\rho_f$  are particle and fluid densities respectively,  $g$  is acceleration due to gravity,  $D_p$  is the particle diameter,  $\mu$  is the fluid viscosity, and  $\varepsilon$  refers to the void fraction, which is a

function of the material, shape, and size of the particles. For nearly spherical particles,  $\varepsilon$  is about 0.40-0.45 [36], which was assumed for first-order calculations using cornstarch.

Equation 6.1 can be simplified using the same assumptions to simplify the terminal velocity Equation 3.4. Assuming standard particle density ( $1000 \text{ kg/m}^3$ ), that  $\rho_p \gg \rho_f$ , and assuming spherical particles with  $\varepsilon = 0.45$ , Equation 6.1 simplifies to:

$$U_c = 585509 D_p^2 \quad (6.2)$$

## 6.2 Hardware Development

One key component of fluidized bed design is having a porous air distributor below the particle bed, whose mesh size is smaller than the smallest particles. This air distributor uniformly distributes the fluid at the base of the bed and prevents air channeling, which can occur if the material packs too much or if the distributor holes are too large.

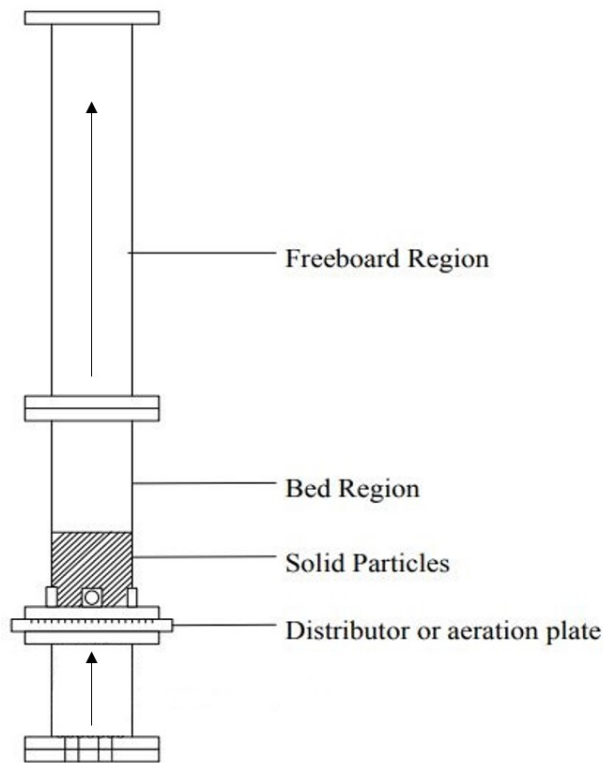
The intriguing components of exploring a fluidized bed were its characteristically low pressure drop once fluidized, the ability to size select which particles to loft based on lofting velocity, the ability to sample fuel concentrations as a function of height above the bed, and the particle density gradient that develops within the fluidized bed which would allow large particles to sink to the bottom of the bed and be processed once more into yet smaller particles.

It was clear that velocities used would need to be greater than the critical fluidization velocity because particle lofting for combustion was desired. Using  $28 \mu\text{m}$  as the mean diameter of cornstarch (Table 3.2), the lofting velocity was estimated to be  $0.0235 \text{ m/s}$  (Eq. 3.5).

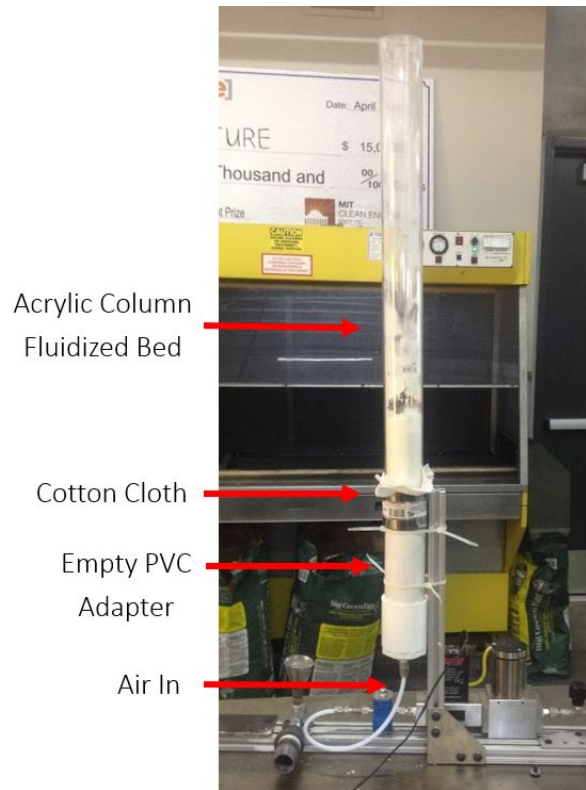
### 6.2.1 First Generation Fluidized Bed Burner

The first fluidized bed burners for this project were made out of acrylic tube to be able to visually inspect the particle bed for fluidization and lofting. Following the general schematic of a fluidized bed (Table 6.2a), a simple fluidized bed column was made out of acrylic tube for the freeboard region, cotton cloth stretched tight for the air distributor, empty PVC tube below the

distributor to diverge the incoming air velocity profile, and incoming air from the bottom controlled by the Alicat mass-flow controller (Figure 6.2b). The acrylic tube for this first generation burner was 1.25 inches in diameter.



(a) General fluidized bed schematic [34]



(b) 1st generation acrylic fluidized bed burner

**Figure 6.2:** Fluidized Bed Burner

Some simple calculations guided initial set points for testing this hardware. The goal was to observe fluidization, but also to loft the particle bed sufficiently to convey particles out of the top of the tube and attempt to create a stable flame. Assuming combustion would happen at or above stoichiometric concentrations, the flame speed would be approximately 0.40-0.50 m/s (Table 3.4), which is well-above the lofting velocity of cornstarch. Equating flame speed with bulk flow out of the tube (the initial simplified assumption of a flat flame), 17.9 SLPM of air would create a local velocity of 0.45 m/s at the nozzle using the 1.25-inch diameter acrylic tube. This was used as the initial air set point and fine-tuned based on observations of flame lift-off or blow-back.

At the onset of testing the fluidized bed, it quickly became clear that cornstarch's propensity to pack tightly was a major challenge of using it as a fuel. As air increased up to and beyond the point of fluidization, the cornstarch bed would begin to create *bubbles* as expected, and the bed height would expand. Then a point came where the bed voids would collapse and pack against itself with the impact. This would cause air channels to form through the bed instead of fluidization. The air channels would remain even as air velocity was increased beyond the particle terminal velocity.

Once channeling occurred, it was possible to create fluidization by *knocking* the side of the apparatus with a blunt object at frequencies of about 1 sec. These strong vibrations made it so that the cornstarch never had a chance to fully settle and create air channels, and the vibrations allowed fluidization to occur. The acrylic was important in allowing direct observation of these packing and vibrating phenomena.

By knocking the side of the apparatus and increasing the air flowrate above the particle terminal velocity, a particle cloud began to exit the top of the cloud. There was no way to control the equivalence ratio of the mixture, but it was observed that higher air flow made the particle cloud more dense. Using 17.9 SLPM as a starting point, a flame was achieved, but it lifted off. Air velocity was decreased until the flame latched to the top of the acrylic tube, at 10.5 SLPM. Figure 6.3 shows the dust cloud and subsequent flame after ignition with a lighter. Knocking the side was necessary and tests remained short to keep the acrylic from melting.

Firepower was estimated by placing the apparatus on a scale and sweeping air flowrates for two minutes each without igniting the dust cloud. Three 2-minute samples were taken at 10, 15 and 18 SLPM air. The starting and ending mass was recorded over two minutes while knocking the tube as if it were burning. The unburned cornstarch was vented through through the fume hood. Figure 6.4 shows the results of the firepower sweep test using cornstarch in the 1.25-inch diameter burner. Based on this data, the flame in figure 6.3b was estimated to be about 275 watts based on the 10.5 SLPM air flowrate. The increase in firepower as a function of air flowrate implies an increase in fuel-air concentration as air velocity increases, which confirmed observations during testing.

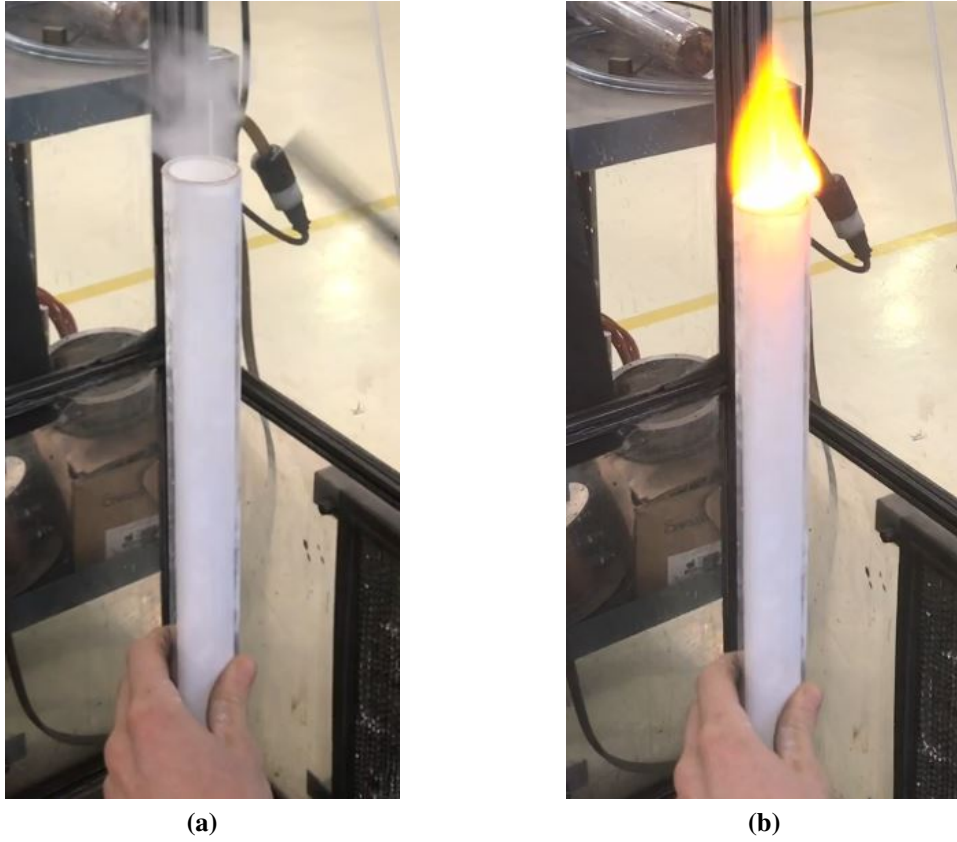


**Figure 6.3:** First generation fluidized burner (a) dust cloud and (b) resulting flame. 10.5 SLPM air, firepower ~275 watts

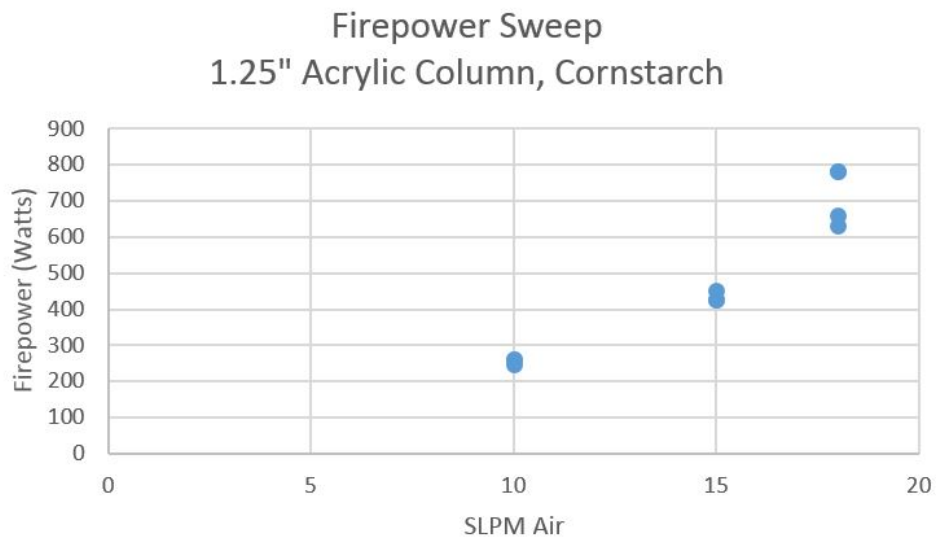


**Figure 6.4:** Firepower sweeps for 1.25" diameter fluidized bed burner

By combining fuel mass flowrate and air volumetric flowrate, fuel-air concentration was calculated as a function of air flowrate (Figure F.1). The fuel-air concentration at 10.5 SLPM was estimated to be  $79.9 \text{ g/m}^3$ , which is near the lower flammability limit. The nozzle velocity under these conditions was  $0.263 \text{ m/s}$ . Table 3.4 suggests a flame speed around  $0.35 \text{ m/s}$ , so equating nozzle velocity to flame speed seemed appropriate for first-order approximation air flowrates.

## 6.2.2 Intermediate Hardware Revisions

Some hardware iterations were explored to address the need to vibrate the tube to keep the fuel fluidized. Vibrating devices were briefly explored, but rejected because of the increased electricity burden and the increased system complexity. Thinking that swirling the incoming air with a higher velocity air-inlet might help reduce the air channeling, a minor revision was made in the first generation fluidized bed burner and is shown in Figure 6.5. Two pieces of 1/8-inch Swagelok tubing were connected to the main air line and routed tangentially into a piece of acrylic tube containing cornstarch.



**Figure 6.5:** Fluidized bed burner with swirl



**Figure 6.6:** Fluidized burner with aluminum nozzle

This ended up having no effect on channeling reduction and was abandoned due to increased complexity.

A diverging aluminum nozzle also was machined to fit on top of the acrylic tube (Figure 6.6). The thought was that the flame would locate itself at a diameter on the nozzle that matched its flame speed and allow for a greater firepower throttle. The nozzle didn't work at all, which pointed to a dependence on secondary air entrainment at the nozzle edge. This was the first evidence that pointed to the flame being a partly pre-mixed and part diffusion flame. This was surprising because the fuel-air concentration was lean, which implies that there should have been enough oxygen in the mixture to fully combust. Nonetheless, all future fuel-air mixtures were strongly fuel-rich and had a dependency on secondary air fueling diffusion combustion. Perhaps the error in the initial firepower estimates didn't take into account buoyant forces induced in the flame preheat zone, which may have increased the fuel velocity and resulted in a higher firepower and fuel-air concentration.

### **6.2.3 Second-Generation Fluidized Bed Burner**

The first generation burner was scaled down to see if an even smaller stable flame could be sustained. The cotton cloth air distributor was abandoned (because the knocking was enough to induce fluidization), and a U-shaped base was constructed at the base of the burner so that powder did not fall back into the air supply. This second-generation burner body was fabricated from 1/2-inch black pipe. Using a stoichiometric fuel-air concentration ( $230 \text{ g/m}^3$ ) and flame speed from generation 1 data as a set point, the nozzle exit diameter and air flowrate was calculated. The exit velocity was held constant from the first generation at  $0.263 \text{ m/s}$ . By necking down the top of the nozzle to a 1/8" NPT fitting (0.33" ID), a 55 watt flame would result from an air flowrate of 0.73 SLPM. Anticipating the equivalence ratio to possibly be  $\phi = 2$ , the resulting firepower would be 110 watts for the same air flowrate.

Figure 6.7 shows the second-generation apparatus with the 1/8" NPT nozzle. A stable flame (Fig. 6.8) was achieved with this setup at 1.5 SLPM of air. Frequent knocking with a wrench was necessary to keep the cornstarch fluidized.



**Figure 6.7:** Second-generation fluidized bed burner



**Figure 6.8:**  
Second-generation flame.  
~100-200 watts, 1.5 SLPM air.

Firepower tests were performed identically to the first generation hardware. The average firepower over three tests was estimated to be 165 watts, with the air flow rate at 1.5 SLPM. The average fuel-air concentration was quite rich at an average of 335.6 g/m<sup>3</sup>. These and other data points are summarized in Table 6.1

## 6.3 Conclusions

A brief summary of operating condition differences between the two versions of the fluidized bed burners is contained in Table 6.1. Note the increase in equivalence ratio as the burner becomes smaller. Keep in mind that firepower and fuel-air concentrations were estimates to quickly guide further iterations of hardware development. More rigorous tests would need to be done in order to have higher confidence in these numbers, but their role is well-served in quickly providing reference points through the quick hardware iterations.

**Table 6.1:** Summary of fluidized bed burner operating parameters, cornstarch as fuel

<b>Burner Version</b>	<b>Nozzle Diameter (in.)</b>	<b>FP (W)</b>	<b>Air Flow Rate (SLPM)</b>	<b>Nozzle Velocity (m/s)</b>	<b>Fuel-Air Concentration (g/m<sup>3</sup>)</b>
Gen 1	1.25	275	10.5	0.263	79.9
Gen 2	0.33	165	1.5	0.540	335.6

The dramatic reductions in firepower from the venturi nozzle to the first and then second-generation fluidized bed burner were promising steps in the Nano-Combustor development. A number of concerns remained that required further hardware development. First, there was little control over the fuel-air concentrations. It was clear that fuel-air concentration was a function of velocity through the tube (higher velocity increased the fuel concentration), but there was not a way to independently control fuel and air flowrates while keeping nozzle geometry constant. Second, the need to continuously knock the side of the tube to keep the bed fluidized was unacceptable in a the final Nano-Combustor design. Third, these designs weren't able to accommodate fuel additions in their current configuration. These three concerns inspired the next stages of hardware development.

# Chapter 7

## Fuel Delivery System

With the relative success scaling down firepowers with the fluidized bed burners, the next challenge was addressing fuel delivery. None of the systems tested to this point included a way to convey fuel into the burner, which was a necessary design criteria for the final Nano-Combustor. This chapter discussed the evolution of the fuel-deliver system.

It was at this point in the project that the choice of using cornstarch as an ideal fuel was reconsidered. Many of the challenges encountered thus far were due to its propensity to pack tightly and form dense clumps. Even though it ignited well, it was very difficult to convey. Because of this, at this stage in the project lycopodium began taking the place of cornstarch as an ideal fuel. Even though lycopodium was much more expensive, the scale of the system was small enough that tests remained economical. By observation, the lycopodium powder was very free-flowing, which was necessary in the development of a fuel delivery system. Unless otherwise specified, assume future tests are performed with lycopodium powder, whose properties can be reviewed in Section 3.3.

### 7.1 Auger Design

The most logical way to introduce fuel into a vertical nozzle burner was horizontally. Horizontal conveying is most easily done on this scale using a hopper and horizontal auger. A conveyor belt was also considered, but abandoned because of the complexity.

MSR designed and 3D-printed a hopper and selection of various augers that were tested at CSU. 3D-printing provided quick iterations and easy manufacturing considering an auger's complex geometry.

Many auger iterations were made as the Nano-Combustor progressed. The first versions and tests will be discussed here and later iterations will be discussed in Chapter 8. The initial hopper

and auger assembly is shown in Figure 7.1 alongside the simple Arduino controller for the stepper-motor speed. The Arduino control system will be described in more detail in Section 7.3.

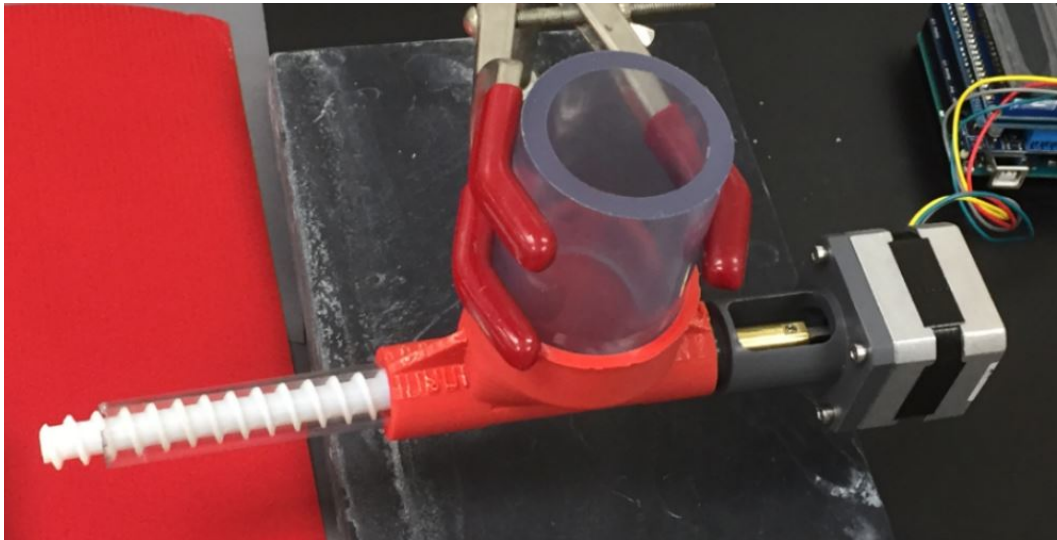


**Figure 7.1:** First generation auger and hopper assembly

The auger was initially driven by a NEMA-17 stepper motor [37]: 200 steps/rev, 12VDC, 350mA, 20 N-cm torque. But after a few days of testing the auger became slightly warped (from the 3D-printing process) and internal friction increased to the point where the motor couldn't provide sufficient torque. The motor was upgraded to a higher-torque stepper motor from Sparkfun [38]: 400 steps/rev, 12VDC, 1.7A, 40 N-cm torque. Insufficient torque was never again an issue with the second motor.

Three augers were fabricated in the first round of 3D-printing. All had an outside diameter of 1/2", a shaft diameter of 0.33", and three different pitches: 3/8", 1/4", and a variable pitch starting at 3/8" and finishing with 1/4". The first generation of Arduino code ramped the motor from 0-15 RPM and displayed the current RPM on a LCD display (Fig. 7.3).

As hardware development progressed, auger pitch, outer diameter, shaft diameter and length changed slightly. These changes will be addressed mainly in the next chapter because they occurred alongside total system design.

## 7.2 Firepower Set points

It was necessary to correlate motor RPM with expected firepower by measuring mass flowrate for each auger design. The auger assembly was suspended above a scale and lycopodium powder was run 5, 10 and 15 RPM for 10-30 minutes. Using the LHV of lycopodium and Eq. 2.5, a firepower vs. motor RPM line was generated for the three augers and is shown in Figure 7.2.

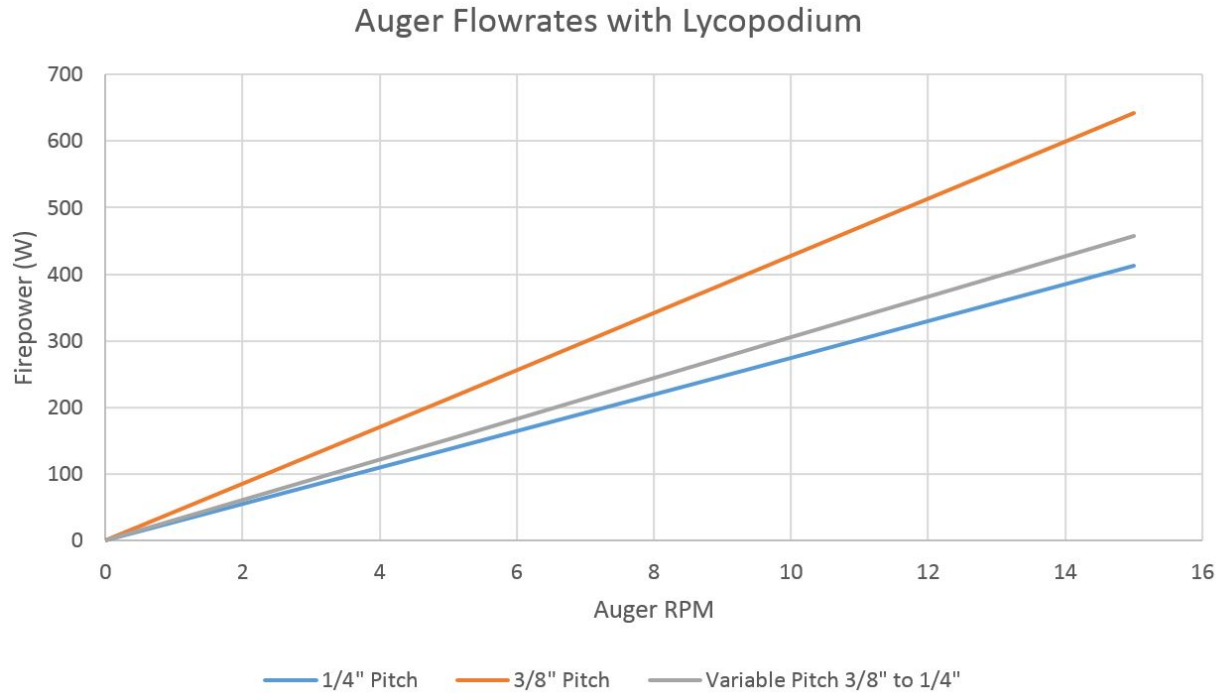


**Figure 7.2:** Firepower vs RPM curve, first generation auger versions

It was observed that the fuel fell out of the auger in pulses, the frequency of which corresponded to the auger flight passing the lip of the acrylic tube. The shortest pitch, therefore, created less pulsing because it had to move at a faster rpm to deliver the same amount of material. Therefore, the 1/4" auger was selected as the first primary auger for fuel feed experiments. The slope of the 1/4" line in Figure 7.2 was 27.5 W/RPM, which was used as a linear multiplier for RPM to firepower conversion. Key firepower set points for the 1/4" pitch auger are below:

**Table 7.1:** 1/4" pitch auger firepower setpoints

Set Point (RPM)	Expected Firepower (Watts)
3.6	100
7.3	200
10.9	300
15.5	426

### 7.3 Control System

An Arduino was programmed to control the stepper motor with a potentiometer and output the RPM on a LCD display. The original code developed by MSR was eventually revamped by CSU to improve performance by eliminating inconsistencies in rotational speed (which were present in the first batch of code: the motor would *hiccup* every second). The updated code also stepped in increments of 5 RPM. A complete copy of the final Arduino code can be found in Appendix D.

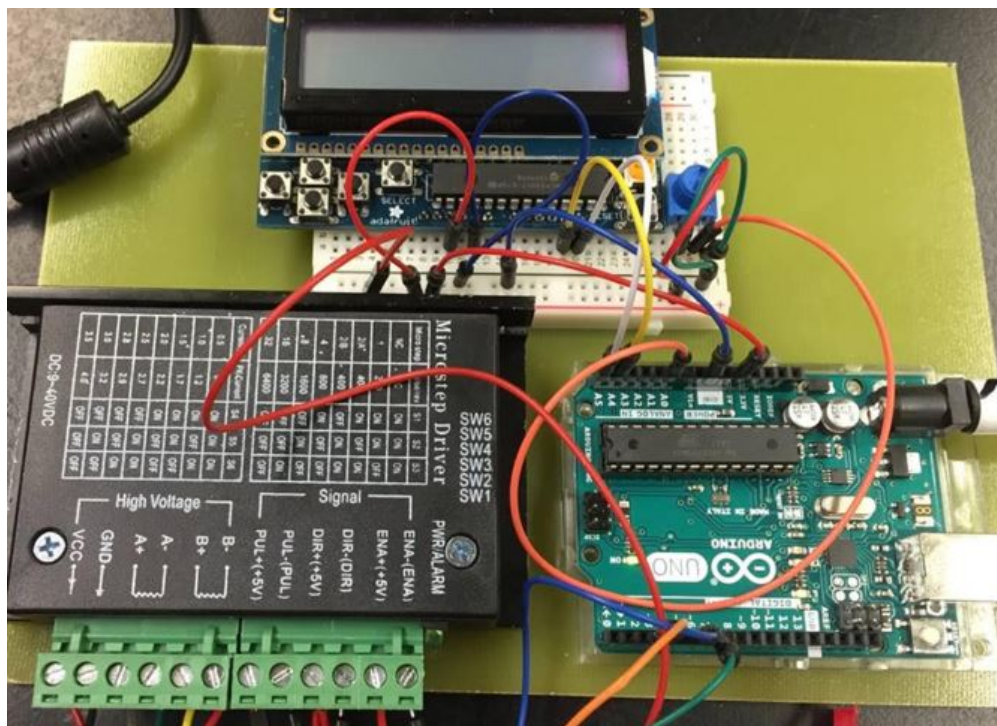


**Figure 7.3:** Arduino stepper-motor controller

# Chapter 8

## Final Nano-Combustor Design and Testing

The final stage of Nano-Combustor development involved incorporating the fuel-feed mechanism from Chapter 7 into a revamped version of the second-generation fluidized bed burner (Section 6.2.3). The aim of revamping the fluidized bed burner was to actually move away from the fluidized bed concept, which required frequent knocking on the side of the burner to keep the powder fluidized, while keeping similar nozzle geometry and air flowrate set points.

The concept that was developed involved *dosing* fuel with the auger into a high-velocity air stream, where fuel and air mixing would occur and then loft to the nozzle exit. All of the stable flame burners discovered in the literature review (Section 5.1) used fluidized beds and baffles to loft the particles and have control over fuel-air ratios. None of the technology reviewed used an auger system to incorporate the fuel and air. This updated approach developed at CSU provided two independent *knobs*: one for fuel flowrate, and another fully independent control for air flowrate. Incoming air velocity was controlled by the size of an orifice upstream of the fuel addition, and bulk velocity in the nozzle was controlled by the nozzle diameter and air flowrate.

This configuration went through two major iterations: the *third-generation Nano-Combustor* and the *final Nano-Combustor*. The final generation will conclude CSU's hardware development, though MSR continues development of hardware through 2018. A discussion of continued development is presented in Chapter 10.

### 8.1 Third-Generation Nano-Combustor

The second-generation fluidized bed burner utilized a 180° bend at the bottom to keep fuel out of the air line. In the third-generation Nano-Combustor, an orifice was fabricated to increase the air velocity and keep the fuel lofted. To calculate the proper orifice diameter, first the settling velocity of lycopodium was calculated to be 0.035 m/s using Equation 3.4. Using the air set points from the previous tests as a guide, flowrates over 1.5 SLPM were unlikely for a burner in the 100-300 watt

range with a nozzle diameter less than 1/4". A hypothetical fuel-rich concentration of 1000 g/m<sup>3</sup> with 0.1 SLPM air would create a 60 watt flame, which seemed like an appropriate low-firepower extreme of operation. Using a 1/16" orifice with this air flowrate creates an orifice velocity 29 times greater than the terminal velocity of lycopodium. This was a good starting point for lofting velocity and ensured that fuel would not fall below the orifice so the 180° bend was abandoned. The orifice was fabricated by welding a 3/8" MNPT stainless steel Swagelok fitting over the small end of a 3/8" MNPT X 1/16" S.S. Swagelok fitting. Upstream of the orifice, 3/8" tubing attached to the Alicat mass-flow controller via barb fittings.

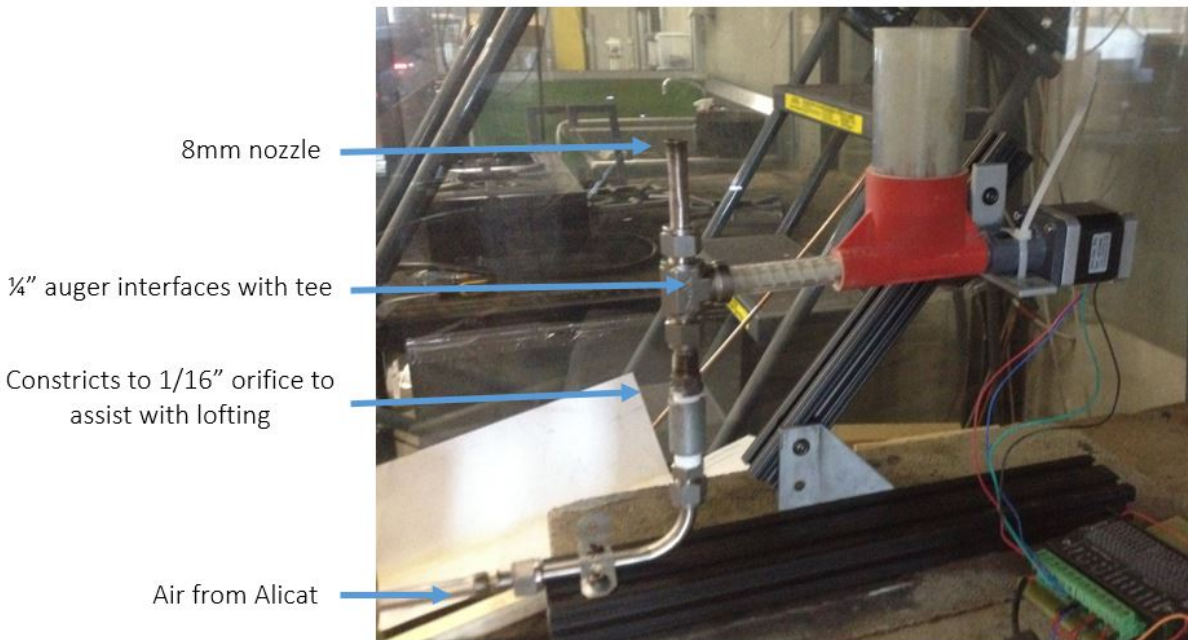


**Figure 8.1:** Third-generation Nano-Combustor

The auger system integrated into the burner above the orifice via a FNPT tee fitting. The auger housing was machined down to fit snugly into the threads of the tee fitting. The end of the auger extended 1/8" beyond the end of the housing, and the auger face was lined up halfway between the center axis of the burner and the inner wall of the tee fitting. At that location, the auger would deliver fuel into the high-velocity air stream without occluding the bulk air flow. Ideally, the orifice

would be closer to the auger to increase lofting and mixing, but this design was limited by the size of the fittings.

The nozzle diameter was an important consideration and was calculated using the EES code in Appendix E. The design constraints included: starting with an assumed fuel-air concentration of 336.6 g/m<sup>3</sup> and a nozzle velocity of 0.54 m/s (from the 2nd-generation fluidized burner). A flame at 275 watts was initially the target. These constraints suggested starting with an 8mm diameter nozzle and 1.35 SLPM air. Having decided on the 1/4" pitch auger from Chapter 7, an auger set point at 10 RPM would produce a 275 watt flame. This process formed the logic and calculations for the geometry of the third-generation Nano-Combustor, shown in Figure 8.1.

The revisions of the third-generation burner will be summarized below. Even though each revision involved a plethora of testing, the final set points and conclusions are labeled *rev. 1, rev. 2... etc.*

### 8.1.1 Gen-3, Revision 1 Results

The initial revision results of the third generation Nano-Combustor provided some critical guidance for further iteration. A flame existed for about 10-15 seconds maximum before self-extinguishing, but could be repeated indefinitely. The set points of a stable flame occurred slightly differently than the initial calculations, which was expected. The final set points are summarized in Table 8.1 next to the initial expected set points.

**Table 8.1:** Summary of first revision results with third-generation Nano-Combustor using lycopodium fuel

<b>Burner Version</b>	<b>Nozzle Diameter (mm)</b>	<b>FP (Lyco.) (W)</b>	<b>Air Flow Rate (SLPM)</b>	<b>Nozzle Velocity (m/s)</b>	<b>Fuel-Air Concentration (g/m<sup>3</sup>)</b>
Gen 3, Rev. 1 (expected)	8	275	1.35	0.540	335.6
Gen 3, Rev. 1 (actual)	8	426.3	1.0	0.395	702.4

The stable flame (Figure 8.2) was achieved by beginning with the expected set points, then adjusting fuel and air flowrates based on flame observations. If the flame was extinguishing be-

cause of lift-off, the air flowrate was decreased. If the flame flashed-back into the nozzle, the air velocity was increased. Fuel concentration was adjusted with the auger speed and firepower was back-calculated from Figure 7.2. The flame seemed to stabilize as fuel-air concentration increased. Table 8.1 shows an actual fuel concentration of  $702.4 \text{ g/m}^3$ , which was about 2-times greater than the fluidized bed burner. This explains the higher-than-expected firepower. The fluidized bed did not offer control over the fuel-air concentration with the fidelity that this generation offered. This test offered an updated set point for expected concentration moving forward.



**Figure 8.2:** third-Gen Nano-Combustor, Rev. 1 flame

This test also revealed a *pulsing* flame that seemed to correspond with the auger rotations. It was observed in the initial auger firepower tests (Ch. 7) that the fuel delivery was inconsistent because the auger's flight would block powder delivery each time it passed through the bottom of its rotation. The 1/4" auger was chosen for this reason, but this test suggested the necessity to reduce flight volume by increasing the relative shaft diameter and/or decreasing pitch so that the

auger could spin at a faster rate without increasing the firepower. Additional auger development will be discussed in Section 8.1.5.

Because this first revision had a higher fuel-air ratio than expected the firepower was higher than desired. The next revision aimed to reduce the nozzle diameter and achieve a 200 watt flame.

### 8.1.2 Gen-3, Revision 2

The design constraints for revision 2 used the nozzle velocity and fuel-air concentration results from revision 1 and then iterated the nozzle geometry and fuel-air flowrates for a 200 watt flame. The same EES calculator was used (App. E) and suggested a nozzle diameter of 5.4mm and an air flowrate of 0.47 SLPM. 5mm stainless tubing was used for the nozzle and was installed on the third-generation Nano-Combustor.

A stable flame was more difficult to achieve with this configuration because the flame kept lifting off. It was theorized that the flame needed a way to anchor itself to the geometry of the nozzle rim, and the stability difference between Rev 1 and 2 involved the difference in nozzle edge perimeter. Advised by MSR about the importance of *flame-holders*, a simple flattened wire was placed in the bulk flow just above the nozzle exit and flame stability was immediately achieved. Flame holder theory will be briefly discussed later in Section 8.1.3. Table 8.2 summarizes the expected and actual results for Rev. 2, and Figure 8.3 shows the flame and flameholder. Notice how the flame is lifted off of the nozzle rim, but anchored to the flameholder.

**Table 8.2:** Summary of third-gen. Rev 2 Nano-Combustor using lycopodium fuel

<b>Burner Version</b>	<b>Nozzle Diameter (mm)</b>	<b>FP (Lyc.) (W)</b>	<b>Air Flow Rate (SLPM)</b>	<b>Nozzle Velocity (m/s)</b>	<b>Fuel-Air Concentration (g/m<sup>3</sup>)</b>
Gen 3, Rev. 2 (expected)	5	200	0.47	0.395	702.4
Gen 3, Rev. 2 w/ flameholder (actual)	5	275	0.5	0.5058	906.3

This flameholder stabilized the flame, but powder would quickly accumulate on the bottom of the flattened wire and slough off, occluding the bulk flow. Revision 2 revealed the importance



**Figure 8.3:** third-Gen Nano-Combustor, Rev. 2 flame, with flattened-wire flameholder

of utilizing a flameholder as the nozzle diameter (and thus firepower) decreased, but it was clear that placing anything directly in the fluid path at this point was detrimental to the longevity of the flame. Flameholders can occur within the bulk flow or around it (external), so the next path of development became iterating nozzle rim geometry to create an external flameholder.

### **8.1.3 Nozzle Rim Flameholders**

A simplified flame model was described in the beginning of Section 2.1.4 with Equation 2.6. In the simplified model, the flamespeed is balanced by the normal component of the unburned fuel-air mixture's bulk flow velocity. The second half of Section 2.1.4 describes the complexities around the perimeter of a flame. In summary, the three factors that can reduce local flamespeed and anchor a flame are: heat loss to the nozzle, micro eddies at an edge, and the no-slip condition which creates slower bulk-flow velocity near the outer edges of the flow.

With this criteria in-mind, four nozzles were designed with different rim characteristics, and shown in Figure 8.4. These nozzles were constructed out of 1/4" brass tubing, which fit snugly

over the 5mm stainless steel Swagelok nozzle and allowed for a quick exploration of nozzle rim flameholders. Three of the nozzles had 1/16" holes drilled below the rim, with the intention to draw air into the bulk flow and lean-out the already high fuel-air ratio. Two of the nozzles had constricting rim geometry, and two were flared at 45° with a flaring-tool. One of the flared nozzles had no holes.



**Figure 8.4:** Nozzle rim flameholders

Some quick tests with these nozzles revealed that the holes were not beneficial. The bulk fuel-air velocity was not sufficiently high to draw in air. Instead, fugitive unburned powder exited the holes. Additionally, the constricting rim geometry was ultimately undesirable due to concerns of powder impacting and accumulating at the constriction. A stable flame was achieved using the 45° flared nozzle without holes, and Section 8.1.4 describes the results from this test. The flared nozzle increases the surface area for heat transfer to the nozzle, which may be the primary factor stabilizing the flame. Secondary stabilizing effects likely come from micro-eddies at the sharp 45° divergence as well as the lowered bulk-flow velocity at the flow perimeter.

### 8.1.4 Gen-3, Revision 3

The addition of a flameholder at the nozzle rim greatly stabilized the flame. Since the brass tubing slipped over the top of the already-existing 5mm stainless tubing, the expected set point parameters were taken from the rev 2 results: 0.5058 m/s nozzle velocity and 906.3 g/m<sup>3</sup> fuel-air concentration coupled with the new 0.25" nozzle diameter. The calculated flow rates were 0.81 SLPM and 16.1 RPM auger rotation for a 444 watt flame. This was a higher firepower than ideal, but it was expected for a 1/4" nozzle diameter. The third revision test was primarily to study the stability of the flame with the flared rim flameholder.

Once more, the flow rates were adjusted to produce a stable flame. The comparison of expected and actual parameters are shown below in Table 8.3:

**Table 8.3:** Summary of Third-Gen. Rev 3 Nano-Combustor using lycopodium fuel

<b>Burner Version</b>	<b>Nozzle Diameter (in)</b>	<b>FP (Lyc.) (W)</b>	<b>Air Flow Rate (SLPM)</b>	<b>Nozzle Velocity (m/s)</b>	<b>Fuel-Air Concentration (g/m<sup>3</sup>)</b>
Gen 3, Rev. 3 (expected)	0.25	444	0.81	0.5058	906.3
Gen 3, Rev. 3, flared rim (actual)	0.25	289	0.3	0.1882	1586

The flame produced with the flameholder was quite stable and remained lit for about 5 minutes before extinguishing (Figure 8.5). The point of failure was char and powder accumulating on the nozzle rim and occluding the flow. As the char built-up, the nozzle exit diameter decreased, which increased the nozzle velocity and eventually caused the flame to lift-off.

The results of the third revision testing show that the nozzle velocity was quite reduced from previous revisions. This could reveal the role the flared flameholder played in stabilizing the flame by reducing the average flamespeed. Also of note is the increasingly rich fuel-air concentration, which became the norm in future tests. Table 8.6 shows a summary of the final operating set points for all three revisions of the third-generation Nano-Combustor.



**Figure 8.5:** Third-Gen Nano-Combustor, Rev. 3 flame, with flared nozzle

Having stabilized the flame with the flared nozzle flameholder, the attention turned to redesigning the auger system to help reduce the pulsing in the flame from inconsistent fuel delivery.

**Table 8.4:** Summary of third-generation Nano-Combustor set points using lycopodium fuel

<b>Burner Version</b>	<b>Nozzle Diameter (in)</b>	<b>Burn Time</b>	<b>FP (Lyco.) (W)</b>	<b>Air Flow Rate (SLPM)</b>	<b>Nozzle Velocity (m/s)</b>	<b>Fuel-Air Concentration (g/m<sup>3</sup>)</b>
Gen 3, Rev. 1	0.315	10-15 sec.	426.3	1.0	0.395	702.4
Gen 3, Rev. 2	0.197	20 sec.	275	0.5	0.5058	906.3
Gen 3, Rev. 3	0.25	5 min.	289	0.3	0.1882	1586

### 8.1.5 Further Auger Development

A new auger and hopper was developed and 3D-printed by MSR. The new auger was shorter in length and had a 3/8" outside diameter, no change in shaft diameter, and 3/16" pitch. This auger ended up having the same dimensions as the final auger used. The differences between the two main augers used are summarized in Table 8.5 and shown in Figure 8.6. The clear tubing surrounding the auger had the same outer diameter to fit inside the tee fitting, so the auger revision was a simple change.

**Table 8.5:** Differences in primary augers' geometry

Auger Version	OD (in.)	ID (in.)	Pitch (in.)	Length (in.)
Original	1/2	0.33	1/4	7.25
Final	3/8	0.33	3/16	6.125



**Figure 8.6:** Original and final augers

A new firepower set point curve had to be generated, so the methods described in Section 7.2 were repeated for the new auger. The results are shown in Figure 8.7. The slope of the linear regression was 7.411, which was the multiplier used to convert RPM to firepower.

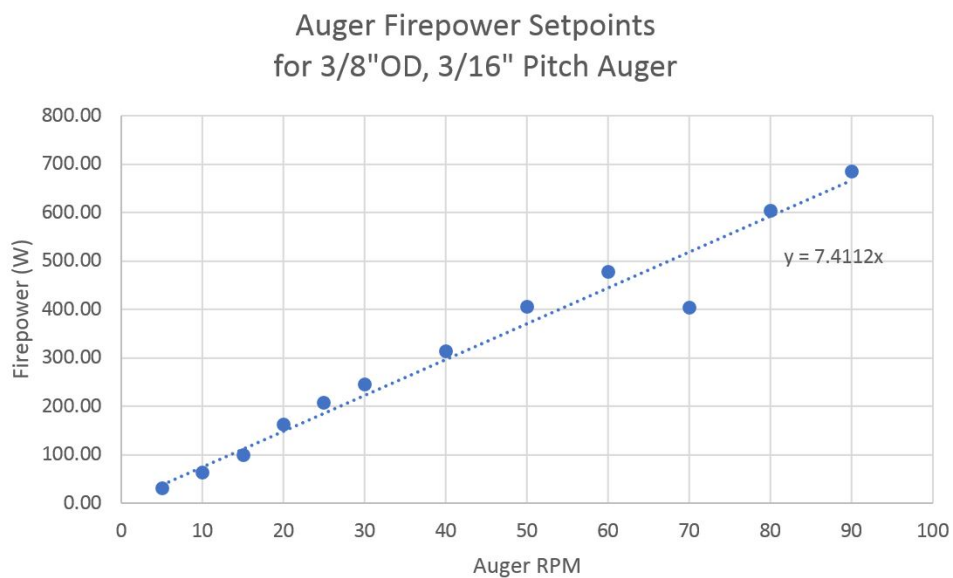


**Figure 8.7:** 3/8" OD auger firepower set points

## 8.2 Final Nano-Combustor

Having achieved a 5 minute burn at 289 watts with the third-generation Nano-Combustor, the focus turned to create a finalized hardware package that would maintain a stable sub 500 watt flame for greater than 15 minutes, achieve a sub 100 watt flame, and establish hands-free operation by integrating an igniter. The new auger and hopper package (Section 8.1.5) was integrated into this final Nano-Combustor design.

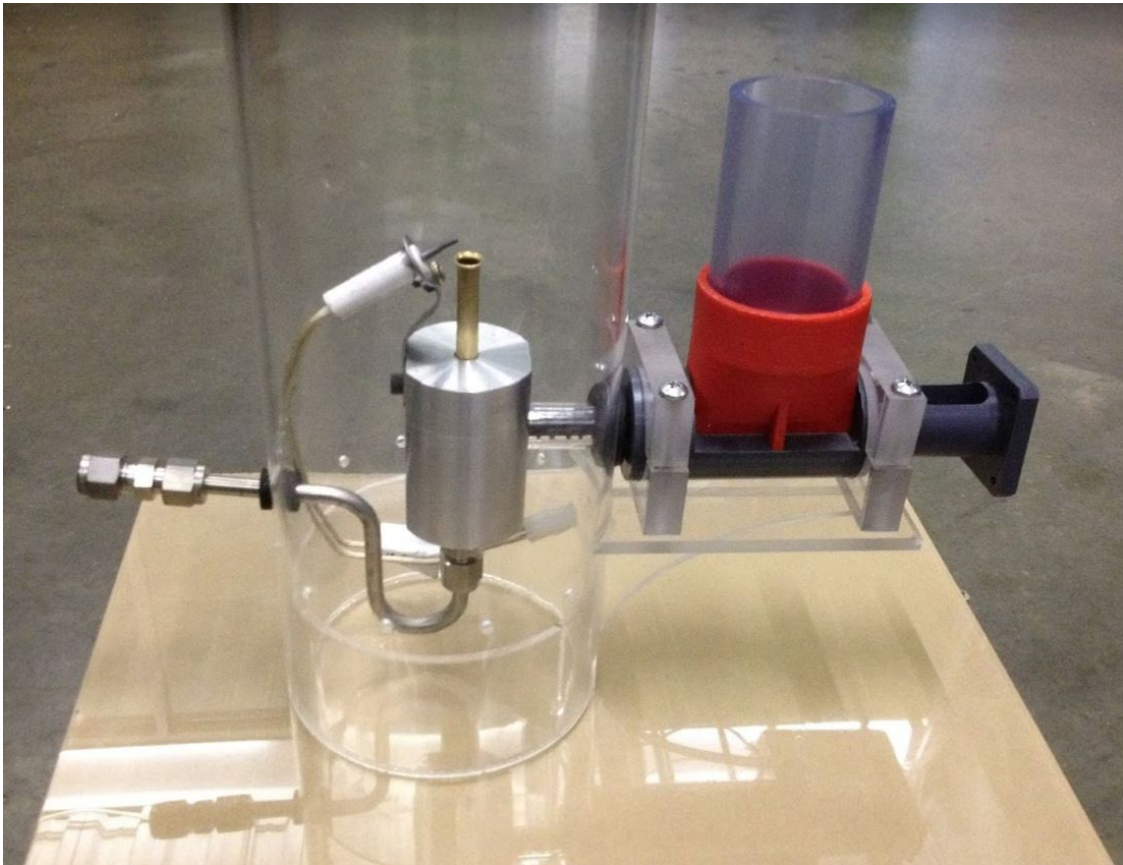


**Figure 8.8:** Final Nano-Combustor Assembly

The final design aimed to create a benchtop model used for testing and demonstration purposes. This design would also be the launching-point for testing with feces powder. As such, a 4.5" diameter acrylic cylinder was designed to contain the flame and extend beyond the top of the nozzle to restrain any fugitive unburned powder. This cylinder would also help maintain a quiescent environment around the flame and buffer it from any drafts in the hood or test room. The hopper

and auger assembly was designed to fasten to the outside of the acrylic cylinder. The bottom of the acrylic cylinder had twelve  $5/32$ " diameter holes drilled around the base to provide sufficient fresh air for combustion.

Another primary design update was to consolidate the  $1/16$ " orifice and tee fitting into one machined aluminum piece. This allowed an opportunity to reduce the distance between the auger and orifice, as well as create a tight-fitting interface between the auger housing and the tee fitting. The new tee fitting had a hole machined into the top to accommodate a  $9/32$ " brass tubing nozzle (0.253" ID). Shims would be utilized to test smaller diameter nozzles, if desired. The  $9/32$ " tubing was flared to  $45^\circ$  at the top for a flameholder, but it was made slightly smaller than Gen-3 Rev-3 to reduce powder buildup.

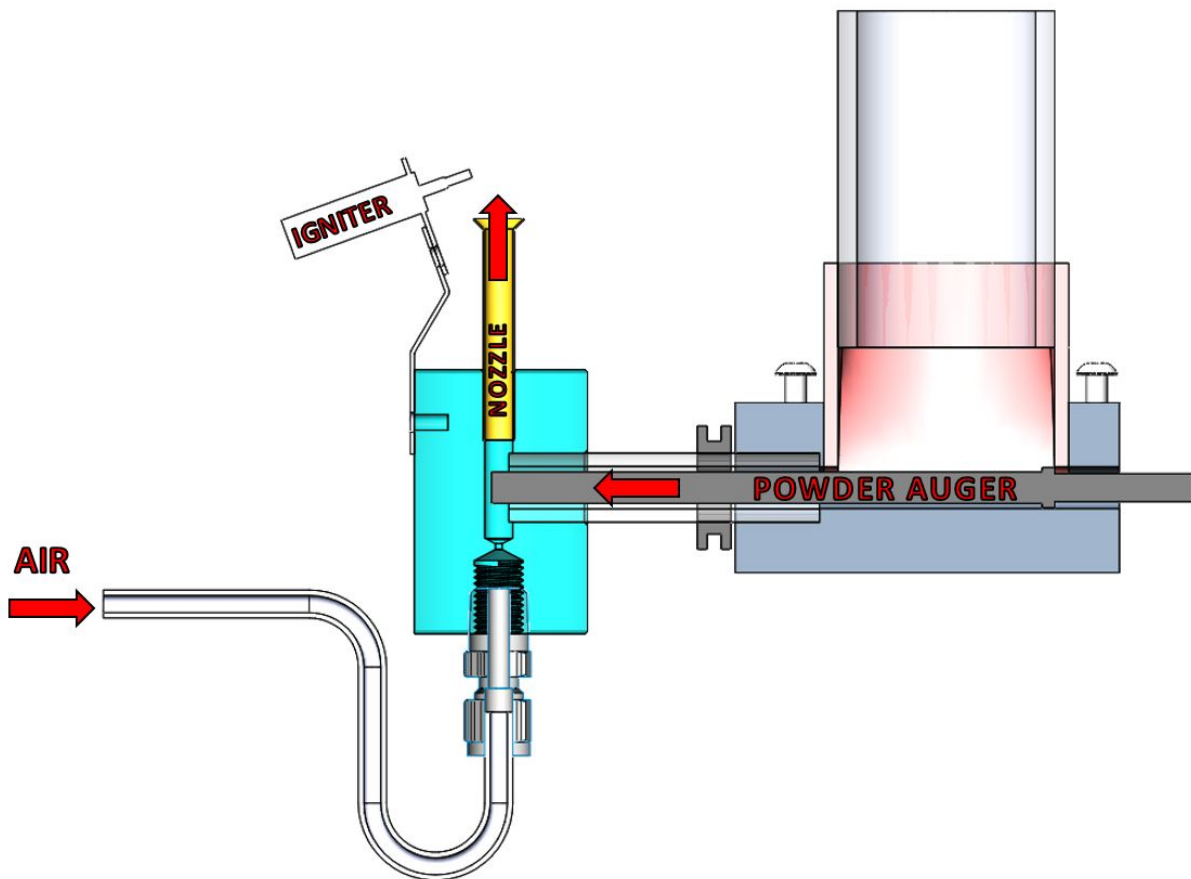


**Figure 8.9:** Section view schematic of final Nano-Combustor

A 12VDC hot surface igniter [39] was integrated into the Arduino control panel with a toggle switch so that the burner could be ignited from a distance (e.g. when feces testing). It was mounted at the tip of the nozzle.

The Nano-Combustor assembly was designed in Solidworks and the acrylic parts were cut out on a waterjet and joined together with acrylic glue.

Figure 8.8 shows a picture of the finished Nano-Combustor and Figure 8.9 shows a schematic section view from Solidworks.

### 8.2.1 Testing Results and Summary

The results from Gen. 3 Rev. 3 (Table 8.6) guided the set points for the final round of tests. The goal was to achieve a stable flame over a range of firepowers. The first test involved using Gen. 3 Rev. 3 set points: nozzle velocity at 0.1882 m/s and fuel-air concentration of 1586 g/m<sup>3</sup>. The expected firepower for these conditions was 169 watts, auger at 22.75 RPM, and air at 0.1751. The expected and actual results are shown below:

**Table 8.6:** Summary of initial test with the final Nano-Combustor design using lycopodium fuel

<b>Burner Version</b>	<b>Nozzle ID (in)</b>	<b>Auger RPM</b>	<b>FP (W)</b>	<b>Air Flow Rate (SLPM)</b>	<b>Nozzle Velocity (m/s)</b>	<b>Fuel-Air Concentration (g/m<sup>3</sup>)</b>
Final, Test 1 (expected)	0.253	39.9	295.8	0.3	0.1882	1586
Final, Test 1 (actual)	0.253	40	296.4	0.4	0.245	1221

This result shows a strong agreement with the expected set points. The nozzle velocity was slightly faster than expected because the fuel-air concentration was lower than anticipated. A flame did exist at 0.3 SLPM air, but appeared more well-anchored at 0.4 SLPM. It started to become clear that there was a range of set points and conditions for which a stable flame can exist. These conditions seemed to correlate to a broad range of fuel-air concentrations, where more stable flames existed above 1000 g/m<sup>3</sup> but could also exist in the 500-1000 g/m<sup>3</sup> range. It was perhaps difficult to become more stoichiometric because the pulsing of the auger (which was greatly improved with

the new revision, but still present) dropped the concentration below an ignitable limit causing the flame to extinguish.

Clearly there was also a nozzle velocity range that produced a stable flame. Figure 3.3 suggests that flamespeed is strongly related to fuel-air concentration, but also exists as a range at a specific concentration. The remaining goals of the final Nano-Combustor tests were to sweep firepowers and achieve a minimum 15-minute below 500 watts and a stable flame below 100 watts. To achieve a sub 100 watt flame the auger was set at 10 RPM, which corresponds to a 74 watt flame. The air was then swept until a flame stabilized. A stable flame was achieved and lasted about 5 minutes before extinguishing. As it burned, its length oscillated with the timing of the auger flight.

Through observation, higher firepower flames were more stable. Firepowers were swept from 150-300 watts and burn times greater than 15 minutes were achieved for all of the tests. Table 8.7 summarizes the primary test set points for different firepowers in the final Nano-Combustor design. Each firepower set point had a range of about  $\pm 0.1$ - $0.2$  SLPM from the stable central air flow rate. At the risk of over-complicating the results by giving the full air flowrate ranges for each firepower, only the stable central air flowrates are provided, and the concentrations and nozzle velocities are calculated using this number.

**Table 8.7:** Summary of final Nano-Combustor set points with lycopodium. All firepowers except the 75 watt burned for greater than 15 minutes

<b>Firepower (W)</b>	<b>Auger RPM</b>	<b>Nozzle ID (in)</b>	<b>Air Flow Rate (SLPM)</b>	<b>Nozzle Velocity (m/s)</b>	<b>Fuel-Air Concentration (g/m<sup>3</sup>)</b>
74.1	10	0.253	0.2	0.1225	611
148.2	20	0.253	0.2	0.1225	1221
185.3	25	0.253	0.4	0.245	763
222.3	30	0.253	0.3	0.1837	1221
296.4	40	0.253	0.4	0.245	1221
333.5	45	0.253	0.4	0.245	1374

As the firepower increased and testing continued for longer than 15 minute burns, the acrylic tube began to bubble and melt. Surely, a future combustor should incorporate glass for this cylinder.

After these tests concluded, experimentation continued, but the original 3/8" OD, 3/16" pitch auger broke due to overuse. More augers were 3D-printed, but the flight thickness decreased minimally. New firepower/RPM curves were created and are shown in Figure 8.11 next to the older curve. The new slope multiplier to calculate firepower from RPM became 9.055. It makes sense that the slope increased minimally because the thinner flights allowed for more powder volume in the auger. The old and new augers are shown in Figure 8.10 and the difference in flight thickness is evident. Although the data presented here corresponds to the thicker-flight auger, future tests should consider the subtle change in manufacturing and adjust the firepower flowrates accordingly.



**Figure 8.10:** 3/8" OD 3/16" pitch augers. New auger on top with thinner flights

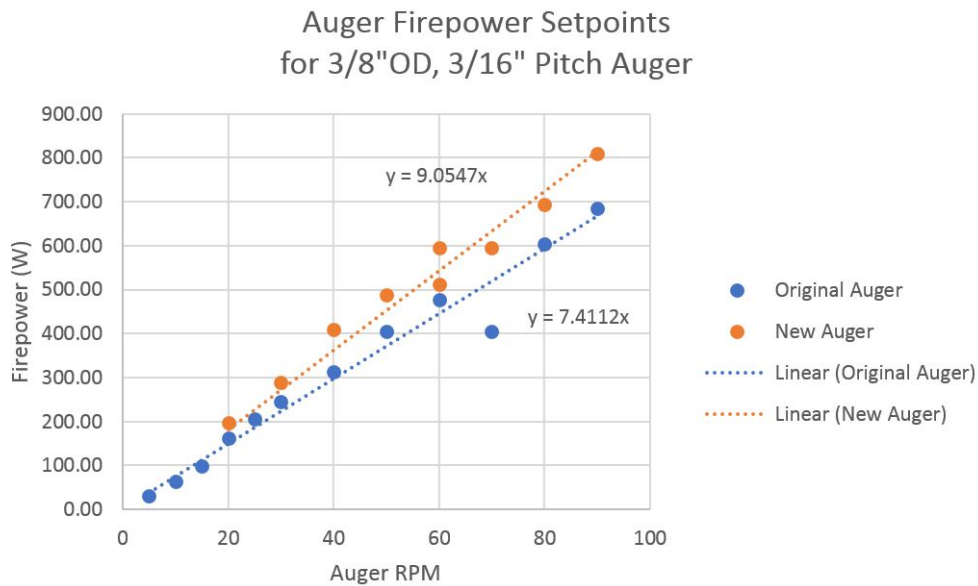


**Figure 8.11:** Firepower set points for old and new 3/8" OD augers

# Chapter 9

## Fuel Challenges

### 9.1 Observations From Testing

Fuel characteristics are crucial to the success of a stable powder burner. The project began by using cornstarch, which provided important insights but was ultimately abandoned because of its inability to flow and willingness to pack. Lycopodium used fresh from the container was an ideal fuel around which to develop the Nano-Combustor. But there were times during testing that *used* unburned lycopodium was used in the burner. The used lycopodium came from the firepower sweep tests for determining auger set points and had been run through the auger multiple times, but remained unburned. When this used lycopodium was burned, it clearly did not loft homogeneously and stable flames became difficult to achieve under the same conditions as the fresh lycopodium. It seemed that the surface of the lycopodium had changed in a way that caused it to clump to neighboring particles. Surface charge, shape, or moisture content could all contribute to the used lycopodium agglomerating. This reveals the challenges that will need to be faced when non-ideal (e.g. fecal) fuel is used. It also provides an opportunity to use the used lycopodium as the primary fuel to guide future hardware development on the path to eventually burning feces. Han et al. observed agglomeration in Lycopodium flames as well, but did not offer any insight to mitigating it [40] and [15].

When the flame would extinguish in the final Nano-Combustor tests, it was almost always due to buildup of ash and unburned powder on the outer rim of the nozzle. This occurred mostly in the low-firepower range (sub 175 watts). Figure 9.1 shows the potential severity of this build-up. As the fuel accumulated around the nozzle, unburned fuel would stick to the ash and occlude the main flow, causing the nozzle velocity to increase and the flame would eventually blow-off. This is beginning to be addressed by MSR with additional flameholder designs as of August, 2018 and is discussed in Chapter 10.



**Figure 9.1:** Lycopodium accumulating on Nano-Combustor nozzle and occluding bulk flow

## 9.2 Flow Regimes

Assuming fully developed flow in the nozzle, which is a fair assumption because of the nozzle's length, the Reynolds number was calculated as a function of air flow rate for the 9/32" OD brass nozzle. The *velocity factor*, defined as the nozzle velocity divided by the lycopodium terminal velocity was also calculated as a function of air flowrate to see how much higher than terminal velocity the flowrate in the nozzle was. These results are shown in Figures 9.3 and 9.2.

Figure 9.2 shows that the lower firepowers (which correspond to 0.1-0.2 SLPM air) on the 9/32" OD nozzle are only lofting the particles at 2-4 times the terminal settling velocity. These numbers assume 1-dimensional flow in a cylinder, but since the flow profile in a tube is parabolic for laminar flow, the low lofting velocities could become problematic. This might be why the

### 9/32" OD Nozzle Velocity Factor above Lycopodium Terminal Velocity

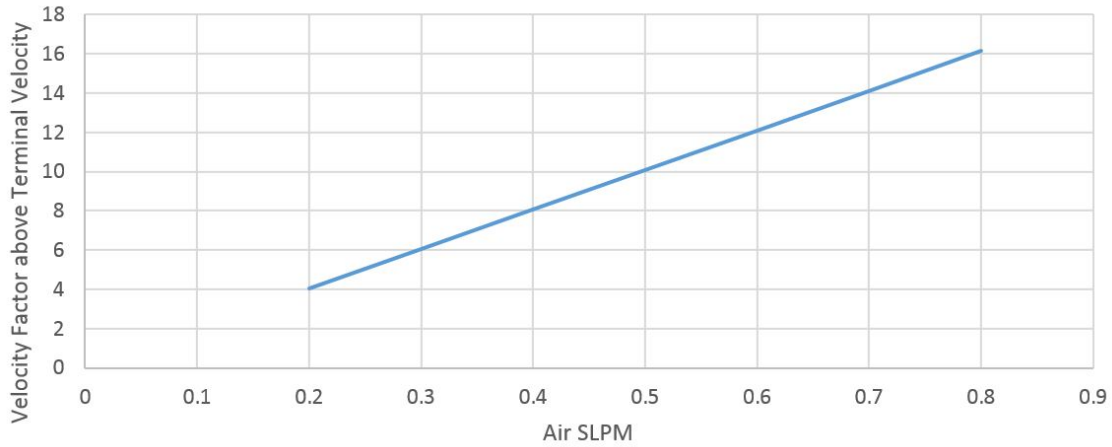


**Figure 9.2:** 9/32"OD nozzle velocity factor with lycopodium

particles settled out of the bulk flow and landed on the nozzle rim. Perhaps constricting the nozzle to a smaller diameter for low firepower testing would help fuel accumulation on the nozzle.

Figure 9.3 shows that the Reynolds number for the air set points were mostly in the transition zone. If there was a way to bring the flow into fully turbulent, fuel-air mixing may increase, but nozzle exit velocities may become too high and liftoff might become an issue.

### Reynolds Numbers for 9/32"OD Nozzle, Fully Developed Flow

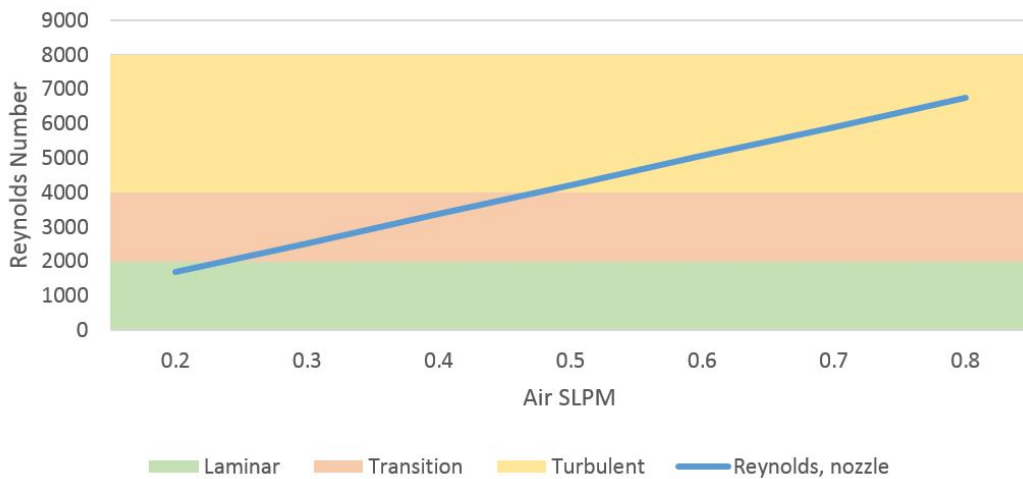


**Figure 9.3:** 9/32"OD nozzle Reynolds numbers

### 9.3 Agglomeration and Particle Microscopy

In an effort to begin to understand the particle agglomeration occurring with the used lycopodium and feces (which is discussed in-depth in Chapter 11), particles were observed under a microscope. A small amount of powder was dropped onto each slide from a height of 1.5-2 feet to try and disperse clumps naturally. Some images from the microscopy are shown below, with additional images in Appendix F.



**Figure 9.4:** Fresh lycopodium, 80x magnification

The agglomerates in the used lycopodium (Fig. 9.5) are clearly distinguishable from the well-separated particles of fresh lycopodium (Fig. 9.4). The clumps in the human feces (Fig. 9.6) are also evident, especially because the fecal particles had been sifted to 0-44  $\mu\text{m}$ , yet the clumps exceed 100  $\mu\text{m}$  in diameter.

An understanding of agglomeration from fuel processing and handling is clearly a facet from this study that needs to be explored further. It would be interesting to examine the aerodynamic diameter distribution of agglomerated particles from different grinding and handling situations.

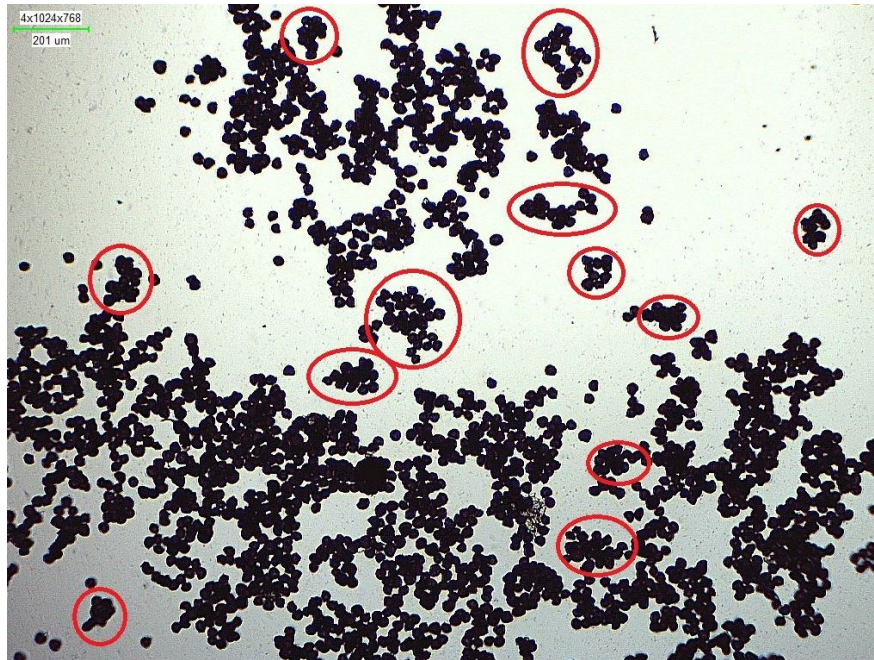


**Figure 9.5:** Used lycopodium, 80x magnification, agglomerates circled

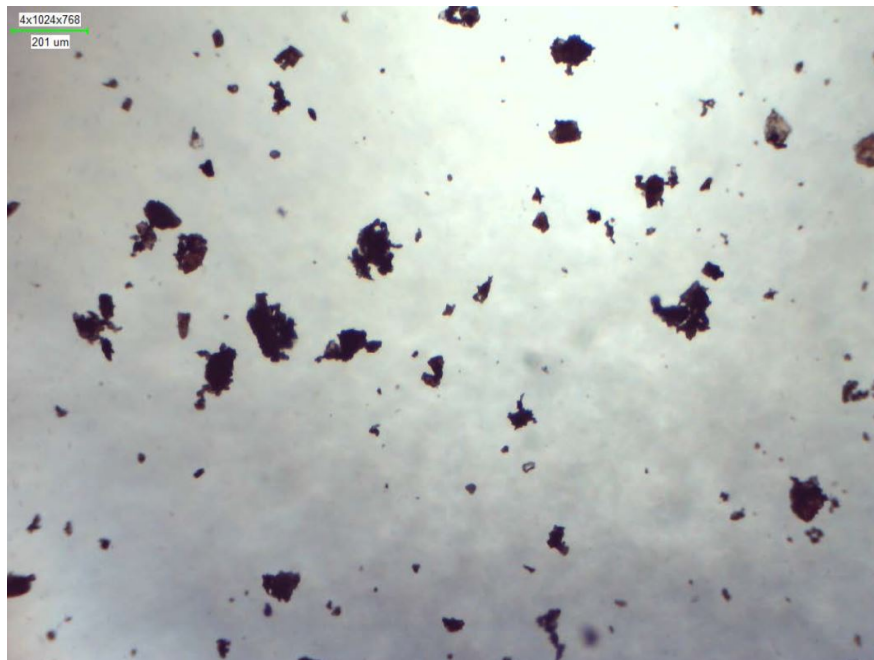


**Figure 9.6:** Human Feces, 0-44  $\mu\text{m}$ , 80x magnification

Designing flowrates for terminal velocities of agglomerated particles may be necessary for successfully lofting and burning these particle groupings.

Fuel handling can be revamped as well. One simple solution is to create a variable-pitch auger whose pitch increases toward the exit (Figure 9.7). This would prevent particles from packing through the entire auger and it would create some space in the auger flights for the particles to flow freely. MSR is exploring auger redesign as of August 2018 and variable pitch augers are showing some promise when handling used lycopodium.

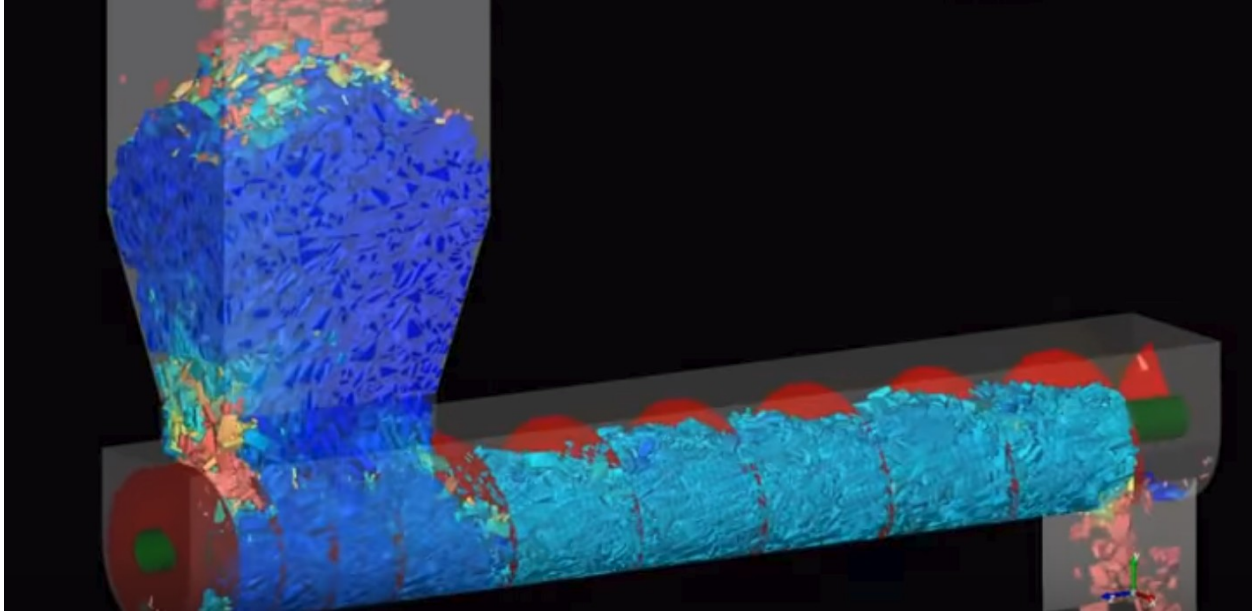


**Figure 9.7:** Auger with decreasing pitch creates partially-full flights [41]

# Chapter 10

## Further Hardware Improvements

After demonstrating a sub-100 watt flame using idealized biomass fuel, CSU stepped back from the primary development on the project and MSR began further hardware development in order to eventually transition to a powdered fecal burner. The main foci to improve upon are: prevent fuel build-up on the nozzle rim, improve fuel delivery consistency, and improve lofting when using highly agglomerated or larger diameter (40-100  $\mu\text{m}$ ) particles. These are currently addressed respectively through an investigation of alternative flameholder shapes, auger redesign, and interchangeable lofting orifices.

The hardware development detailed in this chapter is current as of August, 2018. It is still too early to provide conclusive evidence on the efficacy of the different hardware iterations, but the following summary of the project's state of the art will help guide future work.

### 10.1 Flameholders

The flared nozzle used in CSU's Nano-Combustor worked well for achieving stable flames below 500 watts, but there were some tests where ash and fuel accumulated on the nozzle rim and the occlusion of bulk flow caused the flame to lift-off and extinguish. Figure 9.2 shows the bulk flow velocity divided by particle terminal velocity as a function of air flowrate. It shows that for flowrates creating a 100 watt flame, the air velocity was only 2-4 times the lofting velocity of a particle (for 1-dimensional flow). When taking into account varying particle size, agglomeration, and 3-dimensional flow it isn't surprising that fuel and ash collected on the nozzle rim. This is being addressed by increasing air velocity (by increasing air flowrate and decreasing nozzle diameter) and incorporating redesigned flameholders.

The new flameholders developed at MSR are guided by their experience in the camp-stove industry. Various shapes and patterns were laser cut and tested. They are mounted to a sleeve that can index at any height on the nozzle, which allows testing various distances from the nozzle rim.



**Figure 10.1:** Examples of flameholder designs at MSR

In these tests, the flared nozzle used by CSU was abandoned because the external flameholder apparatus takes its place. Figure 10.1 shows some of the different flameholder styles explored. Some of them locate the flame above the flameholder and others hold the flame within the flameholder. The notches on the flameholder may act as fins, increasing heat transfer and locally decreasing the flamespeed, which helps anchor the flame. These tests are currently being carried out with fresh lycopodium powder with the goal of testing other more difficult fuels including feces.

The initial results are encouraging because the higher air velocities do prevent fuel buildup. The flame still has difficulty locating itself at a stable location on the flameholder; although the flame persists, it will often jump along the vertical axis which decreases its stability.

## 10.2 Fuel Delivery

Achieving constant fuel delivery was a challenge through the entire project. As firepower decreased, auger RPM also decreased and the pulsing in the fuel delivery from the auger flight passing the fuel exit point became more apparent. This was initially addressed by decreasing outer flight diameter and decreasing the auger pitch. MSR has continued with this concept by

exploring an even more compact outer diameter to shaft diameter ratio (decrease flight volume). As discussed in Chapter 9, variable pitch and variable shaft diameter augers were also 3D-printed to try and reduce fuel packing along the length of the auger. Initial tests with used lycopodium through these variable augers indicates that the redesign helps increase powder flowability. Figure 10.2 shows some of the MSR-redesigned augers.

Vibratory fuel delivery is current in the nascent stages of investigation at MSR. An engraver and a cell phone vibrator were used to deliver vibration to a fuel feeding tube with cornstarch. The vibrations caused the cornstarch to flow freely out of the tube. This investigation could provide a promising alternative technology to using an auger for fuel delivery. It is unclear the effect that vibration frequency and amplitude have on fuel feedrate, as well as any other parameters that may affect fuel delivery.

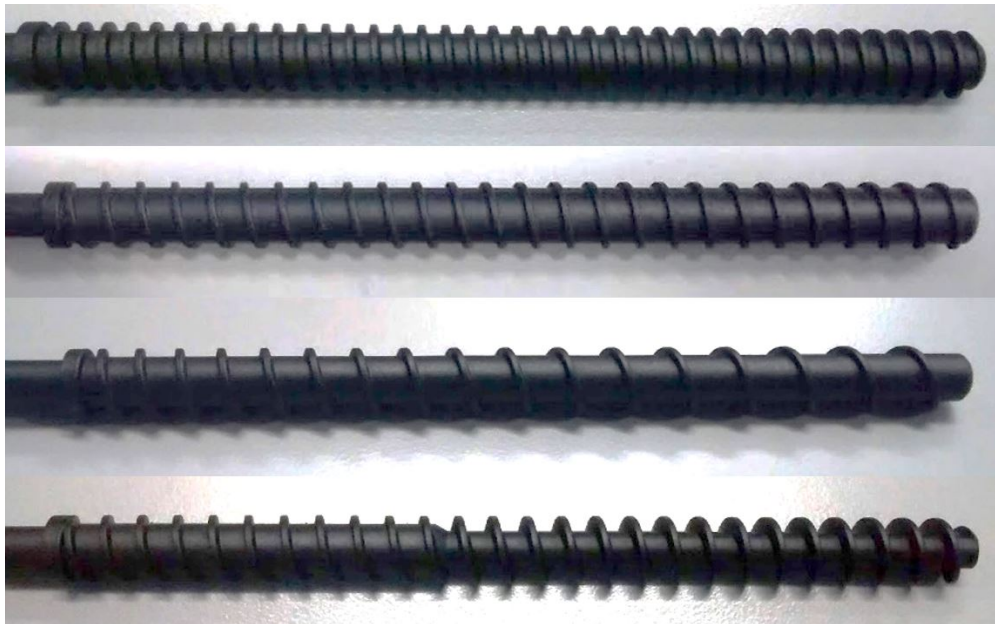


**Figure 10.2:** Redesigned augers at MSR including variable pitch and variable shaft diameter (bottom)

## 10.3 Lofting Orifices

In order to address larger particle size and agglomeration, lofting orifice iteration is being explored by MSR. Their strength as a stove manufacturer makes them ideal for exploring jet diameters. MSR redesigned the tee fitting to accept modular lofting orifices as shown in Figure 10.3. The orifices range in diameter from 0.013" to 0.125" (Figure 10.4).

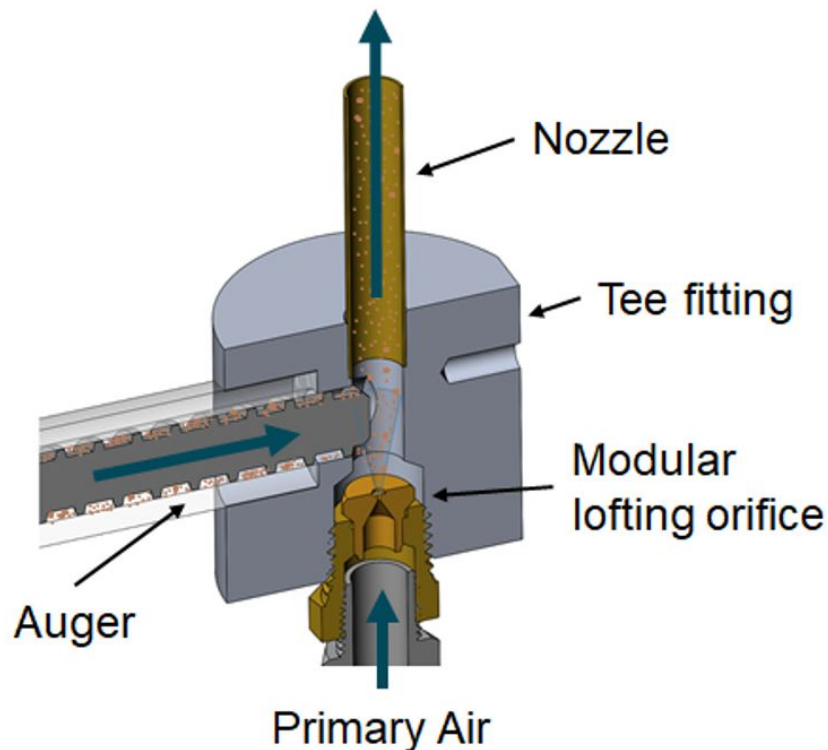


**Figure 10.3:** Updated tee-fitting with interchangeable lofting orifices, developed at MSR

It is possible that the high velocity through the smallest orifices may actually be strong enough to break up particle agglomerates. This must be explored further with a thorough exploration of particle clumping using optical examination. Initial tests indicate an improved flame using small orifices and used lycopodium.

Of course, the added energy burden of a small orifice must be recognized. The energy required to overcome the pressure drop in a 0.013" orifice is likely far too great for the final product de-

velopment. It is a valuable exploration at this point in the project, though, especially with the upcoming transition to powdered feces testing.



**Figure 10.4:** Lofting orifices ranging from 0.013" to 0.125" developed at MSR

# Chapter 11

## Fecal Processing and Testing

### 11.1 Grinding and Size Selection

Although feces was not the focal fuel for this version of the Nano-Combustor, feces nonetheless was tested in the final version of the Nano-Combustor. Since the importance of small particle size became clear during the project, a feces grinding and sieving system was developed that provided an *ideal-sized* powdered fecal fuel.

ASTM dust combustion tests screen particle samples to below  $75\ \mu\text{m}$  [42], so  $75\ \mu\text{m}$  was decided as the upper size limit of fecal fuel. Three ASTM screens were purchased: 40 mesh ( $420\ \mu\text{m}$ ), 200 mesh ( $74\ \mu\text{m}$ ), and 325 mesh ( $44\ \mu\text{m}$ ). The sieves were stacked with the coarsest mesh on top and a solid tray on the bottom, which allowed the feces to be classified into 4 size bins:  $0\text{-}44\ \mu\text{m}$ ,  $44\text{-}75\ \mu\text{m}$ ,  $75\text{-}420\ \mu\text{m}$ , and  $> 420\ \mu\text{m}$ .



**Figure 11.1:** Sieve stack with coarsest mesh on top

The dried feces was obtained by RTI via the RTTC fecal gasifier project. A standard coffee grinder was used to pulverize the dried feces, and then the fecal material was placed in the sieve-stack. The stack was vibrated until the material settled into each respective size bin.

### 11.1.1 Sieve Vibrator

A professional-grade sieve vibrator was initially purchased for this project [43], but the processing duration overheated the motor, so a vibrator was built out of a re-purposed palm sander. The sander body was mounted via sheet metal to a piece of 12" X 12" X 1/2" plywood. The sieve stack was sandwiched between this piece of plywood on the bottom and an identical one on top. It was an effective low-cost solution to classifying fecal powder by size.



**Figure 11.2:** Sieve vibrator made out of a re-purposed palm-sander

## 11.2 Fecal Combustion Testing

### 11.2.1 Test Enclosure

A sand-blasting cabinet [44] was purchased and assembled to be used as a feces test enclosure. The cabinet is portable, sealed from the outside, has built-in gloves, and a clear top for viewing. It also has the ability to be retrofitted with a chimney vent containing an in-line HEPA filter, and dust collection ports for cleaning. For this phase of the project, though, a fume hood sufficed for the minimal feces testing, and the blast cabinet remains unused but available for future phases of fecal testing.

### 11.2.2 Nano-Combustor Fecal Testing

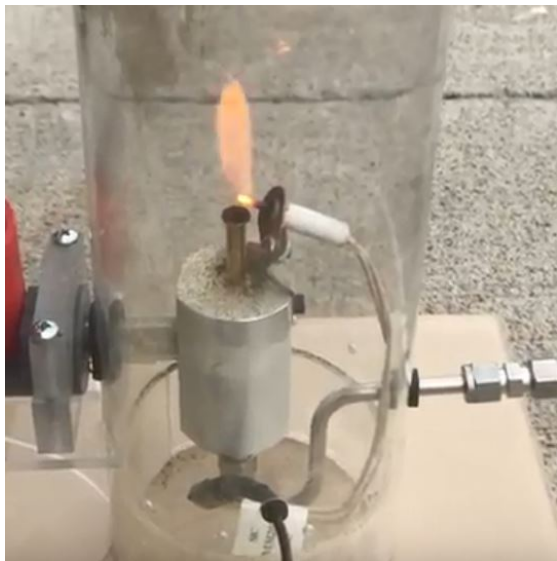
Feces was tested in the final Nano-Combustor revision (Ch. 8). Four main tests were run with powdered feces based on fuel sizing: one with 0-44  $\mu\text{m}$  feces, one with 44-74  $\mu\text{m}$  feces, one mixed 50/50 of those two size bins of feces, and one with 50% of 0-44  $\mu\text{m}$  feces and 50% fresh lycopodium powder. This phase of the Nano-Combustor project did not require feces testing, these tests were primarily exploratory and qualitative in nature.

In all of the tests, the clumping of the feces was terrible and caused the fuel to *spill* out of the nozzle at times instead of lofting. A number of air flowrates were used to try and loft the fuel more successfully, but there was no success achieving a steady or stable flame. The ignitor was left on through the duration of all tests because the flame was so intermittent. The lycopodium and feces mixture burned slightly better, but the flame remained inconsistent and fuel still clumped. Images of two fecal flames can be seen in Figure 11.3.

**Table 11.1:** Summary of Nano-Combustor fecal testing

<b>Fuel</b>	<b>Nozzle Diameter (in)</b>	<b>FP (W)</b>	<b>Air Flow Rate (SLPM)</b>	<b>Nozzle Velocity (m/s)</b>	<b>Fuel-Air Concentration (<math>\text{g}/\text{m}^3</math>)</b>
44-74 $\mu\text{m}$ feces	0.25	223	0.6	0.367	995
50/50: 0-44 $\mu\text{m}$ feces/fresh lyco.	0.25	366	0.5	0.306	1492

For feces firepower estimates, the main simplifying assumption was that the auger delivered the same grams per second as lycopodium, but firepower was calculated using feces' LHV (India human feces, Table 3.1). In Figure 11.3a, feces sized between 44-74  $\mu\text{m}$  was used, and air flowrate set to 0.6 SLPM. The 3/8" OD auger with 3/16" pitch was used at 40 RPM, which equals an estimated 0.0119 g/s of fuel. This equals about 223 watts firepower, and 995  $\text{g}/\text{m}^3$  concentration (assuming homogeneous and complete lofting, which wasn't the case). Figure 11.3b shows a 50/50 mixture of fresh lycopodium powder and feces sieved below 44  $\mu\text{m}$ . 0.5 SLPM air was used with the same auger at 50 RPM. This equals an estimated 0.0148 g/s of fuel, 365.9 W firepower (averaging the feces and lycopodium LHV), and 1492  $\text{g}/\text{m}^3$  fuel-air concentration. The setpoints from the two fecal tests depicted in Figure 11.3 are summarized in Table 11.1. The feces flame was most stable at these set points, but perhaps would have been more stable if a richer concentration was able to loft. It was difficult to get the fuel-air concentration higher, though, because as fuel flowrate increased, the air flowrate had to increase proportionally to keep the additional fuel lofted. More fuel-rich mixtures would end up spilling out of the top of the nozzle rather than lofting.



(a) 100% powdered feces



(b) 50/50 lycopodium/feces

**Figure 11.3:** Initial powdered fecal flames with Nano-Combustor hardware

These tests foreshadow significant fuel-processing challenges for the future of the project. It is clear that the fuel must loft as discrete particles with the smallest diameter possible to have a successful stable flame.

The mechanism which causes the particles to agglomerate is unknown, though Ogle suggests that many of the challenges faced in dust combustion stem from particle surface conditions [12]. Surface shape and texture can make a particle more likely to stick to other particles, and surfaces can develop static charges that draw them into agglomerations. Additionally, moisture adsorption (or absorption) on the surface of the particle could cause the particles to stick. This was addressed in the fecal testing by running the powdered feces through a kiln at 150°F for 12 hours and then tested in the Nano-Combustor immediately after, but there could be complicating factors.

Another contributor to particle agglomeration may be the fuel conveying system. The packed tumbling that occurs in the auger might create an environment that forces the particles into larger clumps. One change in auger design that will address this in future revisions is an auger with increasing pitch (Fig. 9.7, and discussed in Chapter 9). This would allow the flights at the end of the auger to only be partially full and may allow the feces to be more free-flowing.

Since the powdered feces was severely agglomerated, little design modification went into the nozzle geometry nor specific air or fuel flowrates. Based on the observations gained through the project, the foundation necessity for the dust combustor to work is to have a homogeneous distribution of lofted particles at the nozzle exit. One way to visually check this is to run the mixture very fuel lean and with high air flow rates, which increases the air velocity and would create a best-case situation for particle suspension. These operating conditions did not create a visibly homogeneous dust cloud with feces, and so the focus must turn to fuel processing, conveying, and to a lesser extent, lofting velocity.

As of August, 2018, MSR began testing feces powder with their smallest air orifice in the newest hardware iteration (Chapter 10). The smallest orifice size creates slightly better lofting, but the flame is still inconsistent and very unstable. At this time, MSR is also beginning to look at variable pitch and variable shaft diameter augers to reduce fuel packing.

The observations and challenges with clumping and old lycopodium powder (see Chapter 9) make it a good intermediate surrogate for feces testing. Small amounts of anti-caking additives are also being explored to help keep the feces powder free-flowing and into separate particles, but the combustion properties of any fuel additives must be considered.

# Chapter 12

## Conclusions

### 12.1 Summary of Findings

The process of developing a stable-flame dust burner provided many insights toward the path of a low-firepower fecal dust combustor. CSU exceeded their deliverable of a stable 500 watt flame by demonstrating a stable flame in the 150-300 watt range as well as a less-stable 75 Watt flame. The simple models and calculations used to iterate hardware design were successful in guiding initial fuel and air flowrates. The nozzle velocity and fuel-air concentration were valuable data points to develop hardware around.

Through each hardware iteration, it was found that the concentrations which produced stable flames were well above the stoichiometric values in Table 3.3. Often the equivalence ratio was  $5 < \Phi < 10$ . These fuel rich values might be justified by Ogle's explanation of dust flames as incomplete combustion due to slower rates of transport and kinetics [12]. Han also observes a decreased fuel concentration gradient in the flame preheat zone [40]. The elevated temperature in the preheat zone would create gas expansion and may locally lean-out the fuel-air concentration at the flame front.

The exploration of fluidized beds led to the development of the lofting orifice and the fuel-dosing auger. Auger development led to development of a 3/16" pitch, 3/8" outer diameter auger, which rotated quickly enough in the 150-300 watt range to make fuel pulsing negligible for the success of this phase of the project. Continuing to smooth out the fuel delivery system remains a primary task of the project's future development. Feces' lower LHV means that auger rotation will increase for equal firepower compared to lycopodium tests. This inherent increase in rotation and fuel delivery may help with the success of powdered feces combustion.

Fuel sizing and lofting will remain one of the primary challenges of this project moving forward. Agglomeration was observed microscopically in used lycopodium and feces powder.

Clumping of the fuel should be addressed through preventive measures (e.g. auger redesign, fuel grinding, moisture content, or addition of anti-caking agents) or burner design (e.g. lofting orifices, flameholders, or operating set points).

MSR's continued development of the Nano-Combustor will provide key insights into transitioning to a powdered feces burner. Their development of flameholders is showing promise in stabilizing the flame while mitigating fuel buildup and flow occlusion.

## 12.2 Suggestions for Future Work

In the continued development of the Nano-Combustor, there are some alternative pursuits that might provide some insight into successful fecal combustion. An interesting academic pursuit would be to explore the addition of low levels (well-below stoichiometric) of gaseous fuels into the dust mixture to help stabilize the flame.

Swirl has also been shown to stabilize a flame by increasing turbulence [6]. MSR's recent flameholders allude to this phenomenon but do not introduce strong swirl at the flame. Redirecting the bulk flow path helically before the nozzle exit would be one way to introduce swirl and improve flame stability.

Fluidized bed combustors are an alternative combustor that uses high velocity air to combust pieces of fuel mixed with an inert material (often sand). These combustors offer an interesting pursuit because limestone powder could be added to the feces mixture as the inert material. The limestone powder would be able to sequester sulphur emissions from the feces, which is currently an emissions challenge in the larger fecal gassifier [6] [5].

Emissions will eventually need to be characterized for the fecal Nano-Combustor. Understanding combustion efficiency and exhaust constituents may provide some insight into the particulars of fecal dust combustion.

Fuel processing is a whole facet of the success of the fecal Nano-Combustor that must be thoroughly explored. Differences in grinding methods may affect how easily the feces agglomerates or combusts. A thorough study of the powder under microscope, including utilizing scanning electron

microscope imagery, would prove beneficial. Also studying the aerodynamic properties of fecal powder from different grinding sources would help establish lofting velocities and future hardware design.

# Bibliography

- [1] Otto von Guericke University Magdeburg Germany. Online material: Hopper design. [http://www.mvt.ovgu.de/mvt\\_media/Vorlesungen/Lecture\\_SFPS/Folien\\_SFPS\\_4.pdf](http://www.mvt.ovgu.de/mvt_media/Vorlesungen/Lecture_SFPS/Folien_SFPS_4.pdf). [Online; accessed 17-July-2018].
- [2] World Health Organization. Sanitation. <http://www.who.int/news-room/fact-sheets/detail/sanitation>. [Online; accessed 10-July-2018].
- [3] News Medical Life Sciences. <https://www.news-medical.net/health/What-are-Helminths.aspx>.
- [4] Bill & Melinda Gates Foundation. Water, Sanitation & Hygiene: Reinvent the Toilet Challenge. [https://docs.gatesfoundation.org/Documents/Fact\\_Sheet\\_Reinvent\\_the\\_Toilet\\_Challenge.pdf](https://docs.gatesfoundation.org/Documents/Fact_Sheet_Reinvent_the_Toilet_Challenge.pdf). [Online; accessed 10-July-2018].
- [5] Maxwell Flagge. Development of a Combustion System for Fecal Materials. Master's thesis, Department of Mechanical Engineering, Colorado State University, Fort Collins, CO, 2017.
- [6] Stephen R. Turns. *An Introduction to Combustion: Concepts & Applications*. New York: McGraw-Hill, 3rd edition, 2012.
- [7] T.B. Reed. A Survey of Biomass Gasification, Volume II - Principles of Gasification. Technical report, Solar Energy Research Institute, 1979.
- [8] William C. Hinds. *Aerosol Technology: Properties, Behavior, & Measurement of Airborne Particles*. John Wiley & Sons, Inc, 2nd edition, 1999.
- [9] Gordon L. Dugger. Flame stability of preheated propane-air mixtures. *Industrial & Engineering Chemistry*, 47(1):109–114, 1955.
- [10] Rolf K. Eckhoff. *Dust Explosions in the Process Industries*. Gulf Professional Publishing, 3rd edition, 2003.

- [11] Trygve Skjold. *Flame propagation in dust clouds: Numerical simulation and experimental investigation*. PhD thesis, Department of Physics & Technology, University of Bergen, Norway, June 2014.
- [12] Russell Ogle. *Dust explosion dynamics*. Butterworth-Heinemann Ltd, 2016.
- [13] Arthur W. Adamson. *Physical Chemistry of Surfaces*. John Wiley & Sons, 6th edition, 1997.
- [14] NFPA. *NFPA 654: Standard for the Prevention of Fire and Dust Explosions from the Manufacturing, Processing, and Handling of Combustible Particulate Solids*. National Fire & Protection Association, 2005.
- [15] Ou Sup Han, Masaaki Yashima, Toei Matsuda, Hidenori Matsui, Atsumi Miyake, and Terushige Ogawa. Behavior of flames propagating through lycopodium dust clouds in a vertical duct. *Institute of Advanced Sciences*, 13(6):449–457, 2000.
- [16] Christophe Proust. Flame propagation and combustion in some dust-air mixtures. *Journal of Loss Prevention in the Process Industries*, 19(1):89–100, 2006.
- [17] S.H. Chan, editor. *Transport Phenomena in Combustion: proceedings of the Eighth International Symposium on Transport Phenomena in Combustion*, volume 1, San Francisco, CA, July 1995. Pacific Center of Thermal-Fluids Engineering, Taylor & Francis.
- [18] Martin Hertzberg, Ronald S. Conti, and Kenneth L. Cashdollar. Spark ignition energies for dust-air mixtures: Temperature and concentration dependences. *Symposium (International) on Combustion*, 20(1):1681–1690, 1985.
- [19] Stephanie I. Vogel, Bryan T. Piatkowski, Alton C. Dooley Jr., and DorothyBelle Poli. The effects of fire on lycopodium digitatum strobili. *Jeffersoniana Virginia Museum of Natural History*, (27):1–9, 2011.
- [20] Emmanuel Kwasi Addai. *Investigation of Explosion Characteristics of Multiphase Fuel Mixtures with Air*. PhD thesis, Otto-von-Guericke University Magdeburg Germany, August 2016.

- [21] C. Rose, A. Parker, B. Jefferson, and E. Cartmell. The characterization of feces and urine: A review of the literature to inform advanced treatment technology. *Critical Reviews in Environmental Science and Technology*, 45(17):1827–1879, 2015.
- [22] Chunmiao Yuan, Chang Li, Gang Li, and Peihong Zhang. Determination of kinetic parameters of maize starch in air using thermogravimetric analysis. *Advanced Materials Research*, 508:114–117, 2012.
- [23] Rita Schenck and Douglas Huizenga, editors. *Construction cost of plant compounds provides a physical relationship for co-product allocation in life cycle assessment - Proceedings of the 9th International Conference on Life Cycle Assessment in the Agri-Food Sector*, San Francisco, CA, October 2014. American Center for Life Cycle Assessment.
- [24] Elemental Microanalysis Limited. Certificate of analysis part no. b2274 wheat flour standard. <https://www.elementalmicroanalysis.com/Downloads/B2274-2540-60801.pdf>. [Online; accessed 24-July-2018].
- [25] Sourdough Library. Ash content of american and european flour types. <http://www.sourdoughlibrary.org/flour-ash-content/>. [Online; accessed 25-July-2018].
- [26] A. Patwa, B. Malcolm, J. Wilson, and R. P. K. Ambrose. Particle size analysis of two distinct classes of wheat flour by sieving. *Transactions of the American Society of Agricultural and Biological Engineers*, 57(1):151–159, 2014.
- [27] Ram Shankar Subramanian, Clarkson University. Flow through packed beds and fluidized beds. [https://www.researchgate.net/publication/237496902\\_Flow\\_through\\_Packed\\_Beds\\_and\\_Fluidized\\_Beds](https://www.researchgate.net/publication/237496902_Flow_through_Packed_Beds_and_Fluidized_Beds). [Online; accessed 30-July-2018].
- [28] M.D. Horton, F.P. Goodson, and L.D. Smoot. Characteristics of flat, laminar coal-dust flames. *Combustion and Flame*, 28:187–195, 1977.

- [29] H.M. Cassel, A.K. Das Gupta, and S. Guruswamy. Factors affecting flame propagation through dust clouds. *Symposium on Combustion and Flame, and Explosion Phenomena*, 3(1):185–190, 1948.
- [30] W.E. Mason and M.J.G. Wilson. Laminar flames of lycopodium dust in air. *Combustion and Flame*, 11(3):195–200, 1967.
- [31] Fox Venturi Products, mini-eductor, part # 611210-030-SS.
- [32] Robert C. Weast, editor. *CRC Handbook of Chemistry & Physics*. 49th edition, 1968.
- [33] J.J. Fitzpatrick, S.A. Barringer, and T. Iqbal. Flow property measurement of food powders and sensitivity of Jenike’s hopper design methodology to the measured values. *Journal of Food Engineering*, 61(3):399 – 405, 2004.
- [34] David Escudero Guevara. Bed height and material density effects on fluidized bed hydrodynamics. Master’s thesis, Iowa State University, Ames, Iowa, 2010.
- [35] Clayton T. Crowe. *Multiphase Flow Handbook*. CRC Press, 2006.
- [36] W.E. McCabe, J.C. Smith, and P. Harriott. *Unit Operations of Chemical Engineering*. McGraw Hill, 2001.
- [37] Adafruit, NEMA-17 Stepper Motor, 200 steps/rev, 12VDC, 350 mA, 20 N\*cm Torque. <https://www.adafruit.com/product/324>.
- [38] Sparkfun Stepper Motor, 400 steps/rev, 12VDC, 1.7A, 48 N\*cm Torque. <https://www.sparkfun.com/products/10846>.
- [39] Surface Igniter, 12VDC BBQ Grill Hot Surface Igniter. <http://www.surfaceigniter.com/bbqgrills.html>.
- [40] Ou Sup Han, Masaaki Yashima, Toei Matsuda, Hidenori Matsui, Atsumi Miyake, and Terushige Ogawa. A study of flame propagation mechanisms in lycopodium dust clouds

based on dust particles' behavior. *Journal of loss prevention in the process industries*, 14(3):153–160, 2001.

[41] Cadfem UK, ROCKY DEM - Variable Pitch Screw Feeder. [https://www.youtube.com/watch?v=PQi9U8\\_GAVQ](https://www.youtube.com/watch?v=PQi9U8_GAVQ).

[42] John Passero, lab manager EMSL Analytical Inc. On ASTM combustible dust testing. Personal Communication, 26 February, 2018.

[43] Gilson Co, Inc., Wet/Dry 8" Sieve Vibrator, Model SS-23. <https://www.globalgilson.com/wetdry-sieve-vibrator>.

[44] Central Pneumatic 40. Lb Capacity Floor Blasting Cabinet. <https://www.harborfreight.com/abrasive-blast-cabinet-68893.html>.

# Appendix A

## Combustion Calculator

```
clear; clc;

%% Inputs

% Cornstarch:
% 17572 kJ/kg

% phi = 1;
% m_dot_fuel = 500/3600/1000; %kg/s
% T = 800+273.15; LHV = 0;
%
% % Input mass fractions
% mf.C = 50.62;
% mf.H = 6.78;
% mf.N = 4.79;
% mf.O = 21.9;
% mf.S = 0.99;
% mf.ash = 14.92;

[mf, phi, m_dot_fuel, T, LHV, mass_based] = func_GUI_inputs;

%% Constants
P = (12.3/14.6959)*101325; %Pa, taken to be pressure in Fort Collins
Ru = 8315; % J/kmol-k
%Molar Masses, kg/kmol
MW.C = 12.011;
MW.H = 1.0079;
MW.O = 15.999;
```

```

MW.N = 14.0067;
MW.S = 32.065;
MW.air = 28.9645;
MW.CO2 = MW.C + 2*MW.O;
MW.H2O = MW.H*2 + MW.O;
MW.N2 = 2*MW.N;
MW.SO2 = MW.S + 2*MW.O;
MW.O2 = 2*MW.O;

%% Convert Mass-based to moles
if mass_based == 1
    % Convert to ashless mass fraction
    Y.ashless = mf.C + mf.H + mf.N + mf.O + mf.S;
    Y.C = mf.C/Y.ashless;
    Y.H = mf.H/Y.ashless;
    Y.O = mf.O/Y.ashless;
    Y.N = mf.N/Y.ashless;
    Y.S = mf.S/Y.ashless;

    % Convert to molar fuel chemistry CaHbOcNdSe

    MW.fuel = 1/(Y.C/MW.C + Y.H/MW.H + Y.O/MW.O + Y.N/MW.N + Y.S/MW.S); % ...
        ashless fuel, kg/kmol, EQ 2.12b

    % mole fractions of fuel constituents, eq 2.11b
    a = Y.C*MW.fuel/MW.C;
    b = Y.H*MW.fuel/MW.H;
    c = Y.O*MW.fuel/MW.O;
    d = Y.N*MW.fuel/MW.N;
    e = Y.S*MW.fuel/MW.S;

else % if inputs were already molar-based
    a = mf.C;

```

```

b = mf.H;
c = mf.O;
d = mf.N;
e = mf.S;

MW.fuel = a*MW.C + b*MW.H + c*MW.O + d*MW.N + e*MW.S;
end

%% Combustion Equation: CaHbOcNdSe + A(O2 + 3.76N2) --> aCO2 + b/2H2O + ...
(d/2 + 3.76A)N2 + eSO2 + fO2

A_s = a + b/4 + e - c/2; %Stoich 'A'
A = A_s./phi; % Eq 2.33: N_air_act = N_air_stoich/phi
f = A - A_s; % moles excess air
N_prod = a + b/2 + (d/2 + 3.76*A) + e + f;

%% Flow Rate Calcs
AF_stoic = 4.76 * A_s * MW.air/MW.fuel; %EQ 2.32
AF_act = AF_stoic./phi; % Air:Fuel Flowrate

m_dot_ashless = (1 - mf.ash/100)*m_dot_fuel;

m_dot_air = AF_act * m_dot_ashless; % kg/s

m_dot_exhaust = m_dot_air + m_dot_ashless; %kg/s

%% Molar Fractions Exhaust
mol_frac.co2 = a./N_prod;
mol_frac.h2o = (b/2)./N_prod;
mol_frac.n2 = (d/2 + 3.76.*A)./N_prod;
mol_frac.so2 = e./N_prod;
mol_frac.o2 = f./N_prod;

```

```

%% Exhaust Ideal Gas, Flowrate Calc
P_i = [P*mol_frac.co2, P*mol_frac.h2o, P*mol_frac.n2, P*mol_frac.so2, ...
       P*mol_frac.o2]; %Pa
for idx = 1:numel(T)
    rho_i = (1./(T(idx).*Ru)).*[P_i(1).*MW.CO2, P_i(2).*MW.H2O, ...
        P_i(3).*MW.N2, P_i(4).*MW.SO2, P_i(5).*MW.O2]; %kg/m3
    rho_tot(idx) = sum(rho_i); %kg/m3
end

Q_exhaust = 60000.*m_dot_exhaust./rho_tot; %L/min
SLPM_ex = Q_exhaust.*(P./101325.353).*(293.15./T);

%% Print Chemical Rxn
fprintf('\n\nRESULT:\n\nphi = %.2f: ', phi)
if phi < 1
    fprintf('Fuel Lean')
else
    fprintf('Stoichiometric')
end
fprintf('\n\n      C %.2f H %.2f O %.2f N %.3f S %.4f + %.2f(O2+3.76N2) ...
--> %.2f CO2 + %.2f H2O + %.2f N2 + %.4f SO2', a,b,c,d,e,A, ...
a,b/2,d/2+3.76*A, e);

if phi < 1
    fprintf(' + %.2f O2', f)
end

fprintf(['\n\n M_dot solid fuel: %.2f g/hr\n Exhaust Temp: %.2f C\n\n ...
Exhaust Flowrate: '...
'%.2f LPM \n                %.2f SLPM\n']...
, m_dot_fuel*3600*1000, T - 273.15, Q_exhaust, SLPM_ex)

if LHV ≠ 0

```

```
firepower = m_dot_ashless*LHV*1000;  
fprintf(' Firepower: %.2f W\n', firepower)  
end  
  
fprintf('\n\n')
```

Enter Combustion parameters:

Fuel Composition (% Total)  Mass-Based  Molar-Based

Fuel Composition: C   
H   
O   
N   
S   
Ash

LHV Fuel  kJ/kg

Equivalence Ratio  Phi  
Exhaust Temp  C  
Mass Flow Fuel  g/hr

**Figure A.1:** Matlab combustion calculator GUI

RESULT:

phi = 1.00: Stoichiometric

C 0.36 H 0.53 O 0.08 N 0.026 S 0.0014 + 0.45(O2+3.76N2) --> 0.36 CO2 + 0.27 H2O + 1.70 N2 + 0.0014 SO2

M\_dot solid fuel: 82.00 g/hr

Exhaust Temp: 350.00 C

Exhaust Flowrate: 29.70 LPM

11.69 SLPM

Firepower: 1.06 kW

**Figure A.2:** Example results from combustion calculator

# Appendix B

## Fecal Fuel Analysis

		<b>Hazen Research, Inc.</b> 4601 Indiana Street Golden, CO 80403 USA Tel: (303) 279-4501 Fax: (303) 278-1528		Date October 21 2015 HRI Project 009-980 HRI Series No. J158/15-1 Date Rec'd. 10/14/15 Cust. P.O.#	
CSU Powerhouse Max Flagg 430 North College Avenue Fort Collins, Colorado 80524			Sample Identification HU Run 1		
Reporting Basis >	As Rec'd	Dry	Air Dry		
Proximate (%)					
Moisture	3.98	0.00	3.98		
Ash	14.33	14.92	14.33		
Volatile					
Fixed C					
Total					
Sulfur	0.950	0.989	0.950		
Btu/lb (HHV)	9218	9601	9218		
Btu/lb (LHV)	8574	8972			
MMF Btu/lb	10918	11461			
MAF Btu/lb		11285			
Ultimate (%)					
Moisture	3.98	0.00	3.98		
Carbon	48.61	50.62	48.61		
Hydrogen	6.51	6.78	6.51		
Nitrogen	4.60	4.79	4.60		
Sulfur	0.95	0.99	0.95		
Ash	14.33	14.92	14.33		
Oxygen*	21.02	21.90	21.02		
Total	100.00	100.00	100.00		
Chlorine**					
Air Dry Loss (%)			Lb. Alkali Oxide/MM Btu=		
Forms of Sulfur, as S, (%)			Lb. Ash/MM Btu= 15.54		
Sulfate			Lb. SO <sub>2</sub> /MM Btu= 2.06		
Pyritic			Lb. Cl/MM Btu=		
Organic			As Rec'd. Sp.Gr.=		
Total			Free Swelling Index=		
0.95	0.99		F-Factor(dry), DSCF/MM Btu= 9,720		
Water Soluble Alkalies (%)					
Na <sub>2</sub> O					
K <sub>2</sub> O					
			Report Prepared By:		
			 Gerard H. Cunningham Fuels Laboratory Supervisor		
* Oxygen by Difference.					
** Not usually reported as part of the ultimate analysis.					
An Employee-Owned Company					



**Hazen Research, Inc.**  
 4601 Indiana Street  
 Golden, CO 80403 USA  
 Tel: (303) 279-4501  
 Fax: (303) 278-1528

Date October 21 2015  
 HRI Project 009-980  
 HRI Series No. J158/15-1R  
 Date Rec'd. 10/14/15  
 Cust. P.O.#

CSU Powerhouse  
 Max Flagg  
 430 North College Avenue  
 Fort Collins, Colorado 80524

Sample Identification  
 HU Run 2

Reporting Basis >	As Rec'd	Dry	Air Dry
-------------------	----------	-----	---------

Proximate (%)

Moisture	3.79	0.00	3.79
Ash	14.17	14.73	14.17
Volatile	_____	_____	_____
Fixed C	_____	_____	_____
Total	_____	_____	_____

Sulfur	0.859	0.893	0.859
Btu/lb (HHV)	9247	9611	9247
Btu/lb (LHV)	8582	8961	
MMF Btu/lb	10928	11443	
MAF Btu/lb		11271	

Ultimate (%)

Moisture	3.79	0.00	3.79
Carbon	49.08	51.01	49.08
Hydrogen	6.75	7.01	6.75
Nitrogen	4.61	4.79	4.61
Sulfur	0.86	0.89	0.86
Ash	14.17	14.73	14.17
Oxygen*	20.74	21.57	20.74
Total	100.00	100.00	100.00

Chlorine\*\*

Air Dry Loss (%)  
 Forms of Sulfur, as S, (%)

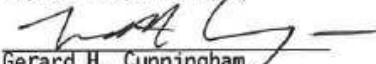
Sulfate		
Pyritic		
Organic	_____	_____
Total	0.86	0.89

Lb. Alkali Oxide/MM Btu=  
 Lb. Ash/MM Btu= 15.32  
 Lb. SO<sub>2</sub>/MM Btu= 1.86  
 Lb. Cl/MM Btu=  
 As Rec'd. Sp.Gr.=  
 Free Swelling Index=  
 F-Factor(dry), DSCF/MM Btu= 9,868

Water Soluble Alkalies (%)

Na<sub>2</sub>O  
 K<sub>2</sub>O

Report Prepared By:

  
 Gerard H. Cunningham  
 Fuels Laboratory Supervisor

\* Oxygen by Difference.

\*\* Not usually reported as part of the ultimate analysis.

An Employee-Owned Company



**Hazen Research, Inc.**  
 4601 Indiana Street  
 Golden, CO 80403 USA  
 Tel: (303) 279-4501  
 Fax: (303) 278-1528

Date October 21 2015  
 HRI Project 009-980  
 HRI Series No. J158/15-2  
 Date Rec'd. 10/14/15  
 Cust. P.O.#

CSU Powerhouse  
 Max Flagg  
 430 North College Avenue  
 Fort Collins, Colorado 80524

Sample Identification  
 K9 Run 1

Reporting Basis >	As Rec'd	Dry	Air Dry
<b>Proximate (%)</b>			
Moisture	3.22	0.00	3.22
Ash	26.06	26.93	26.06
Volatile			
Fixed C			
Total			
Sulfur	0.621	0.642	0.621
Btu/lb (HHV)	6377	6589	6377
Btu/lb (LHV)	5882	6112	
MMF Btu/lb	8874	9293	
MAF Btu/lb		9018	
<b>Ultimate (%)</b>			
Moisture	3.22	0.00	3.22
Carbon	36.22	37.43	36.22
Hydrogen	4.98	5.15	4.98
Nitrogen	3.98	4.11	3.98
Sulfur	0.62	0.64	0.62
Ash	26.06	26.93	26.06
Oxygen*	24.92	25.74	24.92
Total	100.00	100.00	100.00

**Chlorine\*\***

Air Dry Loss (%)  
 Forms of Sulfur, as S, (%)

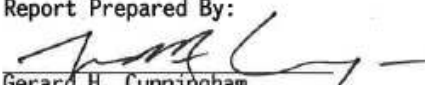
Sulfate		
Pyritic		
Organic		
Total	0.62	0.64

Lb. Alkali Oxide/MM Btu=  
 Lb. Ash/MM Btu= 40.86  
 Lb. SO<sub>2</sub>/MM Btu= 1.95  
 Lb. Cl/MM Btu=  
 As Rec'd. Sp.Gr.=  
 Free Swelling Index=  
 F-Factor(dry), DSCF/MM Btu= 9,877

Water Soluble Alkalies (%)

Na<sub>2</sub>O  
 K<sub>2</sub>O

Report Prepared By:

  
 Gerard H. Cunningham  
 Fuels Laboratory Supervisor

\* Oxygen by Difference.

\*\* Not usually reported as part of the ultimate analysis.

An Employee-Owned Company



**Hazen Research, Inc.**  
 4601 Indiana Street  
 Golden, CO 80403 USA  
 Tel: (303) 279-4501  
 Fax: (303) 278-1528

Date October 21 2015  
 HRI Project 009-980  
 HRI Series No. J158/15-2R  
 Date Rec'd. 10/14/15  
 Cust. P.O.#

CSU Powerhouse  
 Max Flagg  
 430 North College Avenue  
 Fort Collins, Colorado 80524

Sample Identification  
 K9 Run 2

Reporting Basis >	As Rec'd	Dry	Air Dry
<b>Proximate (%)</b>			
Moisture	3.28	0.00	3.28
Ash	29.11	30.10	29.11
Volatile			
Fixed C			
Total			
Sulfur	0.680	0.703	0.680
Btu/lb (HHV)	6291	6504	6291
Btu/lb (LHV)	5791	6023	
MMF Btu/lb	9176	9640	
MAF Btu/lb		9305	
<b>Ultimate (%)</b>			
Moisture	3.28	0.00	3.28
Carbon	36.77	38.02	36.77
Hydrogen	5.02	5.19	5.02
Nitrogen	4.07	4.21	4.07
Sulfur	0.68	0.70	0.68
Ash	29.11	30.10	29.11
Oxygen*	21.07	21.78	21.07
Total	100.00	100.00	100.00

Chlorine\*\*

Air Dry Loss (%)  
 Forms of Sulfur, as S, (%)

Sulfate  
 Pyritic  
 Organic

Total 0.68 0.70

Water Soluble Alkalies (%)

Na2O  
 K2O

Lb. Alkali Oxide/MM Btu=  
 Lb. Ash/MM Btu= 46.27  
 Lb. SO2/MM Btu= 2.16  
 Lb. Cl/MM Btu=  
 As Rec'd. Sp.Gr.=  
 Free Swelling Index=  
 F-Factor(dry), DSCF/MM Btu= 10,461

Report Prepared By:

Gerard H. Cunningham  
 Fuels Laboratory Supervisor

\* Oxygen by Difference.

\*\* Not usually reported as part of the ultimate analysis.

An Employee-Owned Company



**Hazen Research, Inc.**  
 4601 Indiana Street  
 Golden, CO 80403 USA  
 Tel: (303) 279-4501  
 Fax: (303) 278-1528

CSU Powerhouse  
 Max Flagge  
 430 N College Ave  
 Fort Collins, CO 80524

Date March 1, 2017  
 HRI Project 009-976  
 HRI Series No. B49/17-1  
 Date Rec'd. 02/17/17  
 Cust. P.O.#

Sample Identification  
 HU-RTI

Reporting Basis >	As Rec'd	Dry	Air Dry
<b>Proximate (%)</b>			
Moisture	34.47	0.00	2.99
Ash	8.70	13.28	12.88
Volatile	48.55	74.09	71.87
Fixed C	<u>8.28</u>	<u>12.64</u>	<u>12.26</u>
Total	100.00	100.00	100.00
Sulfur	0.350	0.534	0.518
Btu/lb (HHV)	6077	9274	8997
Btu/lb (LHV)	5311	8646	
MMF Btu/lb	6702	10832	
MAF Btu/lb		10694	

<b>Ultimate (%)</b>			
Moisture	34.47	0.00	2.99
Carbon	38.23	58.34	56.60
Hydrogen	4.44	6.78	6.58
Nitrogen	3.43	5.24	5.08
Sulfur	0.35	0.53	0.52
Ash	8.70	13.28	12.88
Oxygen*	<u>10.37</u>	<u>15.83</u>	<u>15.35</u>
Total	100.00	100.00	100.00

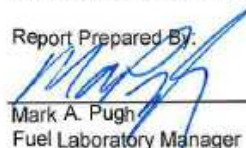
Chlorine\*\*

Air Dry Loss (%)	32.45	Lb. Alkali Oxide/MM Btu =	
Forms of Sulfur, as S, (%)		Lb. Ash/MM Btu=	14.30
Sulfate		Lb. SO2/MM Btu=	1.15
Pyritic		Lb. Cl/MM Btu=	
Organic		As Rec'd. Sp. Gr.=	
Total	0.35	Free Swelling Index=	
		F-Factor(dry), DSCF/MM Btu=	11,613

Water Soluble Alkalies (%)

Na2O  
 K2O

Report Prepared By:

  
 Mark A. Pugh  
 Fuel Laboratory Manager

\* Oxygen by difference

\*\* Not usually reported as part of the ultimate analysis.

An Employee-Owned Company



**Hazen Research, Inc.**  
 4601 Indiana Street  
 Golden, CO 80403 USA  
 Tel: (303) 279-4501  
 Fax: (303) 278-1528

Date March 1, 2017  
 HRI Project 009-976  
 HRI Series No. B49/17-2  
 Date Rec'd. 02/17/17  
 Cust. P.O.#

CSU Powerhouse  
 Max Flagge  
 430 N College Ave  
 Fort Collins, CO 80524

Sample Identification  
 HU-INDIA

Reporting Basis >	As Rec'd	Dry	Air Dry
<b>Proximate (%)</b>			
Moisture	3.64	0.00	3.64
Ash	11.80	12.25	11.80
Volatile	67.98	70.55	67.98
Fixed C	<u>16.58</u>	<u>17.21</u>	<u>16.58</u>
Total	100.00	100.00	100.00

Sulfur	0.438	0.455	0.438
Btu/lb (HHV)	8341	8656	8341
Btu/lb (LHV)	7763	8096	
MMF Btu/lb	9560	9977	
MAF Btu/lb		9864	

<b>Ultimate (%)</b>			
Moisture	3.64	0.00	3.64
Carbon	54.11	56.15	54.11
Hydrogen	5.82	6.04	5.82
Nitrogen	4.61	4.78	4.61
Sulfur	0.44	0.45	0.44
Ash	11.80	12.25	11.80
Oxygen*	<u>19.58</u>	<u>20.32</u>	<u>19.58</u>
Total	100.00	100.00	100.00

Chlorine\*\*

Air Dry Loss (%)	0	Lb. Alkali Oxide/MM Btu =	
Forms of Sulfur, as S, (%)		Lb. Ash/MM Btu=	14.13
Sulfate		Lb. SO2/MM Btu=	1.05
Pyritic		Lb. Cl/MM Btu=	
Organic		As Rec'd. Sp. Gr.=	
Total	0.44	Free Swelling Index=	
		F-Factor(dry), DSCF/MM Btu=	11,495

Water Soluble Alkalies (%)

Na2O  
 K2O

Report Prepared By:  
  
 Mark A. Pugh  
 Fuel Laboratory Manager

\* Oxygen by difference  
 \*\* Not usually reported as part of the ultimate analysis.

# Appendix C

## Venturi Calculations and Hardware Design

### EES Code

```
// Starch
d_p = 15*convert(μm, m)
LHV = 15227*convert(kJ/kg, J/kg)

LEL = 100*convert(g/m^3, kg/m^3) //Lower Explosive Limit
//concen = 100 [g/m^3] //Dust Concentration, Can iterate in parametric Table
Concentration = concen*convert(g/m^3, kg/m^3)

// Constants
FP = 500 [W] //Firepower
P_o = 101300 [Pa] //STP
T_o = 0 [C] //STP

// General EQs

V_p = 4/3*pi*(d_p/2)^3 //Volume sphere

FP = LHV*m_dot_f //Firepower, solve mass flow fuel
m_dot_f_ghr = m_dot_f*convert(kg/s, g/hr) //Fuel
m_dot_f_gs = m_dot_f*convert(kg/s, g/s) //Fuel

m_dot_a = (m_dot_f/Concentration)*density(Air, P=P_o, T = T_o) // air flowrate
SLPM_a = m_dot_a/density(Air, P=P_o, T = T_o)*convert(m^3/s, L/min) //air ...
flowrate
```

```

// Solve for exit nozzle diameter based on flame speed of Lycopodium powder

FlameSpeed = interpolate('Cornstarch Flame Speed', 'Dust Concentration', ...
    'Laminar Flame Speed', 'Dust Concentration' = Concen)

// Exit Velocity of mixture must be ≤ flame speed, assume equal to, Assume ...
    bulk flowrate of fuel/air is flowrate of air (SLPM)

V_exit = FlameSpeed
V_exit = (SLPM_a*convert(L/min, m^3/s))/A_noz
A_noz = D_noz^2*pi/4
D_noz_cm = D_noz*convert(m, cm)

```

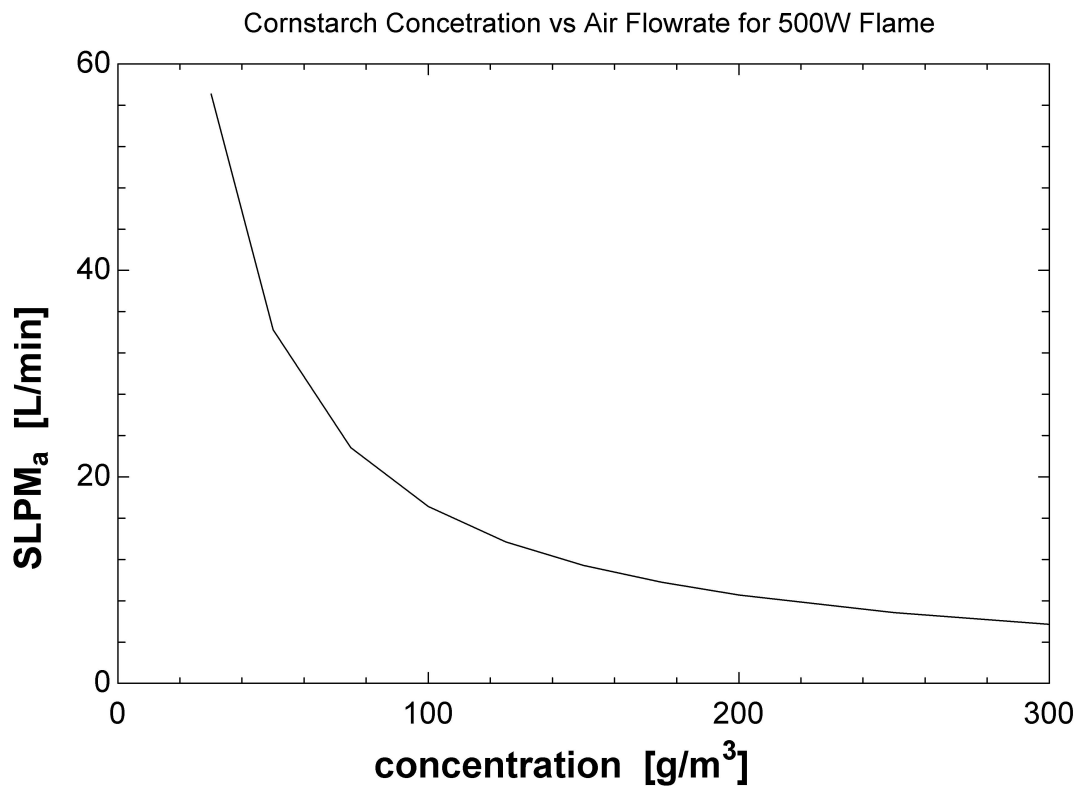


**Figure C.1:** Dust concentration vs. air flowrate

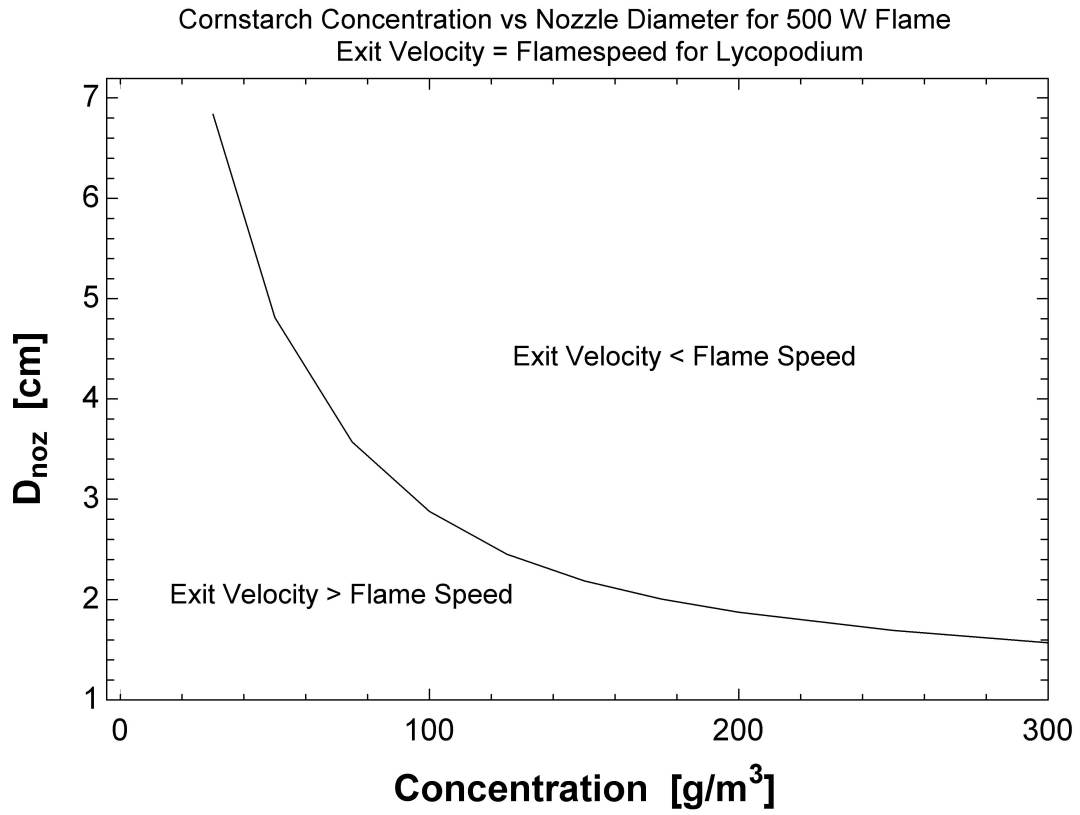


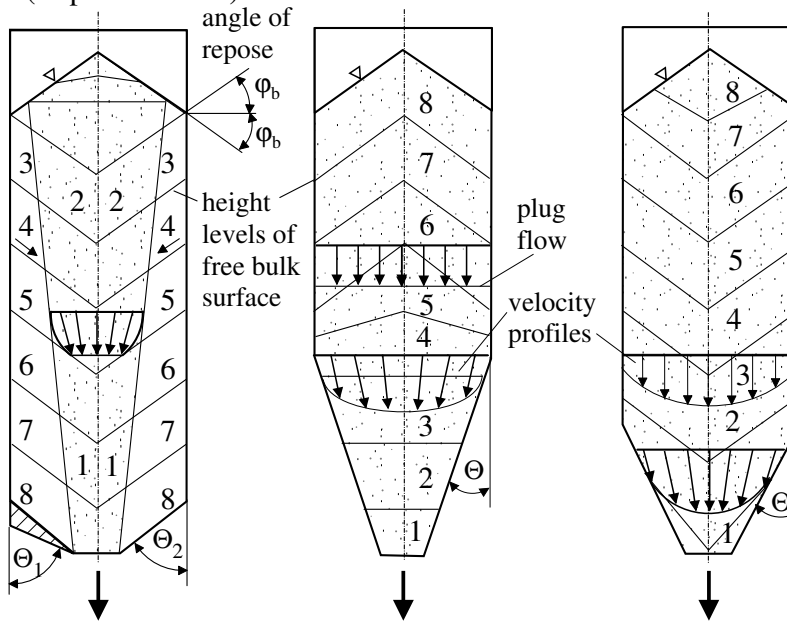
**Figure C.2:** Concentration vs. venturi nozzle diameter

# Hopper Design Equations

## Flow of Particulate Solids in Bunkers and Flow Problems

F 4.2

Funnel or Core Flow (Expanded Flow)    Mass Flow    Mass Flow with Funnel Flow Effect



Channelling,

Piping, Ratholing

Bridging, Arching

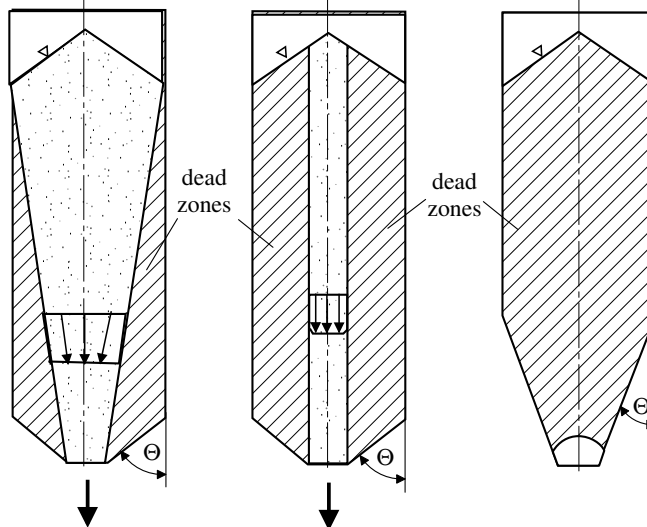


Figure C.3: Hopper design equations [1]

## Apparatus Design of Silo Hopper to Avoid Bridging

F 4.5

### 1. Mass Flow

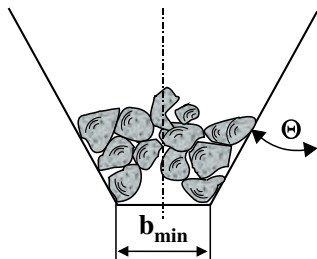
#### - Avoid Channelling:

Hopper angle  $\Theta = f(\text{wall friction angle } \varphi_w, \text{ effective angle of internal friction } \varphi_e)$

see diagrams F 4.6 and F 4.7

#### - Avoid Bridging:

#### 1.1 Free Flowing Bulk Solid (avoid mechanical blocking of coarse lumps or rocks):



$$b_{\min \circ} = 5 d_o \sqrt{k} \quad (1a)$$

$$b_{\min \square} = 5 d_o \sqrt{1,08 k} \quad (1b)$$

$$b_{\min \square} = 5 d_o \sqrt{3} \quad \text{slot width} \quad (1c)$$

$d_o \approx d_{95}$  upper particle size

$k = 0.6 \dots 1.4$  shape dependent parameter

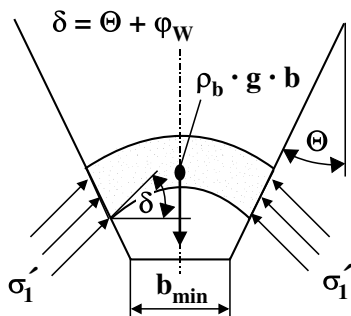
#### 1.2 Cohesive Powder (avoid cohesive bridges):

#### - Effective wall stress at arch:

$$\sigma_1' = \sigma_1 / ff \quad (2)$$

#### - Flow factor (diagram F 4.11):

$$ff = f(\varphi_e, \varphi_w, \Theta) \quad (3)$$



$$b_{\min} = \frac{(m+1) \sigma_{c,crit} \sin 2(\varphi_w + \theta)}{\rho_{b,crit} g} \quad (4)$$

$\sigma_{c,crit}$  critical uniaxial compressive strength

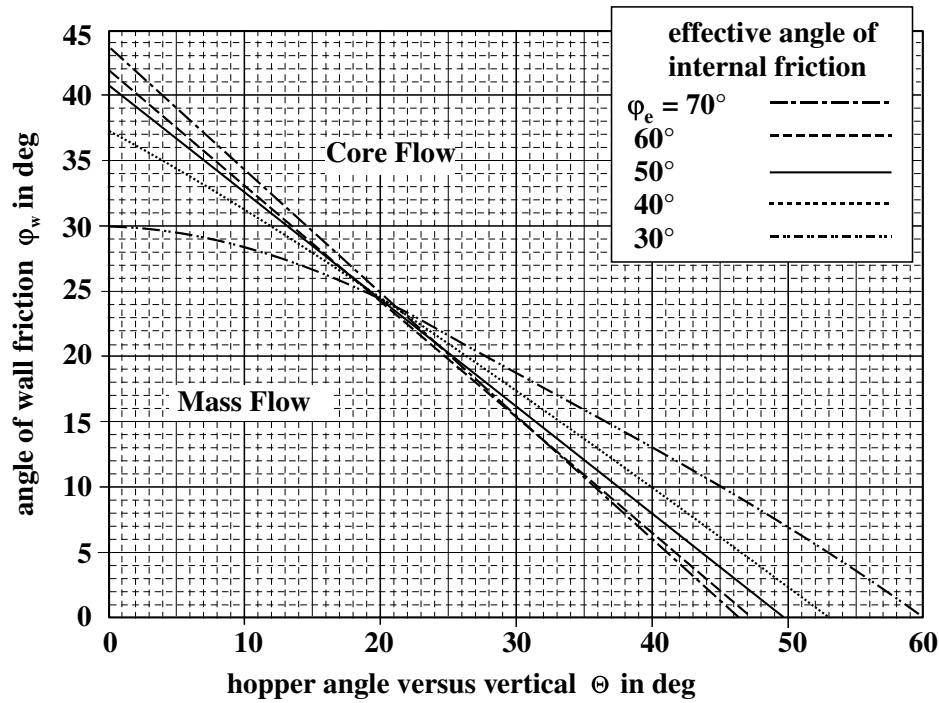
$\rho_{b,crit}$  bulk density at  $\sigma_{l,crit}$   
 $g$  gravitational acceleration

Figure C.4: Hopper design equations [1]

# Bounds between Mass and Core Flow

F 4.6

axisymmetric Flow  
(conical hopper)



$$\Theta \leq \frac{1}{2} \left( 180^\circ - \arccos \left( \frac{1 - \sin \phi_e}{2 \sin \phi_e} \right) - \phi_w - \arcsin \left( \frac{\sin \phi_w}{\sin \phi_e} \right) \right)$$

select  $\Theta := \Theta - 3^\circ$

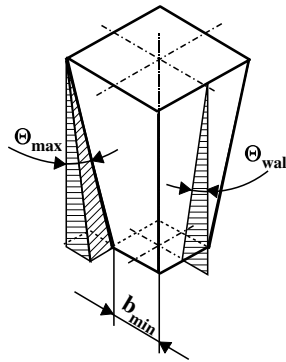
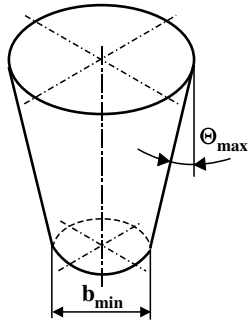
Figure C.5: Hopper design equations [1]

**- Conical Hopper (axisymmetric stress field)**

**F 4.8**

- Cone

- Pyramid

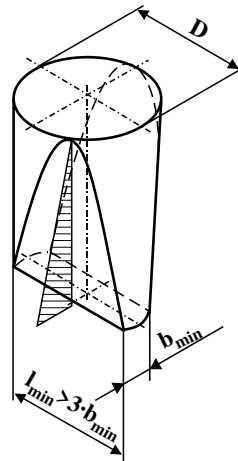
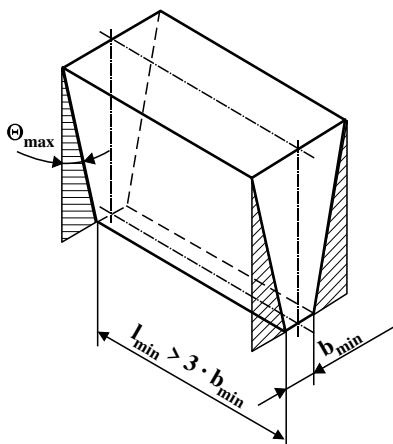


shape factor  $m = 1$

$$\Theta_{\text{wall}} = \arctan\left(\frac{\tan\Theta_{\text{max}}}{\sqrt{2}}\right) \quad [3a]$$

**- Wedge-shaped Hopper (plane stress field)**

- vertical front walls



shape factor  $m = 0$

**Figure C.6: Hopper design equations [1]**

# Appendix D

## Arduino Controller Code

```
/*FOR USE WITH ADAFRUIT DISPLAY SHIELD WITH MICROSTEP DRIVER AND ...
    POTENTIOMETER.
 * MICROSTEP DRIVER NEEDS SEPARATE POWER SUPPLY (E.G. 12V)
 * 5V ACROSS POTENTIOMETER.  ADJUSTABLE PIN TO A0.
 *
 * ORIGINALLY BY LINDEN KLEIN
 * MSR
 * UPDATED BY KYLE GREER, CSU
 */

// include the library code:
#include <Wire.h>
#include <Adafruit_RGBLCDShield.h>
#include <utility/Adafruit_MCP23017.h>
#include <math.h>

// These #defines make it easy to set the backlight color
#define OFF 0x0
#define RED 0x1
#define YELLOW 0x3
#define GREEN 0x2
#define TEAL 0x6
#define BLUE 0x4
#define VIOLET 0x5
#define WHITE 0x7

Adafruit_RGBLCDShield lcd = Adafruit_RGBLCDShield();
```

```

int PUL = 7;           //define Pulse pin
int DIR = 6;          //define Direction pin
int ENA = 3;          //define Enable Pin
float microstep = 4.0; //make sure this matches what's on the driver dip ...
    switch.
int StepPerRev = 400; //using a 400 step per rev stepper motor
int maxRPM = 100;     // let minRPM = 0. **** MaxRPM is 100RPMs for 4 ...
    microsteps. 200RPM for 2 microsteps
int RPM;
int pot;

unsigned int DELAY;
unsigned int dwell;

void setup() {
    pinMode (PUL, OUTPUT);
    pinMode (DIR, OUTPUT);
    pinMode (ENA, OUTPUT);

    Serial.begin(9600); //if using the serial monitor

//RPM & potentiometer setup
    pot = map(analogRead(A0), 0, 1020, 0, maxRPM/5); // map ...
        potentiometer so RPMs step in increments of 5. Map to 1020 instead ...
        of 1023 because max potentiometer is unstable between 1020&1023 so ...
        maxRPM is unstable if max pot = 1023.
    RPM = pot * maxRPM / (maxRPM/5);
    DELAY = round(6E7 / 2 / StepPerRev / microstep / RPM); // DELAY is the ...
        time for a half pulse cycle (high or low). DELAY will be an ...
        microsecond integer, so rounding error will occur. If no ROUND fxn, ...
        then it will just drop the decimal, so use ROUND.

```

```

//LCD Screen Setup
lcd.begin(16, 2);
lcd.setCursor(0, 0);
lcd.print(microstep);
lcd.print(" microsteps");
lcd.setCursor(0, 1);
lcd.print("RPM=");
lcd.print(RPM);
delay(3000);
lcd.clear();
lcd.setCursor(0, 0);
lcd.print("RPM");
lcd.setCursor(0, 1);
lcd.print(RPM);
lcd.print(" FP: ");
lcd.print(RPM*9.0547);

digitalWrite(DIR, LOW); //change this to run in the other direction
digitalWrite(ENA, HIGH); //start spinning motor
}

void loop() {

// dwell times the microseconds it takes to read the analog and check the ...
    if statement.
dwell = micros();
pot = map(analogRead(A0), 0, 1020, 0, maxRPM/5);

// check if the potentiometer was turned. If so, update LCD
if (RPM != pot * maxRPM / (maxRPM/5) ) {
    RPM = pot * maxRPM / (maxRPM/5);
    DELAY = round(6E7 / 2 / StepPerRev / microstep / RPM);
}
}

```

```
//update LCD
lcd.setCursor(0, 1);
lcd.print(RPM);
lcd.print(" FP: ");
lcd.print(RPM*9.0547);
}

// Advance motor one full pulses
digitalWrite(PUL, HIGH);
dwell = micros() - dwell;
delayMicroseconds(DELAY-dwell); // subtract the time for the analog ...
    read from the DELAY time.

digitalWrite(PUL, LOW);
delayMicroseconds(DELAY);
}
```

# Appendix E

## Primary EES Design Calculator

```
// Nano-Combustor Design Calculator, Kyle Greer, 2018
// comment in/out the appropriate constants for helping guide hardware ...
// development
// SLPM -> LPM adjusted for altitude at Ft Collins, CO

//Velocity Constraints:
V_tube = 0.1882
//V_ts = 0.03454 [m/s]

// particle diameter
//dp = 28 //cornstarch
//dp = 31 // lyco

//nozzle diameter
D_tube = .191*convert(in,m)
//D_Tube = 5*convert(mm, m)
d_tube_mm = d_tube*convert(m,mm)
d_tube_in = D_tube*convert(m,in)

//orifice diameter
D_o = 1/16*convert(in,m)

// Air SLPM
//SLPM = 0.3

//Firepower
//FP = 200 [W]
```

```

// LHV Fuel
LHV = 30554 [kJ/kg] //Lycopodium
//LHV = 16500 [kJ/kg] //Cornstarch

// Fuel/air concentration
concen = 1586 [g/m^3]

Q= V_o*A_o
A_o = pi*D_o^2/4

V_tube*A_tube = Q
A_tube = pi*D_tube^2/4

LPM = Q*convert(m^3/s, L/min)
LPM = 101.3/85*SLPM // adjusts for Ft Collins altitude

FP = m_dot*LHV

concen = m_dot/Q

//velfactor_orifice = V/V_ts
//velfactor_tube = V_tube/V_Ts

// Auger RPM to FP:
//RPM*9.0547[W-m] = FP // 3/8 auger for lycopodium, new
RPM * 7.4112[W-m] = FP // 3/8 auger for lycopodium, old
//RPM*27.5[W-m] = FP // 1/4 auger for lycopodium
//RPM = 10.5

//m_dot = RPM*0.00029635 [m*(g/s)] // 3/8 auger flowrate for lyco & assume ...
feces

```

# Appendix F

## Additional Images and Charts

### F.1 Fluidized Bed Burner

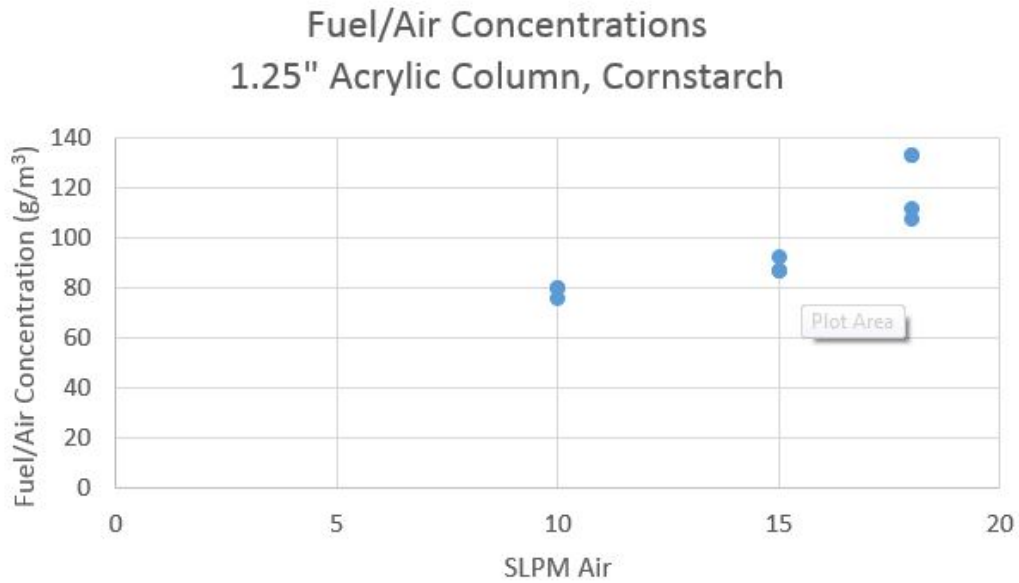


**Figure F.1:** Fuel/Air Concentrations as a function of air flowrate, 1.25" diameter fluidized bed burner

## F.2 Powder Microscopy

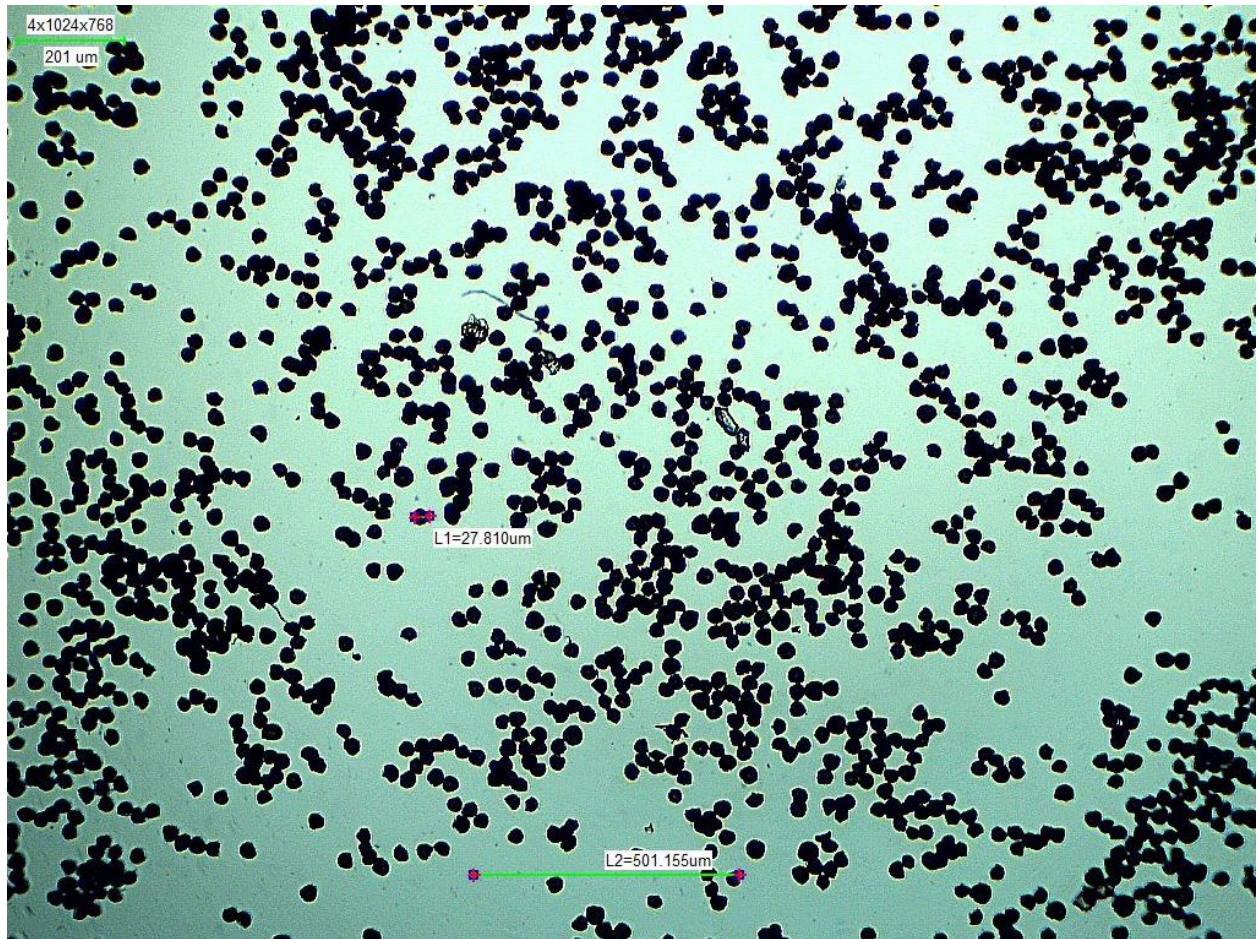
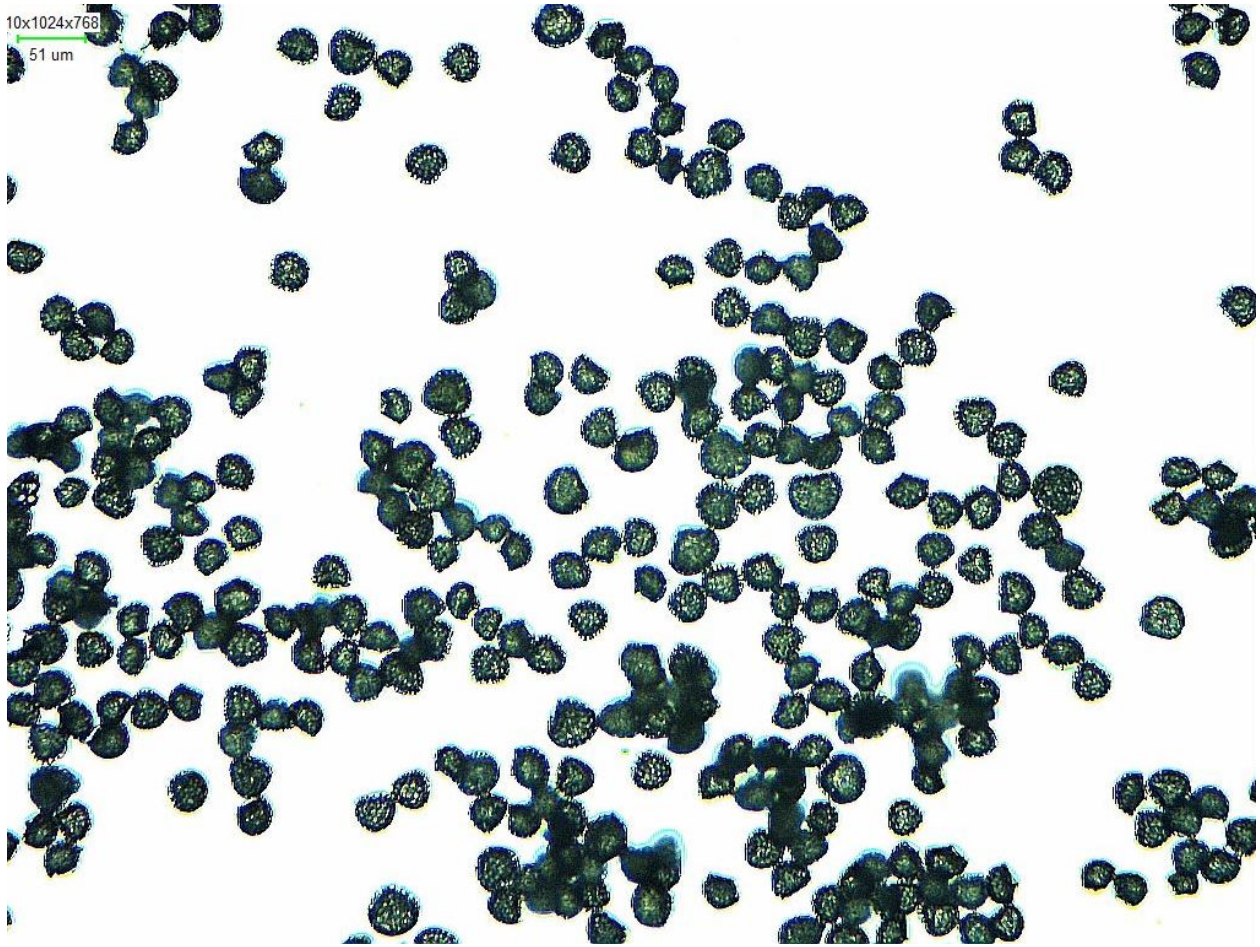
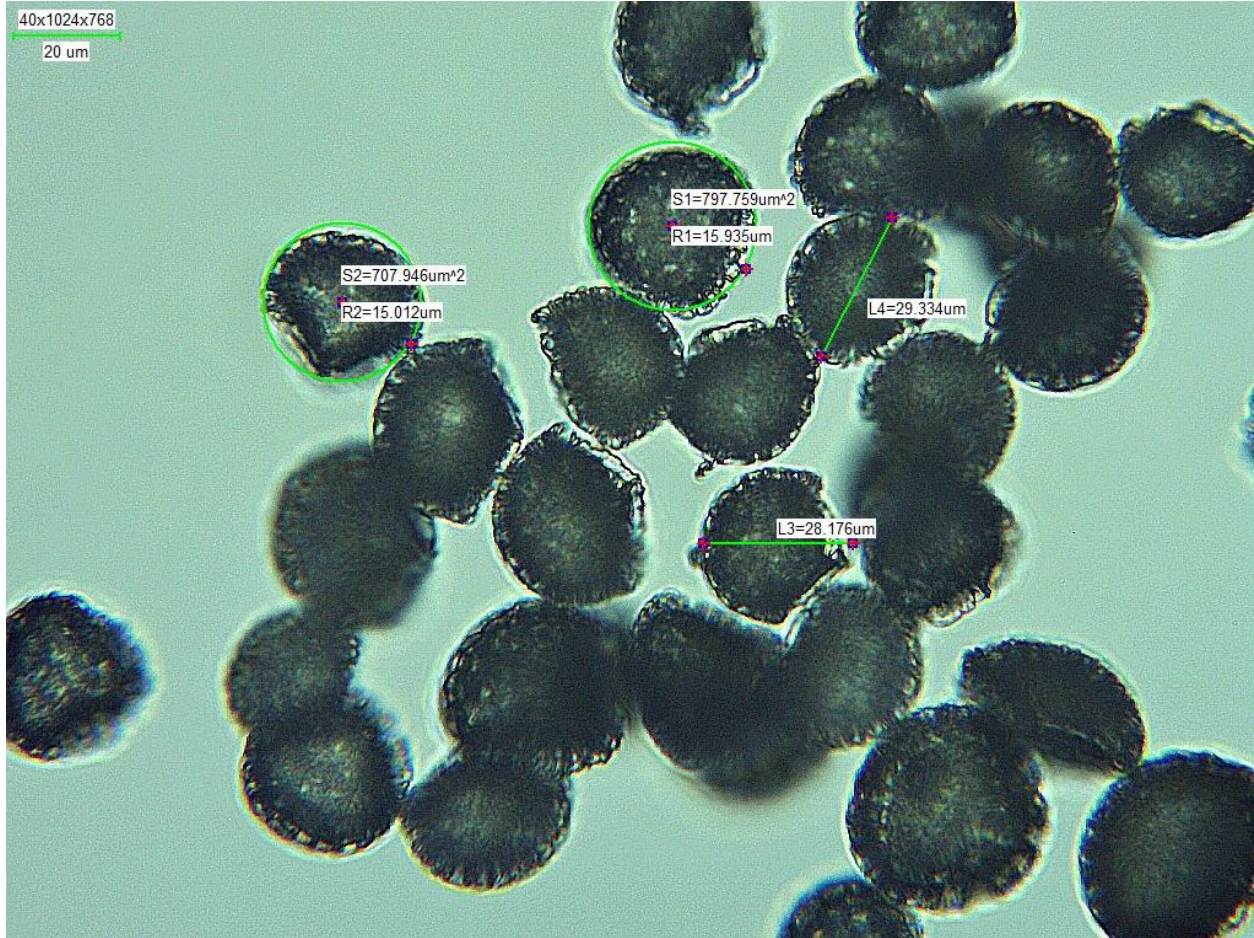


Figure F.2: Fresh lycopodium, 80x magnification



**Figure F.3:** Fresh lycopodium, 200x magnification



**Figure F.4:** Fresh lycopodium, 800x magnification

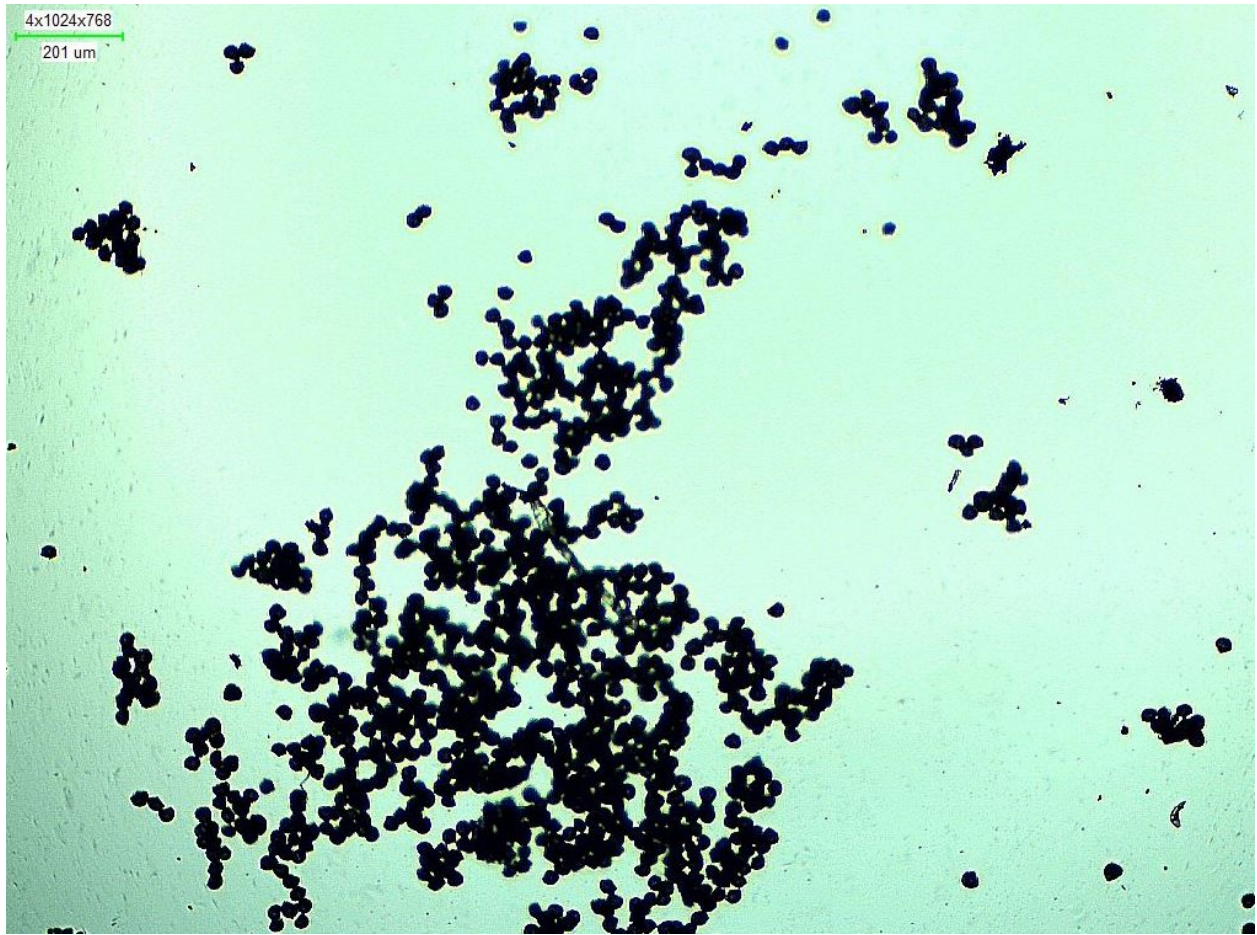


**Figure F.5:** Used lycopodium, 80x magnification

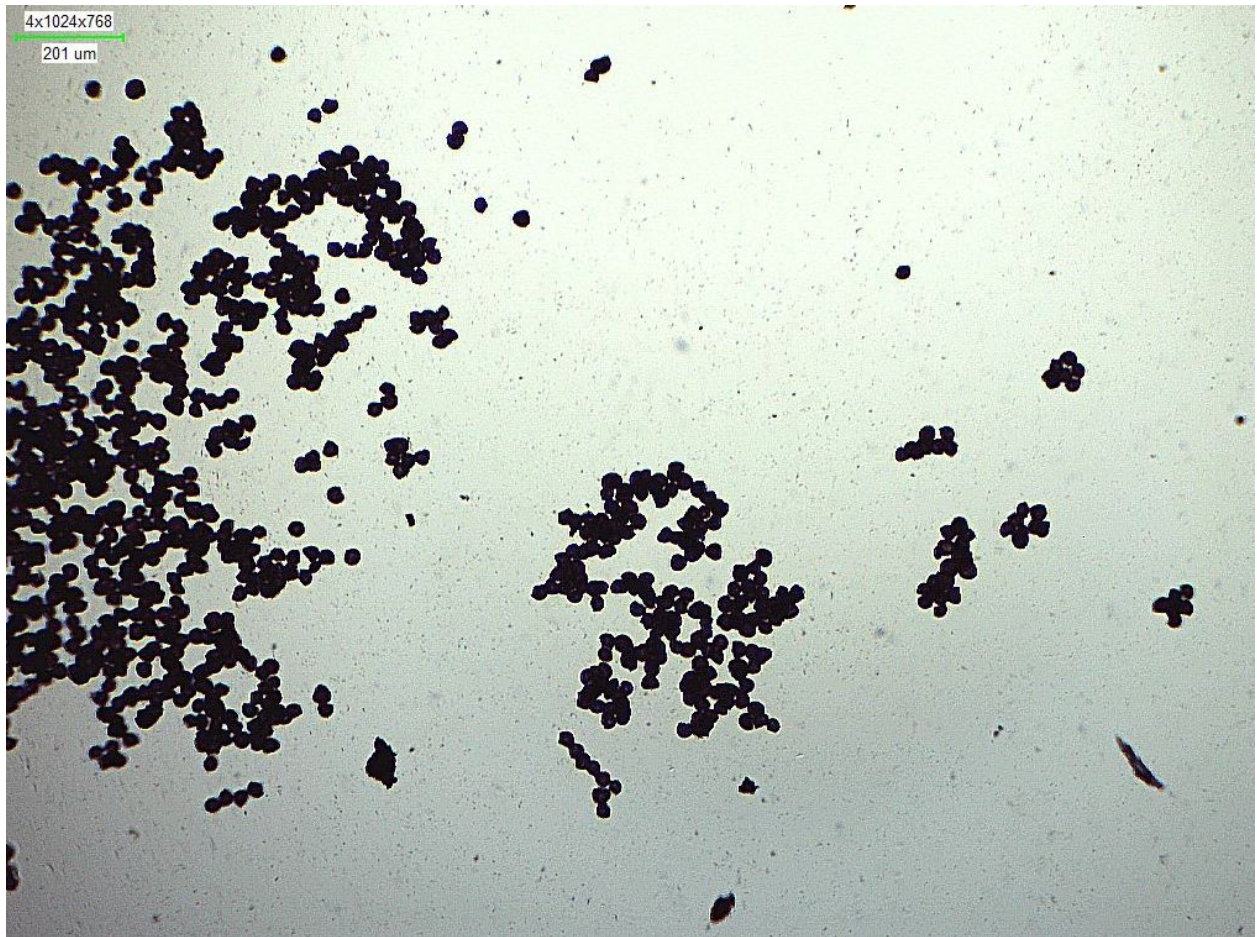


**Figure F.6:** Used lycopodium, 80x magnification

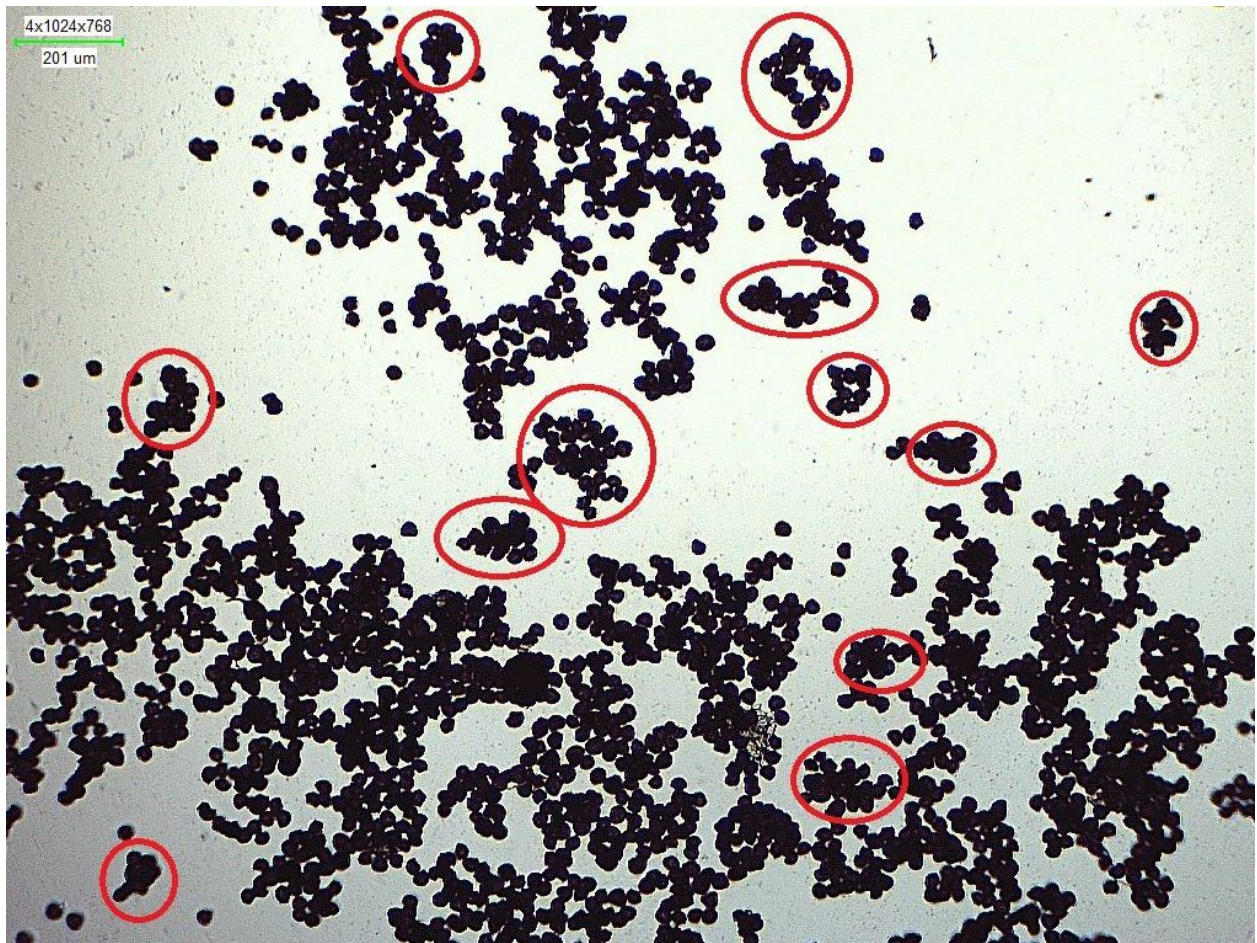


**Figure F.7:** Used lycopodium, 80x magnification, agglomerates circled

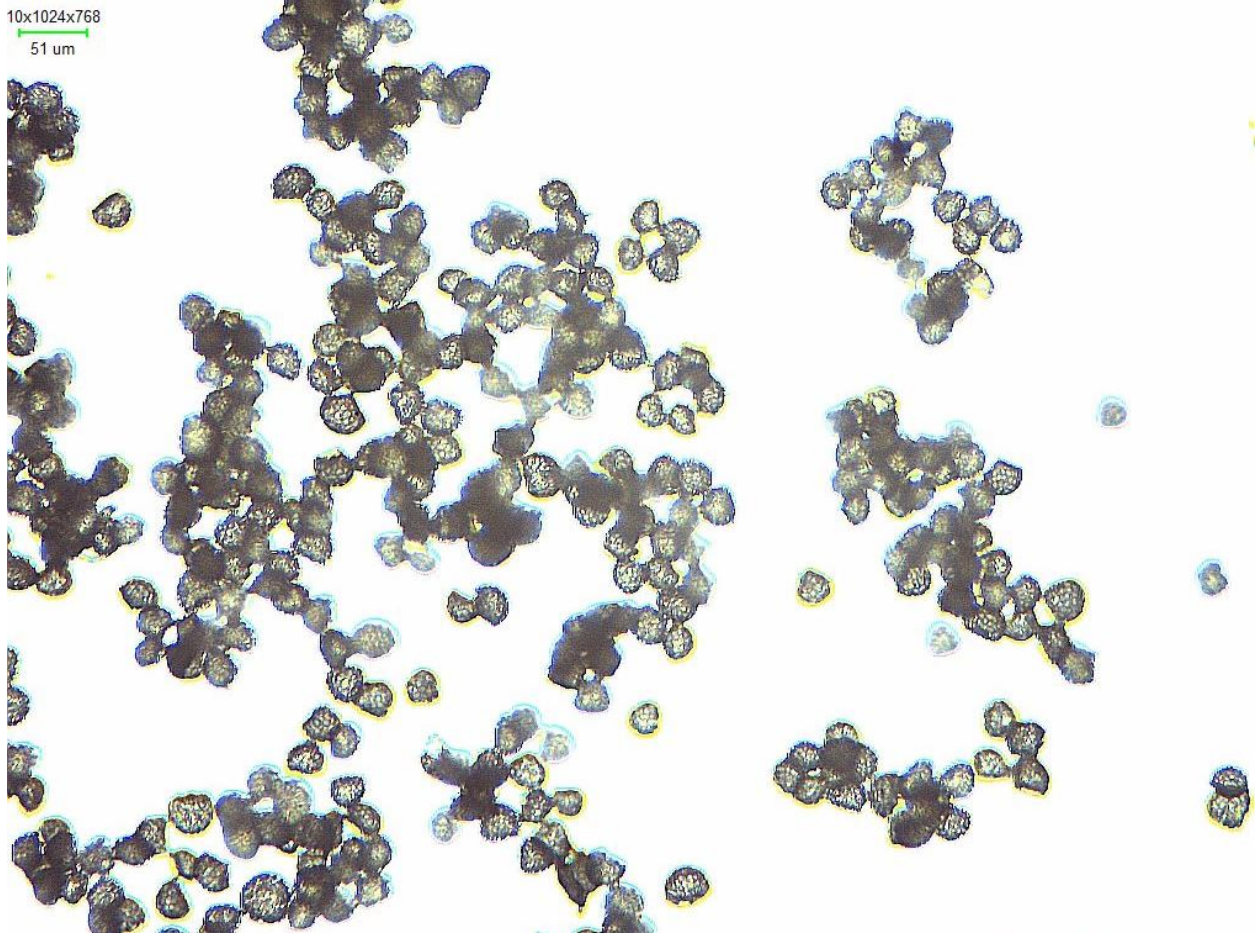
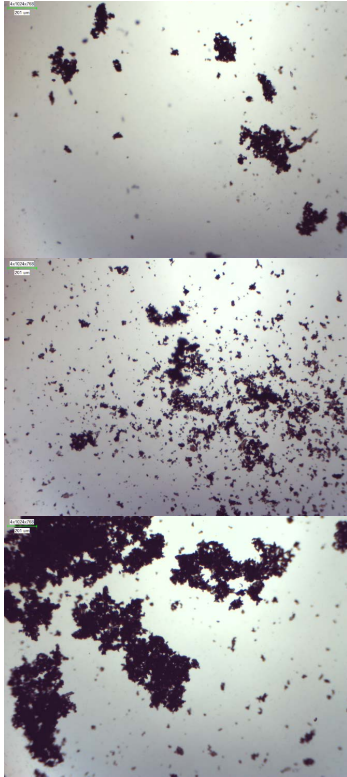
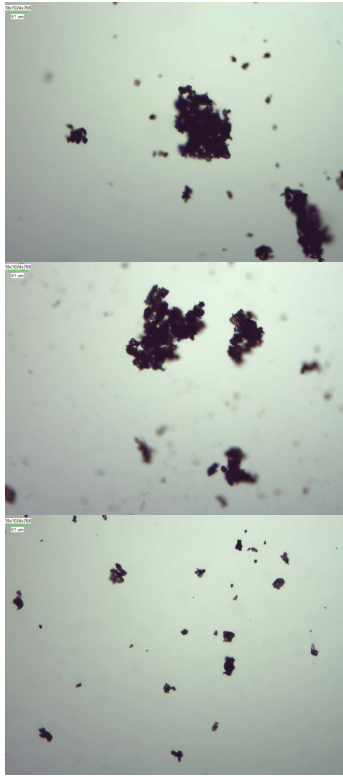


**Figure E.8:** Used lycopodium, 200x magnification



80x Magnification,  
Green Line = 201 um



200x Magnification,  
Green Line = 51 um



800x Magnification,  
Green Line = 20 um

**Figure F.9:** 0-45 um sieved feces powder, taken straight from sieve and sprinkled on microscope slide



**Figure F.10:** 0-45 um sieved feces powder, 80x magnification

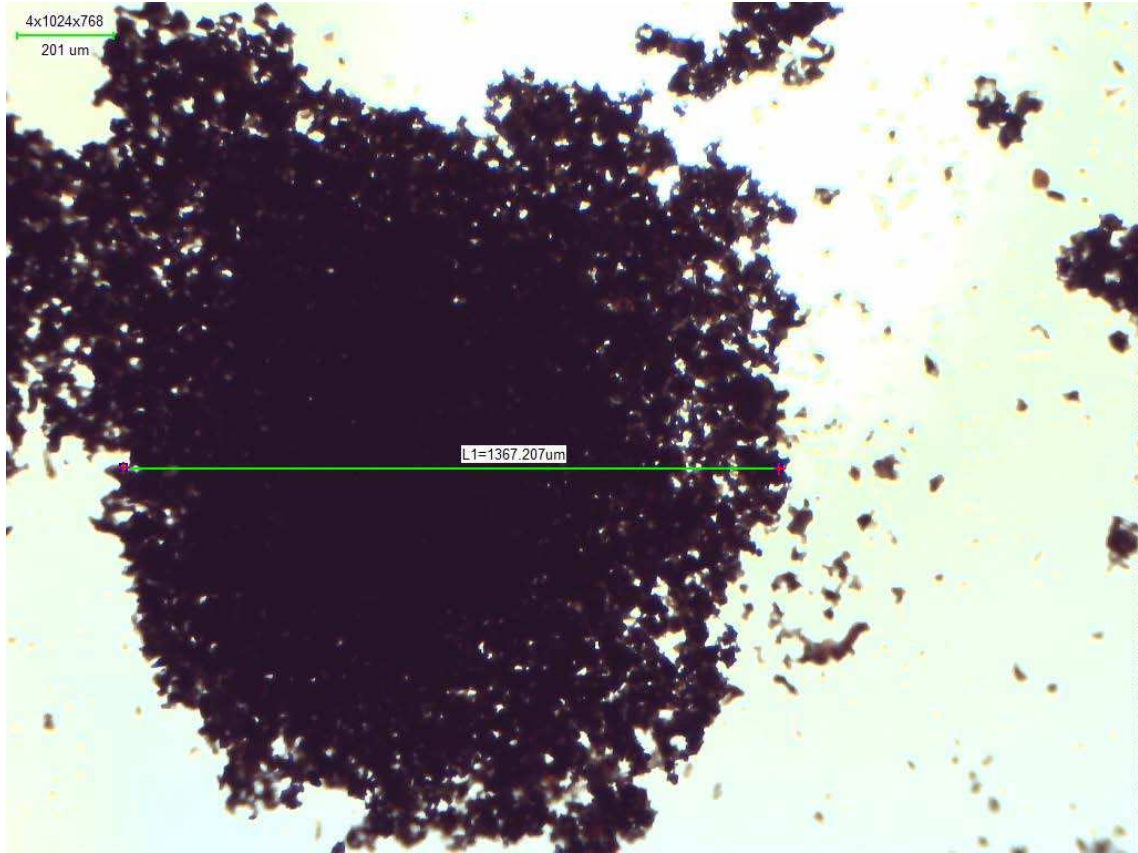


**Figure F.11:** 0-45  $\mu\text{m}$  sieved feces powder, 80x magnification



**Figure F.12:** 0-45 um sieved feces powder, 200x magnification

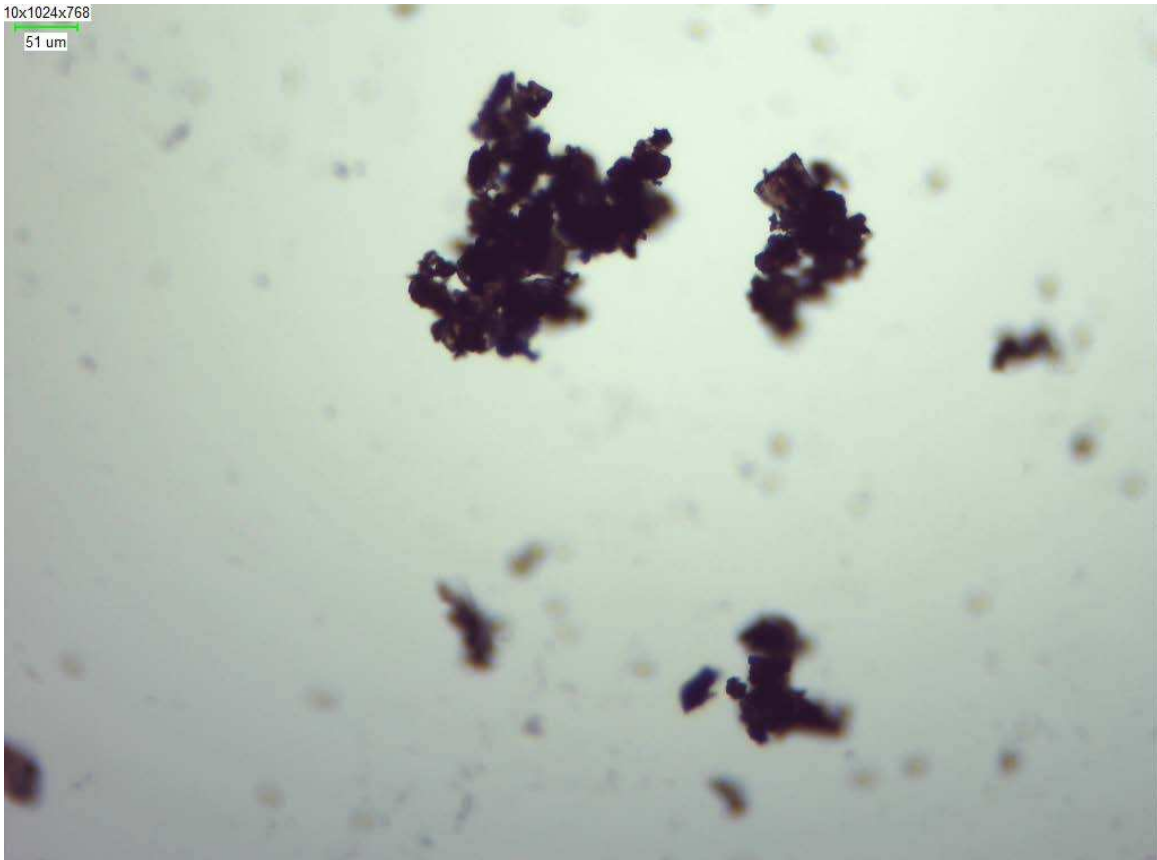


**Figure F.13:** 0-45 um sieved feces powder, 200x magnification

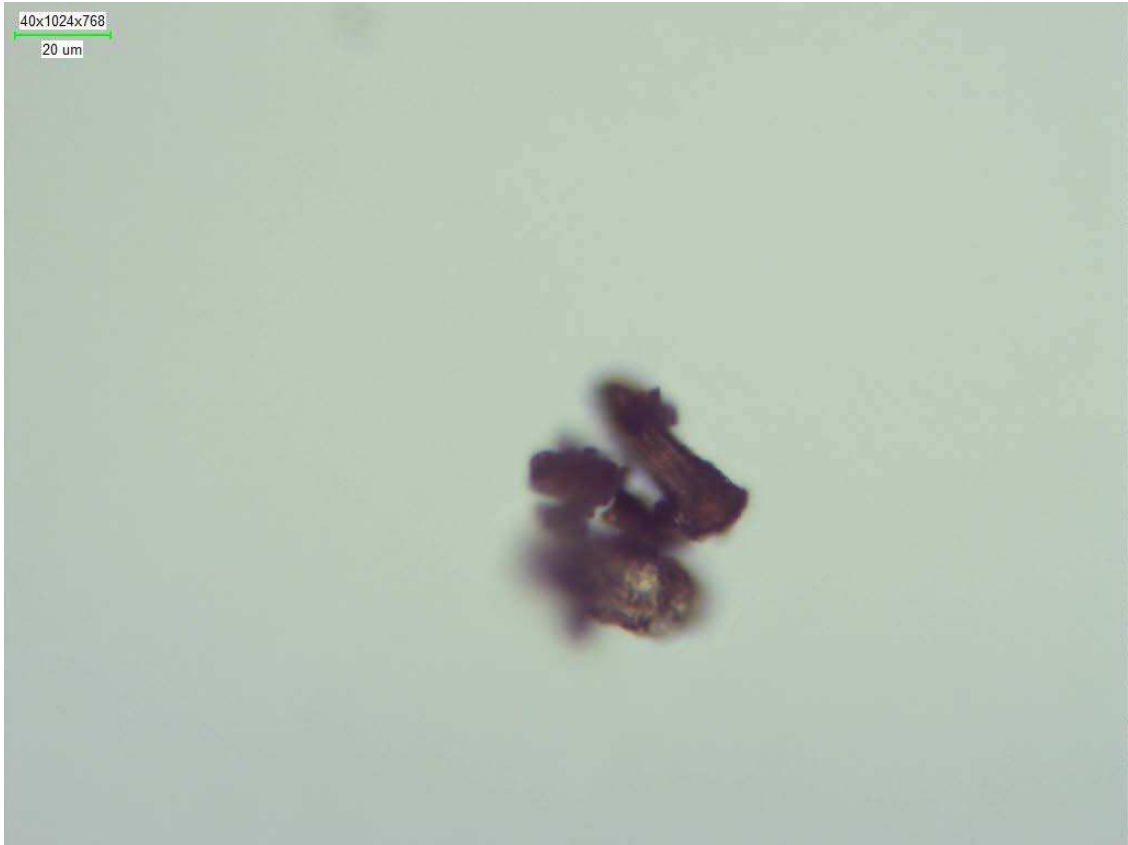


**Figure F.14:** 0-45 um sieved feces powder, 800x magnification

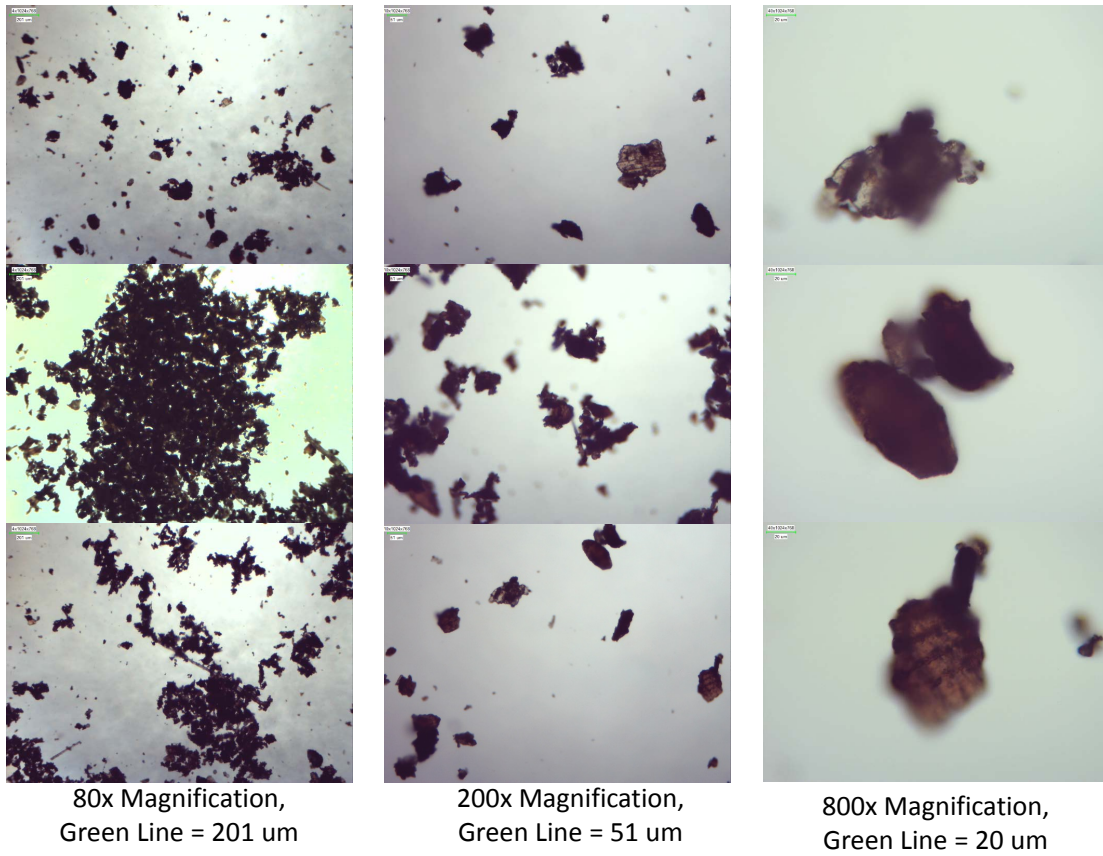


**Figure F.15:** 45-75  $\mu\text{m}$  sieved feces powder, taken straight from sieve and sprinkled on microscope slide



**Figure F.16:** 45-75 um sieved feces powder, 80x magnification



**Figure F.17:** 45-75 um sieved feces powder, 80x magnification

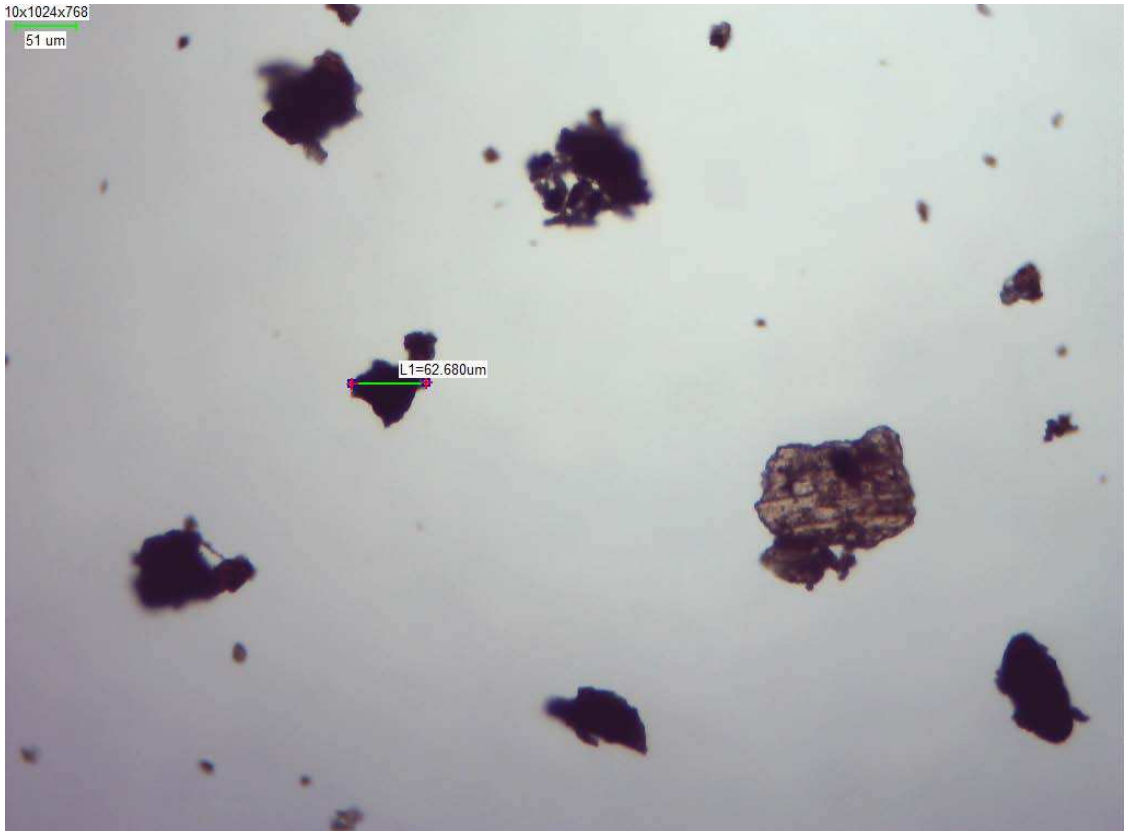


**Figure F.18:** 45-75 um sieved feces powder, 200x magnification

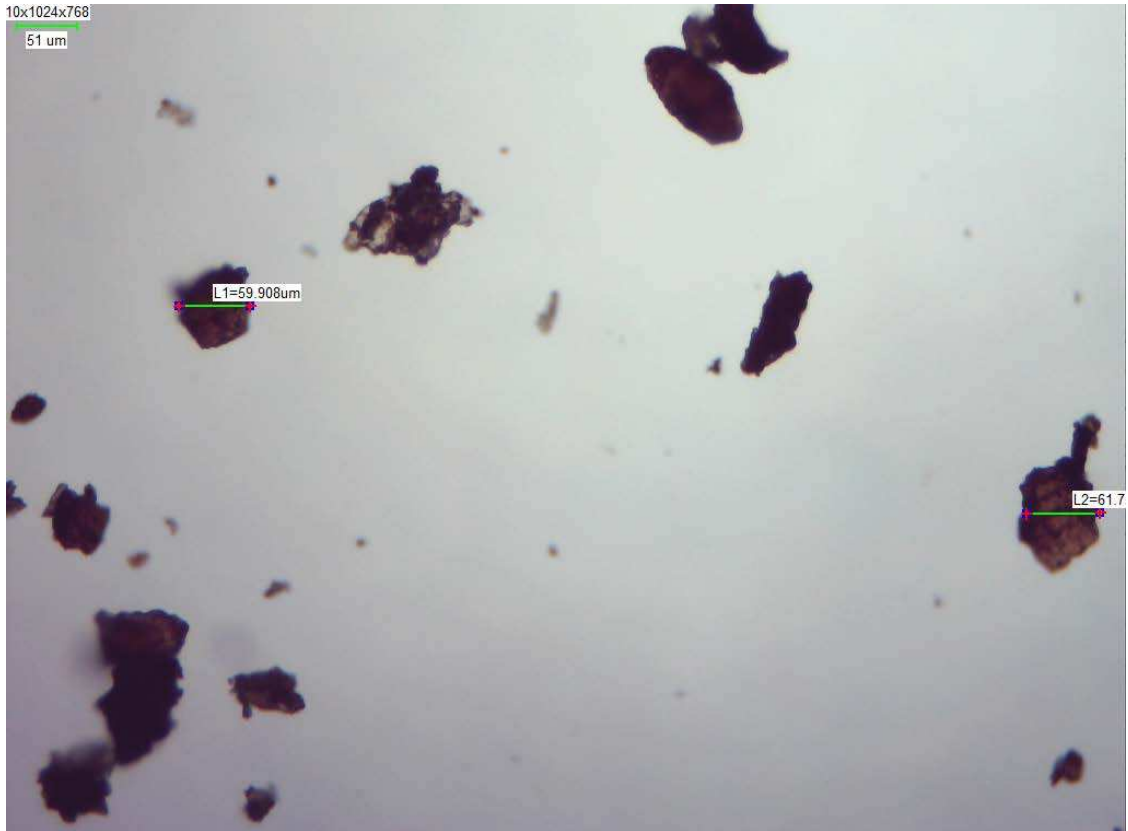


**Figure F.19:** 45-75 um sieved feces powder, 200x magnification

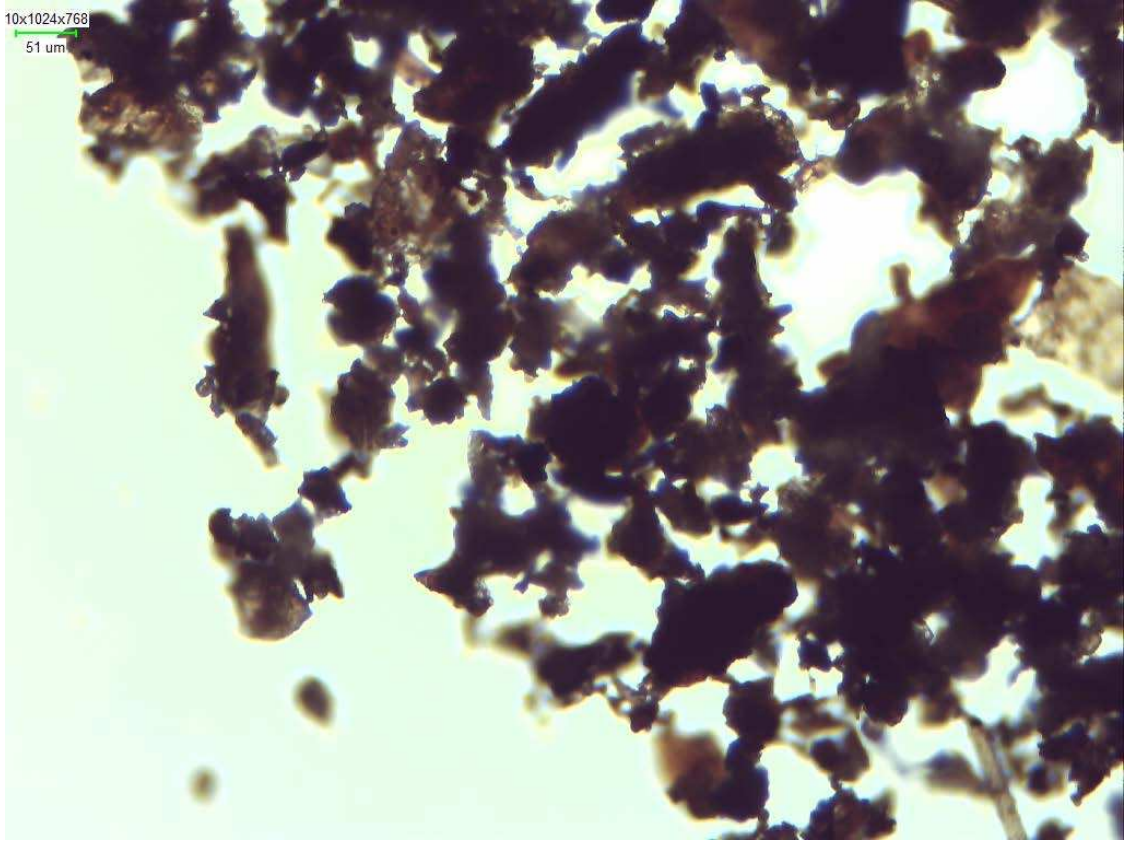


**Figure F.20:** 45-75 um sieved feces powder, 200x magnification

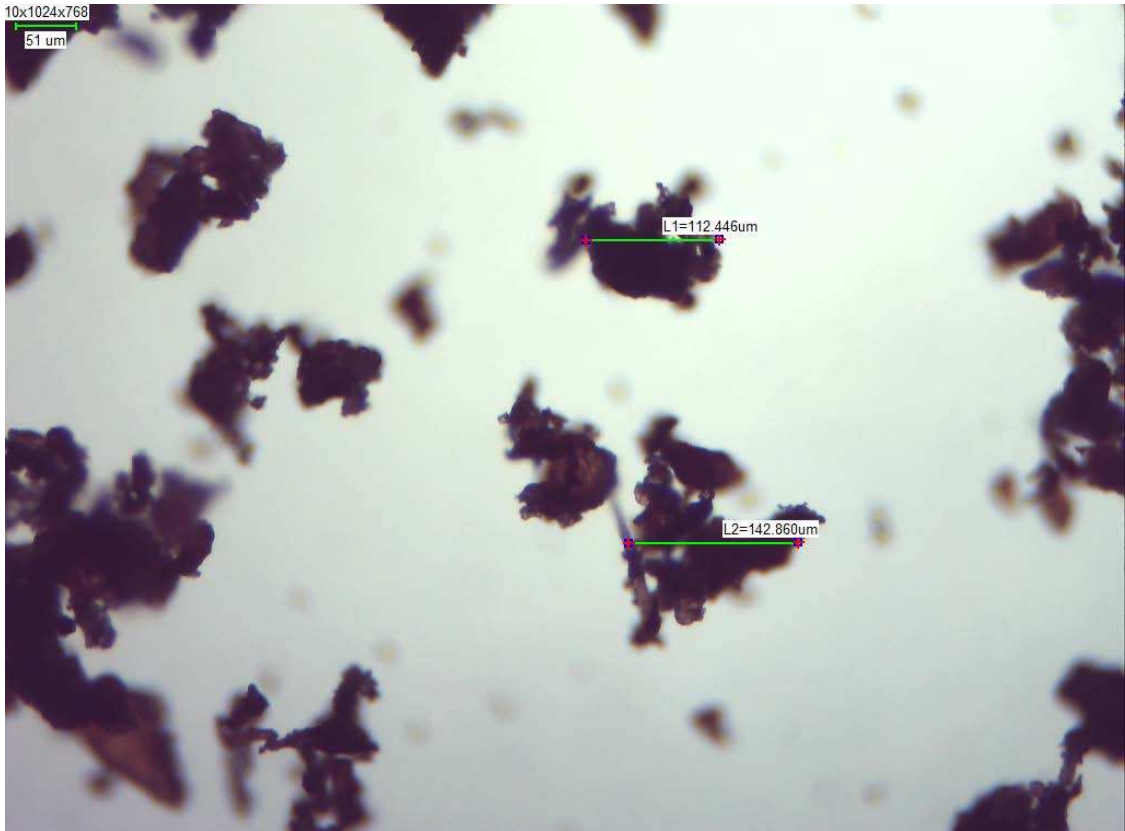


**Figure F.21:** 45-75 um sieved feces powder, 200x magnification

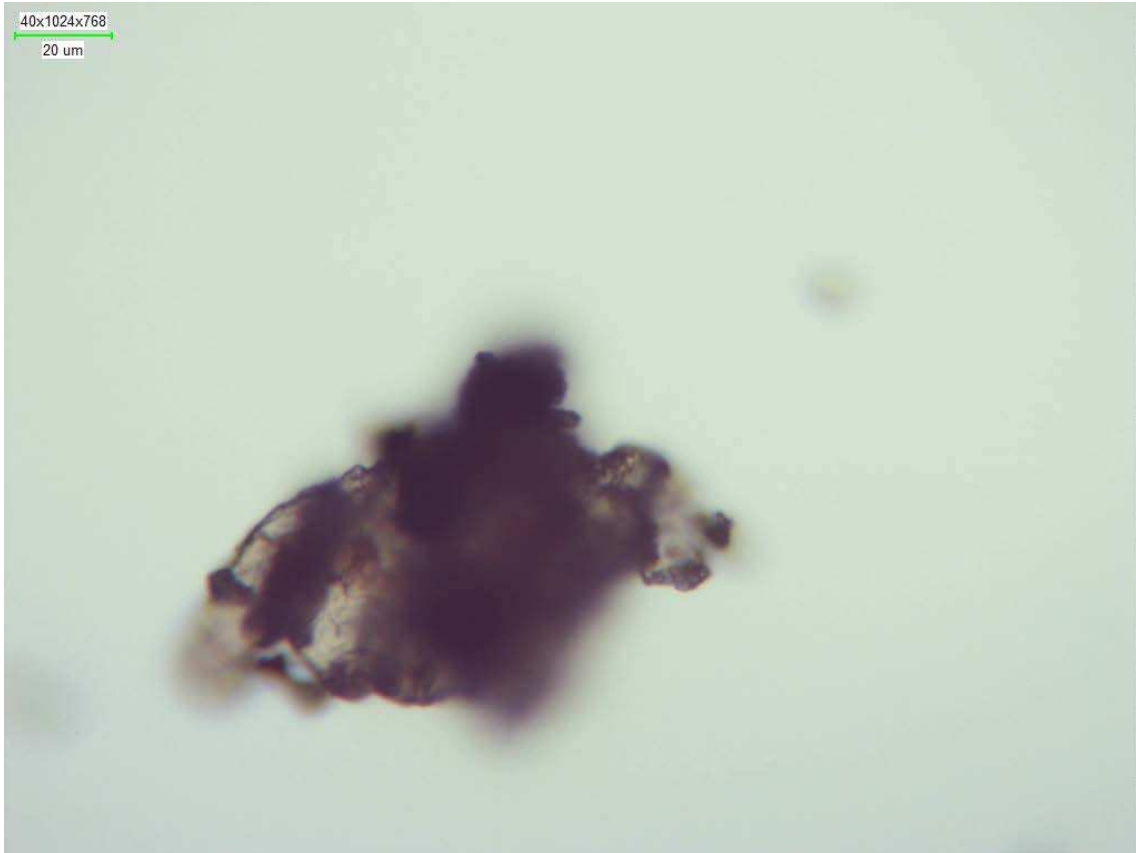


**Figure F.22:** 45-75 um sieved feces powder, 800x magnification